NASA CONTRACTOR REPORT

NASA CR-2452

NASA CR-2452

DEVELOPMENT OF AN ANALYSIS FOR THE DETERMINATION OF COUPLED HELICOPTER ROTOR/CONTROL SYSTEM DYNAMIC RESPONSE

Part I - Analysis and Applications

Lawrence R. Sutton and Stephen A. Rinehart

Prepared by
ROCHESTER APPLIED SCIENCE ASSOCIATES, INC.
Rochester, N.Y.
for Langley Research Center

NATIONAL AERONAUTICS AND SPACE ADMINISTRATION • WASHINGTON, D. C. • JANUARY 1975

1. Report No.	2. Government Accession No.	3. Recipient's Catalog No.
NASA CR 2452		

4. Title and Subtitle	5. Report Date
DEVELOPMENT OF AN ANALYSIS FOR THE DETERMINATION OF COUPLED HELICOPTER ROTOR/CONTROL SYSTEM DYNAMIC RESPONSE, PART I, ANALYSIS AND APPLICATIONS	JANUARY 1975
	6. Performing Organization Code

7. Author(s)	8. Performing Organization Report No.
LAWRENCE R. SUTTON, STEPHEN A. RINEHART	
	10. Work Unit No.

9. Performing Organization Name and Address	11. Contract or Grant No.
ROCHESTER APPLIED SCIENCE ASSOCIATES, INC. ROCHESTER, NEW YORK	NAS1-10856
	13. Type of Report and Period Covered

12. Sponsoring Agency Name and Address	13. Type of Report and Period Covered
NATIONAL AERONAUTICS AND SPACE ADMINISTRATION WASHINGTON, DC 20546	CONTRACTOR REPORT
	14. Sponsoring Agency Code

15. Supplementary Notes

FIRST OF TWO FINAL REPORTS.

16. Abstract

A THEORETICAL ANALYSIS IS DEVELOPED FOR A COUPLED HELICOPTER ROTOR SYSTEM TO ALLOW DETERMINATION OF THE LOADS AND DYNAMIC RESPONSE BEHAVIOR OF HELICOPTER ROTOR SYSTEMS IN BOTH STEADY-STATE FORWARD FLIGHT AND MANEUVERS. THE EFFECTS OF AN ANISOTROPICALLY SUPPORTED SWASHPLATE OR GYROSCOPE CONTROL SYSTEM AND A DEFORMED FREE WAKE ON THE ROTOR SYSTEM DYNAMIC RESPONSE BEHAVIOR ARE INCLUDED IN THE ANALYSIS.

17. Key Words (Suggested by Author(s))	18. Distribution Statement
HELICOPTER ROTOR CONTROL SYSTEM FREE WAKE DYNAMIC RESPONSE	STAR CATEGORY 02

19. Security Classif. (of this report)	20. Security Classif. (of this page)	21. No. of Pages	22. Price*
UNCLASSIFIED	UNCLASSIFIED	114	$5.25

*For sale by the National Technical Information Service, Springfield, Virginia 22151

TABLE OF CONTENTS

DEVELOPMENT OF AN ANALYSIS FOR THE DETERMINATION OF COUPLED HELICOPTER ROTOR/CONTROL SYSTEM DYNAMIC RESPONSE

PART I - ANALYSIS AND APPLICATIONS*

By Lawrence R. Sutton and Stephen A. Rinehart

Rochester Applied Science Associates, Inc.

SUMMARY

A theoretical analysis is developed for a coupled helicopter rotor system to allow determination of the steady-state dynamic response behavior of helicopter rotor systems in steady-state forward flight or maneuvers. The effects of an anisotropically supported swashplate or gyroscope control system and a deformed free-wake on the rotor system dynamic response behavior are included in this analysis.

The analysis involves the utilization of a combination of Laplace transform and transfer matrix techniques such that a set of Laplace transformed equations in matrix form result which include interharmonic coupling of the blades due to the control system and blade aerodynamic coupling. The solution of the matrix equations results in the determination of the harmonic content of the blade response; deflections, slopes, moments, and shears; and of the control system response. The consideration of a deformed free-wake requires an iterative procedure to be applied to the fundamental analysis since the rotor system will respond to a downwash distribution resulting in a modified downwash distribution on the rotor system. Wake-induced velocity influence coefficients and the initial nondimensionalized bound circulation values necessary to determine the initial downwash distribution are obtained from use of an existing free-wake analysis.

A digital computer program based upon the analysis developed was executed for a swashplate controlled, articulated rotor system in steady-state forward and maneuver flight configurations including a deformed free-wake to ascertain the viability of this theoretical analysis. The dynamic response results obtained from these calculations indicate that the coupled rotor system dynamic response analysis provides an accurate and improved simulation of a helicopter rotor system.

---

*PART II - Computer Program Listing is NASA CR-2453.

INTRODUCTION

In recent years the design of helicopter and V/STOL rotor systems has required a more realistic representation of the dynamic and aeroelastic behavior of rotor systems. The prediction of rotor-induced aerodynamic flows has recently undergone extensive refinement, primarily due to the need for improved predictions and to the development of large-capacity digital computer systems. The desire for increased performance and other considerations have stimulated the development of improved analytical tools for use in the design of helicopters. In spite of the technological advances which have been accomplished, helicopters continue to be limited in their operational envelope often as a result of severe oscillatory airloads and rotor system response. There still exists a need for a better understanding of the causative physical phenomena for the behavior of fully-coupled rotor systems.

The analysis which was developed and the computer program which resulted are a part of an increased effort to develop better theoretical methods for the study of helicopter rotor systems. Improved high-harmonic airloads determination alone is of limited usefulness in blade response analysis unless compatible blade models are employed in the dynamic response computations. Inter-blade coupling due to the control system and aerodynamic coupling can have significant effects on the torsional dynamic response behavior of a rotating helicopter blade. In order that the behavior of helicopter rotor systems can be more accurately predicted, a theoretical analysis was developed which includes the effects of; high harmonic airloads, anisotropic control systems, interharmonic blade coupling, and coupling of blade motions with a deformed free-wake.

SYMBOLS*

a	speed of sound
a_m	length of rigid rocker arm attached to $m^{\underline{th}}$ blade, positive if rocker arm aft of quarter chord,m

*All units given in SI units but equivalent English units may be used if applied to all definitions of program variables.

$[A]_m^{(i)}, [\bar{A}]_m^{(i)}$ real time and Laplace transformed blade transfer matrix associated with mass and inertia effects for the $i^{\underline{th}}$ station on the $m^{\underline{th}}$ blade

$A_{Np}^{(i)}$ real part of a Np harmonic state variable inboard of the $i^{\underline{th}}$ station

b_j rigid offset of $j^{\underline{th}}$ linear spring swashplate attachment from neutral axis of ring (positive if offset is toward the center of ring)

$[B]_m^{(i)}, [\bar{B}]_m^{(i)}$ real time and Laplace transformed blade transfer matrix associated with a bend or finite twist of a blade section

$[\bar{B}_{k,n}]_m^{(i)}$ transfer matrix relating contribution to the k-shifted state vector harmonic coefficients at the inboard end of section i of blade m from the n-shifted blade tip unknowns harmonic coefficients, where, for example, a k shift denotes a harmonic -k/rev. relative to the Np/rev. harmonic (this double subscript notation denotes the same form of relationship in other arrays)

$[\bar{\beta}_{k,n}]_m$ portion of final set of rotor and swashplate equations associated with the $m^{\underline{th}}$ blade

$\{\bar{b}_{k,n}\}_m^{(i)}$ matrix relating contribution to state vector for the $m^{\underline{th}}$ blade at $i^{\underline{th}}$ blade station from the control torque applied to blade through rocker arm

$B_{Np}^{(i)}$ imaginary part of a Np harmonic state variable inboard of the $i^{\underline{th}}$ station

c_j linear damper strength of $j^{\underline{th}}$ cyclic spring-damper unit supporting the swashplate, N-sec/m

c_{θ_j} lateral angular damper strength of $j^{\underline{th}}$ cyclic spring-damper unit supporting the swashplate, N-sec/m

c_{ϕ_j} longitudinal angular damper strength of $j^{\underline{th}}$ cyclic spring-damper unit supporting the swashplate, N-sec/m

$c_m^{(i)}$ defines the blade chord at the $i^{\underline{th}}$ blade station of the $m^{\underline{th}}$ blade

$\{\bar{c}_{k,n}\}_m^{(i)}$ matrix relating contribution to state vector at $i^{\underline{th}}$ blade station from the discontinuity in torsional deflection at the pitch bearings

$[\bar{C}_k]_m$ portion of final set of rotor and swashplate equation coefficients associated with the coupling of the $m^{\underline{th}}$ blade with the swashplate response, defined by Equation (150)

$[C]_m^{(i)}$ blade transfer matrix associated with a lumped aerodynamic station, accounts for periodically varying aerodynamic terms involving d/dt

$[C_n]_m^{(i)}$ harmonic blade transfer matrix associated with lumped aerodynamic station obtained by Fourier analysis of previous variable

$[\bar{C}_{n-k,\ n}]_m^{(i)}$ total aerodynamic blade transfer matrix for a transfer across the $i^{\underline{th}}$ station on the $m^{\underline{th}}$ blade

c_ℓ lift coefficient

c_{ℓ_μ} lift coefficient limit for special stall model

c_{ℓ_α} lift curve slope at 0 radians angle of attack

c_d drag coefficient

$c_{m_{2D,\ stalled}}$	two-dimensional stall limit moment
C_G	damper strength of collective spring-damper unit supporting gyroscope, N-sec/m
C_{Gx}	lateral damping coefficient of gyroscope foundation support, N-m-sec/rad
C_{Gy}	longitudinal damping coefficient of gyroscope foundation support, N-m-sec/rad
C	damper strength of collective (foundation) spring-damper unit supporting swashplate, N-sec/m
$\overline{C}$	average of longitudinal and lateral gyroscope damping coefficient, N-m-sec/rad
C'	lateral gyroscopic damping minus the longitudinal damping coefficient /2, N-m-sec/rad
d_m	rigid offset of $m^{\underline{th}}$ control rod attachment point from neutral axis of ring (positive if offset is outward from center of ring), m
$d(\chi_j,t), d(\theta,t)$	definitions involving swashplate deflections to reduce length of equations
$\{\overline{d}_{k,n}\}^{(i)}_m$	matrix relating contribution to state vector at $i^{\underline{th}}$ blade station from the discontinuity in flap angle at the flap hinge
$\{d\}^{(i)}_m$	forcing function due to aerodynamics at an aerodynamic station
$\{d_n\}^{(i)}_m, \{\overline{d}_n\}^{(i)}_m$	real time and Laplace transformed harmonic aerodynamic forcing function obtained by Fourier analysis of the previous variable
$[\overline{\mathcal{D}}_{n-k,n}]_m$	portion of final set of rotor and swashplate/gyroscope equation coefficients associated with coupling of the swashplate or gyroscope response to that of the $m^{\underline{th}}$ blade, defined by Equation (148)

$[D]_m^{(i)}$	blade transfer matrix of terms not multiplied by a time derivative for an aerodynamic station
$[D_n]_m^{(i)}, [\bar{D}_n]_m^{(i)}$	real time and Laplace transformed harmonic transfer matrix based on previous variable
e	blade sweep hinge radial offset, m
$[E]_m^{(i)}, [\bar{E}]_m^{(i)}$	real time and Laplace transformed blade transfer matrix associated with a massless elastic section
$(EI_y)^{(i)}$	local edgewise bending rigidity of $i^{\underline{th}}$ blade section, $N\text{-}m^2$
$(EI_z)^{(i)}$	local flapwise bending rigidity of the $i^{\underline{th}}$ blade section, $N\text{-}m^2$
(EJ_z)	bending stiffness of swashplate, $N\text{-}m^2$
$F(a)$	variable involving swashplate stiffness to reduce equation length as defined after Equation (37)
$\{F\}_m^{(i)}, \{\bar{F}\}_m^{(i)}$	real time and Laplace transformed forcing function due to the mass and inertial effects, k subscript is added for shifted harmonics
$\{F^0\}_m^{(i)}$	steady forcing function due to mass and inertia effects
$\{F^1\}_m^{(i)}$	amplitude of +1/rev forcing function due to mass and inertia effects
$\{F^{-1}\}^{(i)}$	amplitude of -1/rev forcing function due to mass and inertia effects
$\{\bar{F}_k\}^*$	total forcing function effect in final solution as defined by Equation (153)
$\{\bar{F}r_k\}^*$	total swashplate forcing function, always zero

$\{\bar{F}p_k\}_m^*$	total blade forcing function in final solution representation and as defined in Equation (154)
g	gravity constant, m/sec^2
$(GJ)^{(i)}$	local torsional rigidity of $i^{\underline{th}}$ blade section, $N\text{-}m^2$
(GJ_t)	torsional stiffness of swashplate, $N\text{-}m^2$
$[\bar{G}_{k,n}]_m^{(i)}$	real time and Laplace transform version of total section transfer matrix associated with the $i^{\underline{th}}$ section of the $m^{\underline{th}}$ blade
h_{rx}	radial distance (positive outward) of a blade mass point from the origin of the reference coordinate system at the rotor hub when Φ and Θ are zero in value, m
h_{ry}	distance of neutral axis ahead of pitch axis assumed to be at quarter chord,m
$\{\bar{H}_k\}_m^{(i)}$	total forcing function at the $i^{\underline{th}}$ station of the $m^{\underline{th}}$ blade due to all outboard external forces and moments
i	imaginary number, $\sqrt{-1}$
$\bar{I}_{dG}, \bar{J}_{dG}, \bar{K}_{dG}$	orthogonal unit vectors for gyroscope in a perturbed system
$\bar{I}_f, \bar{J}_f, \bar{K}_f$	orthogonal unit vectors for the fixed; shaft, swashplate, and gyroscope systems
$\hat{I}_G$	inertia dyadic of the gyroscope
$\bar{I}_r, \bar{J}_r, \bar{K}_r$	orthogonal unit vectors for the rotating; shaft, swashplate, and gyroscope systems
$\bar{I}_{rb}^{(i)}, \bar{J}_{rb}^{(i)}, \bar{K}_{rb}^{(i)}$	orthogonal unit vectors in local blade coordinate system at the $i^{\underline{th}}$ station

I_{Gx} lateral moment of inertia of gyroscope, $kg\text{-}m^2$

I_{Gy} longitudinal moment of inertia of gyroscope, $kg\text{-}m^2$

I_{Gz} polar moment of inertia of gyroscope, $kg\text{-}m^2$

$I_x^{(i)}$ polar mass moment of inertia of a section about the neutral axis, $kg\text{-}m^2$

$I_y^{(i)}$ flapwise mass moment of inertia of a section, $kg\text{-}m^2$

$I_z^{(i)}$ edgewise mass moment of inertia of a section, $kg\text{-}m^2$

K stiffness of collective spring-damper unit supporting swashplate or gyroscope, N/m

$\overline{K}$ average cyclic stiffness of the gyroscope, N-m/rad

K' lateral minus longitudinal cyclic stiffness divided by 2, N-m/rad

K_b^a variable to reduce equation length as defined after Equations (17) and (18)

$K_{b,k}$ variable to reduce equation length as defined after Equation (157)

$\overline{KC}_a$ variable to reduce equation length as defined after Equation (67)

$\overline{KC}_{\theta_a}$ variable to reduce equation length as defined after Equation (69)

$\overline{KC}_{\phi_a}$ variable to reduce equation length as defined after Equation (69)

k_{GX} lateral angular spring stiffness of gyroscope support, N-m/rad

k_{GY} longitudinal angular spring stiffness of gyroscope support, N-m/rad

k_j stiffness of $j^{\underline{th}}$ cyclic spring-damper unit supporting swashplate or gyroscope, N/m

k_{θ_j} lateral angular spring stiffness of $j^{\underline{th}}$ swashplate or gyroscope support, N-m/rad

k_{θ_j} longitudinal angular spring stiffness of $j^{\underline{th}}$ swashplate or gyroscope support, N-m/rad

k_m stiffness of the control rod attaching the $m^{\underline{th}}$ blade to the swashplate or gyroscope,N/m

k_x stiffness of torsion spring, N-m/rad

k_y stiffness of flapwise moment spring, N-m/rad

k_z stiffness of chordwise moment spring, N-m/rad

$L^{(i)}$ length of the aerodynamic field for the $i^{\underline{th}}$ section if it has aerodynamics,m

$\ell^{(i)}$ length of massless elastic section, m

$L_k^{(i)}$ lift acting on the $i^{\underline{th}}$ section for azimuthal location denoted by k if aerodynamic section, N

L_t operator indicating Laplace transform with respect to time t

m mass of swashplate, kg

$m^{(i)}$ blade section mass, kg

$\bar{M}_b$ moment acting on gyroscope from blade, N-m

M_G	Mass of gyroscope, kg
M_y, M_z, T	flapwise bending moment, edgewise bending moment and pitching moment in a rotor blade, N-m
$(M_z)_\ell$	azimuthal harmonic of bending moment in swashplate, N-m
M_z^{sp}	bending moment in swashplate, N-m
N_b	number of rotor blades
$N_{c.t.}, N_{fea}, N_{flap}$	blade station immediately inboard of which the rocker arm, pitch bearings, and flap hinge occurs, respectively
$N_{e.s.}$	number of concentrated supports below swashplate or gyroscope
N_f	maximum number of harmonics included for interharmonic coupling
N_{ff}	maximum number of blade loading harmonics to be used
N_{max}	highest azimuthal harmonic of swashplate deformation accounted for
N_p, NP	harmonic response of interest
NS	number of stations or segments into which a blade is divided
$P^{(i)}$	centrifugal force components acting in the local spanwise direction, N
$P_m(t), \bar{P}_m(s)$	real time and Laplace transformed counterpart of force in control rod of the m^{th} blade, N
$\{\bar{P}_n\}_m$	column of blade tip unknowns and blade discontinuities
P_ℓ	variable involving swashplate stiffnesses defined to reduce size of equations

$Q(\theta,t)$	distribution of forces acting on swashplate in a downward sense, N/m
$Q_\ell(t)$	$\ell^{\underline{th}}$ fourier harmonic of the loading $Q(\theta,t)$, N/m
$\{\bar{q}_n\}^*$	column containing dependent variables of all blades plus swashplate or gyroscope
R	blade radius from axis of rotation, m
$\bar{r}_m$	position vector of blade attachment point to the gyroscope
$[R]_m^{(i)}, [\bar{R}]_m^{(i)}$	real time and Laplace transformed blade transfer matrix associated with a rigid massless segment-may be used for an offset in neutral axis
$\{\bar{r}_n\}$	column containing harmonics of swashplate deflection or rigid body response of gyroscope
$R_{Np}^{(i)}$	amplitude of a Np/rev variable of interest at the $i^{\underline{th}}$ section
R_p	radius of gyroscope, m
R_{sp}	radius of swashplate, m
$[r_3], [r_4], [r_{11}]$	row vectors having 12 elements, all of which are zero except for a value of unity in the third, fourth, and eleventh positions, respectively
s	complex number which is the Laplace transform variable corresponding to time t, rad/sec
S_a	variable to reduce equation size defined following Equation (37)
$[\bar{S}_{k,n}]$	portion of the final set of rotor and swashplate equation coefficients associated with the swashplate impedance, defined by Equation (147)

$\{S_n\}_m^{(i)}, \{\bar{S}_n\}_m^{(i)}$	real time and Laplace transformed version of the state vector at station i of the $m^{\underline{th}}$ blade, subscript n meaning the Laplace transform variable s is replaced by s-inΩ,- added to superscript denotes vector at inboard end of section where + denotes outboard
$\{\bar{S}_n\}_m^{(Tip)}$	Laplace transformed state vector for n shift and $m^{\underline{th}}$ blade consisting of all twelve state variables
$\{\bar{S}_n\}_m^{*(Tip)}$	Laplace transformed modified state vector for n shift and $m^{\underline{th}}$ blade consisting of six non-zero tip state variables
$[SK]_m^{(i)}, [\bar{SK}]_m^{(i)}$	real time and Laplace transformed version of blade transfer matrix associated with concentrated spring-damper unit (lead-lag spring-damper unit)
t	time, sec
$[\bar{T}_{k,n}]$	contains coefficients for final set of equations governing swashplate or gyroscope response, blade tip unknowns and blade discontinuities, defined by Equation (146)
T_ℓ	azimuthal harmonic of swashplate torque, N-m
T^{sp}	torque in the swashplate, N-m
$u_o(t), \bar{u}_o(s)$	real time and Laplace transformed displacement downward of swashplate base, m
u_x, u_y, u_z	perturbation deflections of blade neutral axis in radial, edgewise, and flapwise senses, respectively, m
$v^{(i)}$	induced velocity at $i^{\underline{th}}$ section if uniform azimuthally, m/sec

$v(\theta,t)$	displacement downward of swashplate as a function of azimuth and time (referred to fixed frame), m
v_{ij}	induced downwash (inflow) velocity at the $i^{\underline{th}}$ blade section and $j^{\underline{th}}$ azimuthal station, m/sec
$V_k^{(i)}$	freestream velocity at the $i^{\underline{th}}$ section and $k^{\underline{th}}$ azimuthal location, m/sec
$v_\ell(t)$	azimuthal harmonic of $v(\theta,t)$
V_y, V_z, N	edgewise shear force, flapwise shear force, and radial force in blade, respectively, N
$(V_y)_\ell$	azimuthal harmonic of V_y^{sp}, N
V_y^{sp}	transverse shear force in swashplate, N
$V_y(\psi_k)^{(i)}$, $V_z(\psi_k)^{(i)}$	chordwise and flapwise shear forces acting at inboard end of section (i) at the azimuthal position ψ_k, N
$\overline{V}_z^{(i)}, N_p$	Np/rev harmonic of the flapwise shear force at the inboard end of section (i), N
$V_z^{(i)-}(t)$	real-time flapwise shear force at inboard end of section (i), N
$\overline{VG}_n^\ell$	gyroscope impedances associated with asymmetry of support configuration
V_o	forward speed of helicopter, m/sec
$w(\phi,t)$	displacement of swashplate as a function of azimuth and time (referred to rotating frame), m
$w_\ell(t), \overline{w}_\ell(s)$	azimuthal harmonic of $w(\phi,t)$, real-time and Laplace transformed versions for swashplate, respectively

$w'_\ell(t), \bar{w}'_\ell(s)$	azimuthal harmonic of $w(\phi,t,)$, real time and Laplace transformed version for gyroscope, respectively
x_f, y_f, x_f	rectangular Cartesian coordinate nonrotating shaft system
x_{dG}, y_{dG}, z_{dG}	perturbed gyroscope coordinate system
x_r, y_r, z_r	rectangular Cartesian coordinate system rotating about z_r axis at Ω radians/second
x_{rb}, y_{rb}, z_{rb}	local right-handed coordinate system attached to blade, Y_{rb} directed along chord, z_{rb} normal to blade
$\bar{X}^{k,n}_{q,\ell}$	swashplate impedances associated with asymmetry of support configuration
$\overline{XG}^{k,n}_{q,\ell}$	gyroscope impedances associated with asymmetry of support configuration
$\bar{Y}^k_m$	complex function characterizing rocker arm length and control rod retardation time
$\bar{Z}^\ell_n$	swashplate impedances associated with symmetric properties of swashplate and its support configuration
$\overline{ZG}^\ell_n$	gyroscope impedances associated with symmetry of support configuration
$\alpha_k^{(i)}$	total blade section angle of attack at the $i^{\underline{th}}$ section and $k^{\underline{th}}$ azimuthal position, rad
$[\alpha]$	boundary condition array on blade root displacements and slopes
α_{co}	amplitude of cyclic input, rad
α_{ls}	lateral cyclic angle, rad
α_{lc}	longitudinal cyclic angle, rad

α_s	shaft tilt angle, rad ($\pi/2$ for hover)
β	cyclic phase angle, $\tan^{-1}(\frac{\alpha_{1c}}{-\alpha_{1s}})$, rad
$\beta(\theta,t)$	applied torque per unit length acting on ring, N-m/m
$\beta_\ell(t)$	Fourier harmonic of $\beta(\theta,t)$, N-m/m
$\beta_{Np}^{(i)}$	phase angle of state variable as shown in Equation (167), rad
Γ	nondimensionalized circulation
$\Gamma_k^{(i)}$	circulation at the $i^{\underline{th}}$ section and $k^{\underline{th}}$ azimuthal position, m/sec
δ_j^i	kronecker delta, equals unity if i=j, equals zero if $i \neq j$
$\delta(\ )$	Delta function
$\{\bar{\Delta}\}_m^{c.t.}, \{\bar{\Delta}\}_m^{fea}, \{\bar{\Delta}\}_m^{flap}$	discontinuity columns defined by Equations (91), (87) and (89), respectively
$\{\bar{\Delta}_n\}_m^{*c.t.}; \{\bar{\Delta}_n\}_m^{*fea}$ $\{\bar{\Delta}_n\}_m^{*flap}$	discontinuity single element arrays defined by Equation (95) with Laplace transform variable shifted by $-in\Omega$
$(\overline{\Delta T})_m, (\overline{\Delta\phi_x})_m, (\overline{\Delta\phi_y})_m$	discontinuities in blade torque, torsional deflection and flap angle of $m^{\underline{th}}$ blade
ε_{ry}	distance of mass center of gravity ahead of elastic axis, m
θ	azimuthal independent coordinate for swashplate unknowns referred to fixed frame of reference, rad
$\Theta(\theta,t)$	local bending slope of elastic ring representation of swashplate, rad

θ_c collective pitch, rad

$\theta_\ell(t)$ Fourier harmonic of $\theta(\theta,t)$, rad

$\{\bar{\lambda}_{k,n}\}_m^{xxx}$ initialization array with xxx superscript equal; c.t. , fea , and flap ; corresponding to control torque, feathering angle, and flap angle, respectively, as defined by Equation (96) for harmonic k and shifted by $-in\Omega$

$[\bar{\lambda}]_m^{Tip}$ 12 by 6 matrix utilized to eliminate zero value tip variables

μ mass per unit arc length of swashplate, kg/m

ρ air mass density, kg/m^3

π Pi, 3.1415927

$[\sigma]$ wake-induced velocity influence coefficient matrix

$\sigma(\theta,t)$ applied moment per unit length acting on swashplate, N-m/m

$\sigma_\ell(t)$ Fourier harmonic of $\sigma(\theta,t)$, N-m/m

τ_m damper time constant associated with spring-damper unit representation of control rod connecting $m^{\underline{th}}$ blade to swashplate, sec

Φ,Θ,Ψ finite angles defining orientation of blade surface at an arbitrary radial point, Φ corresponds to forward sweep, Θ corresponds to downward coning, Ψ corresponds to nose-up pre-twist and/or collective angle of attack, rad

ϕ azimuthal independent coordinate for swashplate motion referred to rotating frame of reference, rad

$\Phi(\theta,t)$ swashplate local twist, rad

$\Phi_\ell(t)$ Fourier harmonic of $\Phi(\theta,t)$, rad

ϕ_m	phase angle of $m^{\underline{th}}$ blade ($2\pi(m-1)/N_b$ for equally spaced blades), rad
ϕ_{mp}	perturbation on ϕ_m or blade wrap-up angle on the $m^{\underline{th}}$ blade, rad
ϕ_x, ϕ_y, ϕ_z	perturbation twist, flapwise bending slope, and edgewise bending slope respectively, rad
$\phi_{x_r}, \phi_{y_r}, \phi_{z_r}$	gyroscope perturbation variables, rad
χ_j	azimuthal angle of $j^{\underline{th}}$ spring-damper unit supporting swashplate, rad
ψ, ψ_k	blade azimuth angle, measured from downstream position plus $\pi/2$ in direction of rotation, rad
Ω	operating speed of rotor system, rad/sec
ω_o	vortex interaction frequency

Subscripts and Superscripts:

i or (i)	superscript denoting $i^{\underline{th}}$ blade station counting inboard from tip to root, has successive values from 1 to NS
j	index
ℓ, n, p, q, k	indices used for harmonic number
m	index indicating $m^{\underline{th}}$ blade
+ -	employed as superscripts to indicate the outboard and inboard ends of a blade segment or radial station, respectively
c.t., fea, flap	employed as superscripts to indicate a matrix product or state vector evaluated at the control torque, pitch bearings, and flap hinges, respectively
( )	as in (r_3) to indicate a row vector
[ ]	indicates a matrix
{ }	indicates a column vector

HELICOPTER ROTOR SYSTEM MODEL

The analysis to be presented is dependent upon the definition of the coupled helicopter rotor system model. Basically, the rotor system configuration is comprised of a rotor consisting of an arbitrary number of flexible blades, arbitrarily located azimuthally, with either a flexible swashplate or gyro control system. To provide model flexibility such that the analysis will be applicable to various rotor systems, the representation of each of these major components consists of several relevant characteristics.

The model of the blades comprising the rotor allows for the inclusion of all blade characteristics believed to be significant. For example, the blade model allows:

(a) arbitrary location of the blade elastic axis and aerodynamic center,

(b) arbitrary location of center of mass relative to blade elastic axis,

(c) arbitrary blade precone and presweep,

(d) arbitrary variable twist distribution,

(e) arbitrary mass and inertia distributions,

(f) arbitrary stiffness distributions,

(g) gyroscopic forces

(h) aerodynamic loading including damping,

(i) flapwise, chordwise, and torsional blade root restraints ranging from rigid to fully articulated and, also, blade root damping.

A lumped parameter approach to the modeling of the blades has been adopted as a suitable means of representation of the blade distributed properties.

The main component of the swashplate control system model is represented by a flexible ring consisting of two parts which is allowed to translate only along the shaft axis but may rotate about two mutually orthogonal axes perpendicular to the shaft axis. The upper portion of the ring is also allowed to rotate about the shaft axis since it is attached to blade pitch arms by control rods having both stiffness and damping characteristics. The lower portion of this ring is supported by an arbitrary number

of supports which have stiffness and damping characteristics and are attached to a ring allowed only translational motion in the shaft direction (collective motion). The support for this final ring has an arbitrary effective stiffness and damping value. This final support is necessary since the collective stiffness can be much lower than the cyclic stiffness of the control system. Thus, by variation of stiffness and damping characteristics of the supports involved any degree of anisotropic support of the swashplate control system can be obtained. Additional capabilities included in the swashplate control system model are presented in a subsequent section.

The gyro control system model considers a rigid gyroscope that is rotating about its center of gravity which is allowed to translate in the shaft axis direction. The gyroscope is supported in such a manner that arbitrary lateral, longitudinal, and collective stiffness and damping values can be associated with the support system. The gyroscope is attached to the blade pitch arms by control rods having stiffness and damping characteristics. Additional information on this control system configuration is presented in a subsequent section.

The general rotor blade coupling to a control system is shown schematically in Figure 1, for a swashplate control system. Also depicted in this figure are aerodynamic load points and their attached trailing vortices representation and the relationship between the rotating shaft coordinate system (r-subscripted) and the nonrotating or fixed shaft coordinate system (f-subscripted) which will be involved in the analysis to be presented.

GENERAL SOLUTION METHOD

In contrast to computation of blade response by use of normal modes of free vibration as generalized coordinates, the method of analysis that is used is based upon a direct inverse of a dynamic matrix. This method eliminates the need for normal mode frequency and mode shape information in determination of the dynamic response of a helicopter rotor system and also eliminates various engineering judgments such as the number and types of normal modes which must be included to yield proper results. The development of the dynamic matrix and its associated forcing function and subsequent solution by taking a direct inverse is straightforward. The basic method of solution can be easily adapted to provide coupling of a deformed free-wake to the blade motions by an iterative procedure.

The analysis for representing blade behavior in the dynamic matrix generation is accomplished by application of a transfer

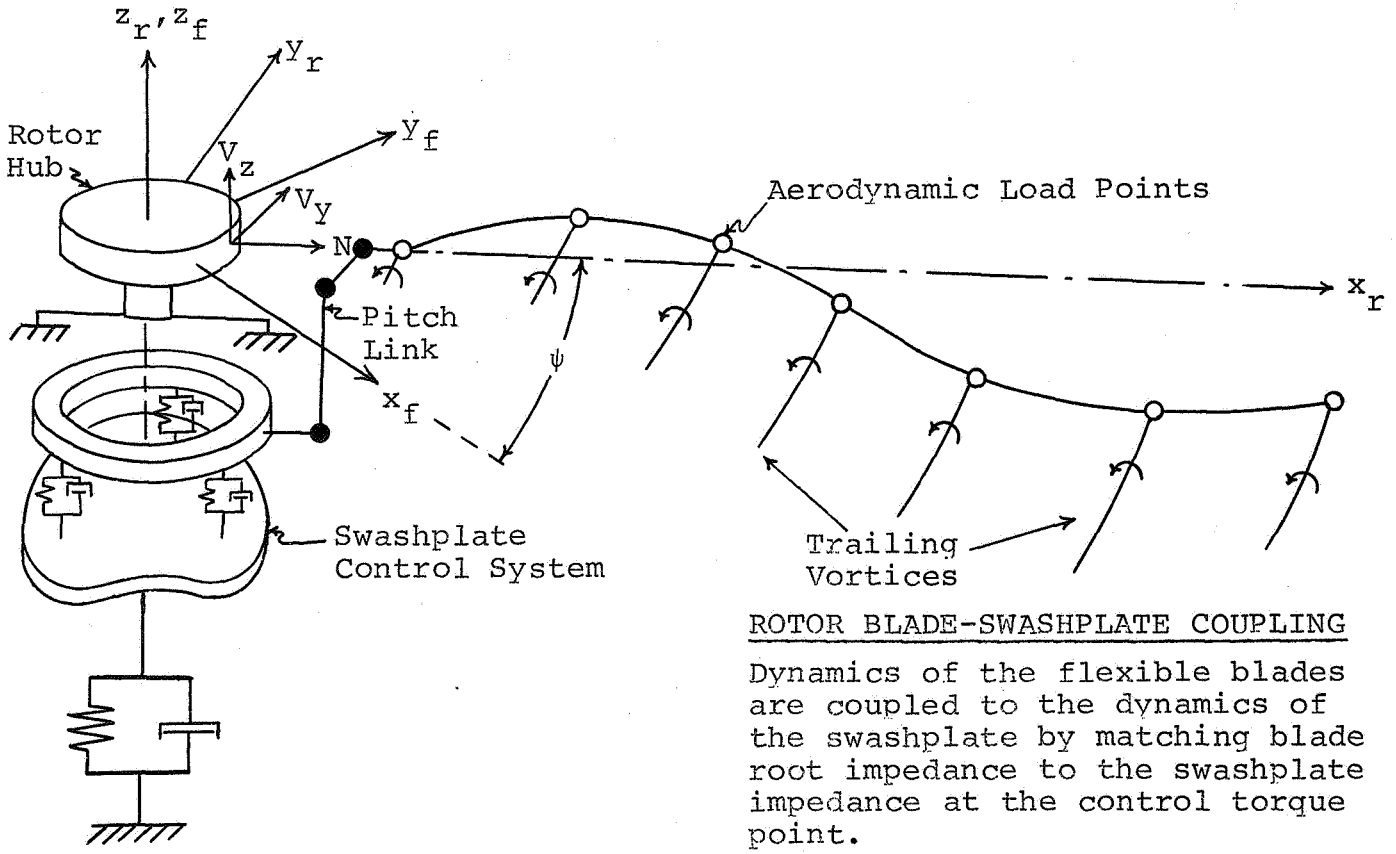

Figure 1. Coupled blade-swashplate representation

matrix approach in the lumped parameter blade model. Basically, the usual transfer matrix procedure consists of the following:

(a) a modeling procedure in which the distributed blade properties are converted to a lumped parameter form representing the blade as consisting of uniform massless elastic beam sections, in tension due to centrifugal loading with point mass, inertias, and aerodynamics located at the ends of the massless lengths,

(b) a process in which section transfer matrices associated with successive sections of a blade and relating shears, moments, slopes, and deflections at each end of the section are multiplied together to form the transfer or associated matrix for the total blade.

The transfer matrix procedure used in this analysis is a modification of that outlined above. The usual transfer matrix technique involves arrays of real numbers since the governing equations from which the transfer matrices are developed are ordinary linear differential equations with constant coefficients and have no damping or gyroscopic terms. For natural frequency prediction, the second time derivative may be replaced by the negative of the natural frequency squared. However, for an n-bladed rotor system which is subject to aerodynamic, gyroscopic, and damping forces, the governing differential equations have periodically varying coefficients such that it is no longer possible to simply replace the differential operator by a natural frequency term. By applying the Laplace transform to all variables, including periodically varying coefficients and differential operators, in the real-time transfer matrices, the transfer matrices are altered to arrays of complex numbers. The process of combining the complex transfer matrices to form the associated matrix module representing the rotor blades is straightforward but differs considerably from the common transfer matrix procedure because of harmonic coupling introduced by the aerodynamic time-varying coefficients.

Application of the modified transfer matrix procedure across the blade sections from blade tip to blade root yields the definition of the shears, moments, slopes, and deflections at the blade root in terms of the corresponding unknown tip values. Boundary conditions that are used in the generation of the final blade governing equations require that the shears and moments at the blade tip be zero and that the slopes and deflections at the blade root are zero.

The anisotropically supported swashplate or gyroscope control

system is represented by analytical expressions for the control system motion obtained from application of the differential equations of continuity and equilibrium to the control system model. Since the blade and control system reference coordinate systems differ, the resulting equations of motion which include coupling to the blades thru the control rod forces are transformed to the blade reference coordinate system to provide compatibility of force application. Also, the control system equations of motion are Laplace transformed to replace differential operators with a complex number representation compatible with the blade analysis.

The control system equations and the blade equations resulting from application of blade boundary conditions are used to construct a dynamic matrix and a forcing function column. The solution for the unknown tip quantities and the control system unknowns is obtained by multiplication of the forcing column by the inverse of the dynamic matrix. From a knowledge of the blade tip unknowns the transfer matrix procedure is repeated across the blade sections to obtain the radial distributions in complex number form representing both amplitude and azimuthal phasing for shears, moments, slopes, and deflections. This method of solution obtains the blade response by harmonics of the rotational speed where the value for the Laplace transform variable determines for which harmonic the analysis is being solved. The total real-time radial and azimuthal distributions of a dynamic response variable is obtained by a proper summation of harmonic components of that variable.

A general representation of the solution method without free-wake coupling included is presented in flow chart form in Figure 2. The notation,"intermediate terms", denotes terms that are not a function of the Laplace transform variable and therefore need not be recalculated for different harmonics of dynamic response. Downwash velocities may be taken as uniform, radially varying, or both radial and azimuthally varying in this solution form in which the blade response includes downwash velocity effects on the aerodynamic terms but coupling of the free-wake and blade motion is not allowed.

Deformed free-wake effects on the helicopter rotor system dynamic response are included in the analysis by modifying the solution method to include an iterative procedure which couples the free-wake to the blade motions. The iterative procedure developed requires the execution of a free-wake analysis program (wake geometry program) developed for reference 1 but a similar free-wake analysis program could be substituted if it provides the necessary information. The wake geometry program with flapping and cyclic blade positions defined from either an airloads

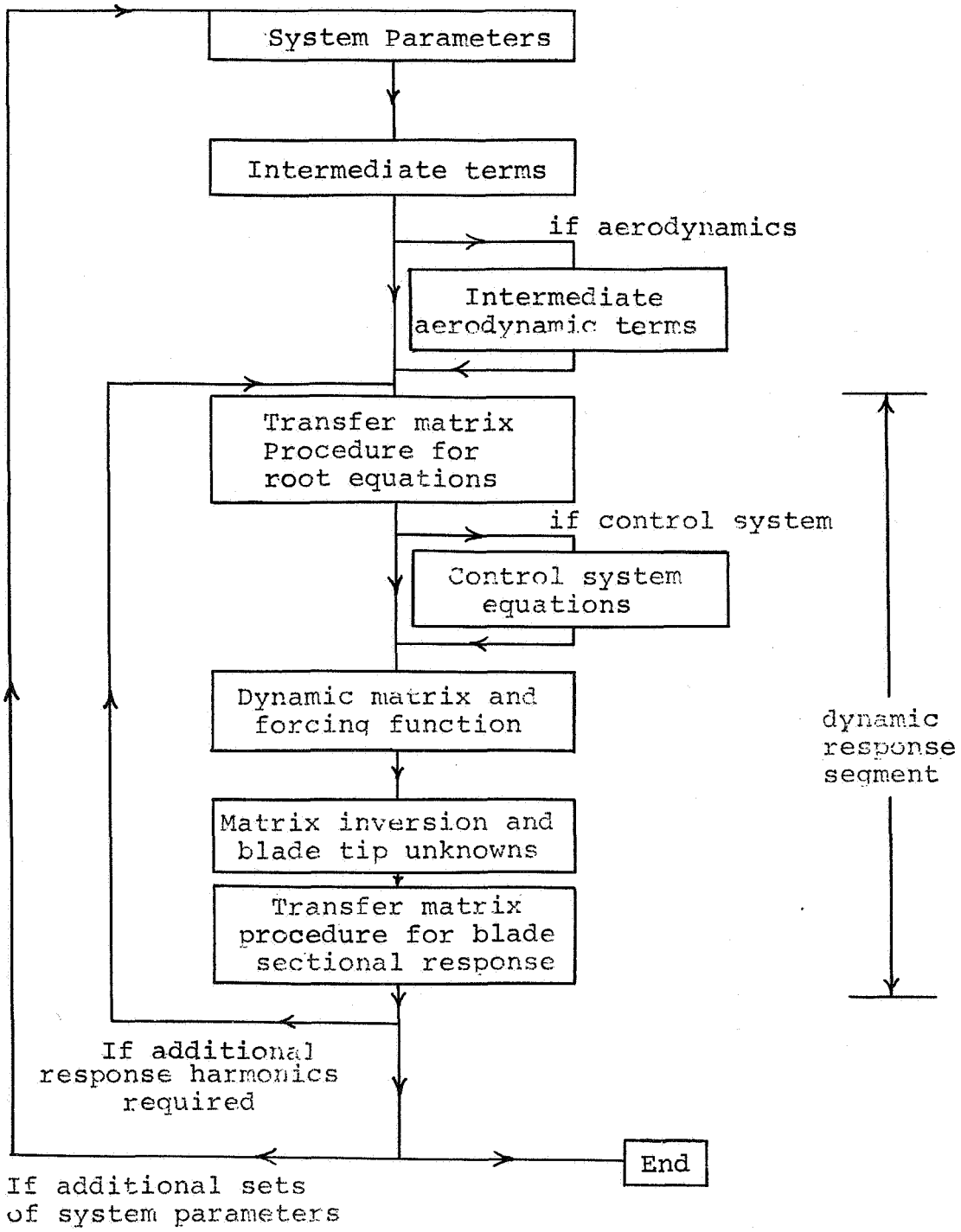

Figure 2. Solution method without free-wake coupling

calculation or experimental values uses a real-time analysis to generate a fully deformed free-wake corresponding to the blade positions. In addition, the wake-induced velocity influence coefficient matrix, $[\sigma]$, and the nondimensionalized bound circulation distribution, $\{\Gamma\}$, are determined and available for use in the dynamic response iteration procedure.

The σ's and Γ's from the wake geometry program are used to determine the initial wake-induced velocity (downwash) at the blade radial and azimuthal loading points (i. e. $[\sigma]\ \{\Gamma\} \propto \{v\}$). This initial downwash distribution is introduced into the aerodynamics analysis in which associated angles of attack and resultant velocities are used to determine the harmonics of blade aerodynamic loadings. With these loadings, the harmonics of dynamic response including control system effects from steady response up to the highest harmonic of response to be included in the wake iteration procedure are determined. But the dynamic response of the system includes blade motions which alter blade aerodynamic loading. From consideration of the total shear responses acting on both sides of the blade aerodynamic load points, radially and azimuthally located, a lift distribution can be obtained which provides a new bound circulation distribution, $\{\Gamma\}$. A new downwash distribution is obtained by use of the initial wake-induced velocity coefficient matrix and the new $\{\Gamma\}$. This new set of downwash values which includes coupling of the free-wake to the blade motions is then inserted into the aerodynamics analysis and the procedure repeated.

The procedure involved from one set of downwash values to the obtaining of a modified set of downwash values (an iteration) can be repeated until a specified maximum number of iterations between blade circulations and blade motions are performed or the values of blade circulations for successive iterations agree to within a certain specified value (convergence criteria). When either of these conditions occur, the harmonic content, in complex form, of the blade moments, shears, slopes, and deflections along the blade and of the swashplate motion can be obtained.

A general representation of the solution method with free-wake coupling to blade motions included is depicted in flow chart form in Figure 3 where the segment with the notation,"dynamic response segment", represents operations which are part of the basic solution method and is labeled on Figure 2. Aerodynamic analysis must be included in the free-wake iteration solution method.

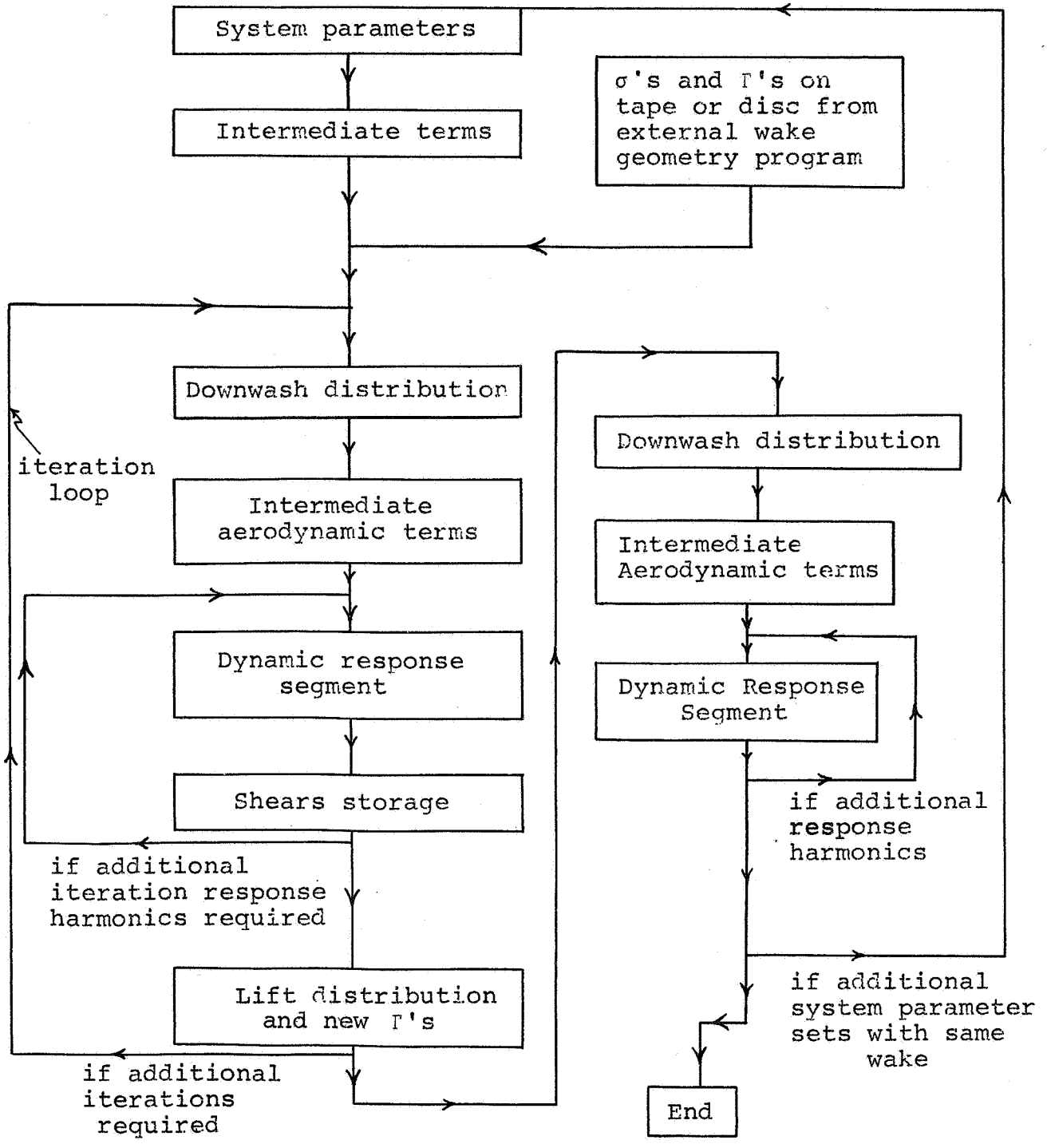

Figure 3. Solution method with free-wake coupling

ANALYSIS

Derivation of the Governing Equations for an Anisotropically Supported Gyroscope

In order to allow flexibility in the choice of control systems which may be utilized in the analysis representing a coupled helicopter rotor system, the analysis for a form of a gyroscopic control system is developed. This analysis provides the necessary representation for the gyroscope control system behavior and for the coupling which occurs between this control system and the blade behavior.

Gyroscope control system model.- The model chosen for the development of analysis representing a gyroscope control system consists of a rigid gyroscope, which may be nonsymmetrical, that is supported by a set of spring-damper units to allow anisotropic support. In addition, the gyroscope is attached to the rotor blades by flexible control rods having both stiffness and damping characteristics. The complexity of the analysis is restricted by assuming the gyroscope to be allowed only translational motion of its center of gravity in the shaft direction and rotational motion about three mutually orthogonal axes located at the center of gravity. Analysis based on these assumptions should represent the major portion of the gyroscope control system effects on the blade dynamic response behavior.

Coordinate systems involved.- A development of analysis to represent the gyroscopic control system behavior requires the definition of three mutually orthogonal coordinate systems. These three coordinate systems consist of a fixed (stationary) system, a rotating system, and a perturbation (local) gyroscope coordinate system.

The fixed gyroscope coordinate system is located in space such that the gyroscope center of gravity location in an unperturbed situation (point O) coincides with its origin as shown in Figure 4 where the fixed system unit vectors $\bar{i}_f$, $\bar{j}_f$, and $\bar{k}_f$ correspond to the x_f, y_f, and z_f axes, respectively. This fixed coordinate system has its axes oriented in the same directions as the shaft fixed coordinate system which will be used in later sections. These two fixed systems are different in that their origin locations may occur at different positions in the shaft direction.

The rotating gyroscope coordinate system has the same origin and z axis as the fixed coordinate system but its x and y axes are rotating at a rotational speed of Ω relative to the fixed system x and y axes. The rotating coordinate system axes and unit

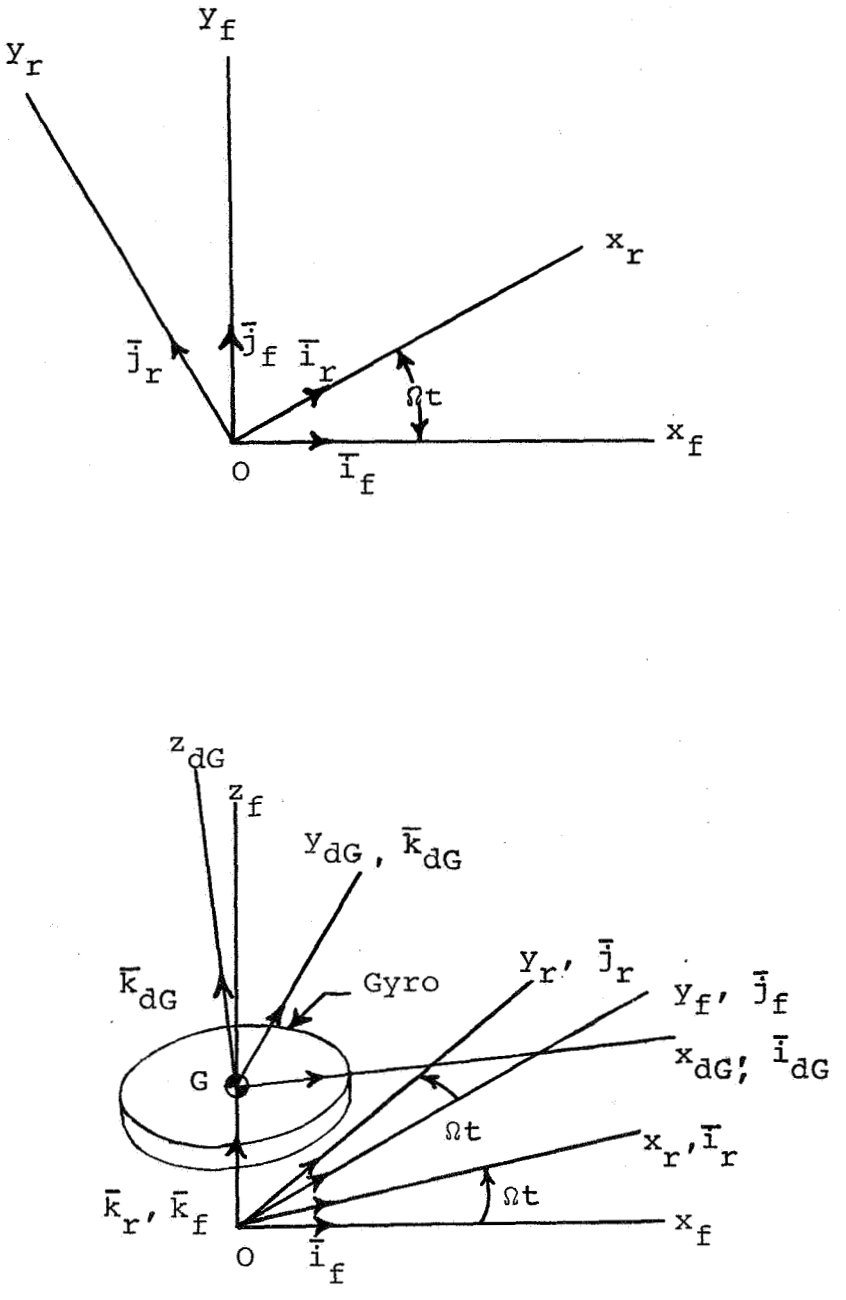

Figure 4. Coordinate systems and orientation relative to fixed coordinate system Ox_f, y_f, z_f.

vectors are denoted by r subscripts as shown in Figure 4. Also shown in Figure 4 is a top view of the coincident x-y planes of the fixed and rotating gyroscope coordinate systems from which the rotating coordinate system can be seen to be related to the fixed coordinate system by the coordinate transformation

$$\begin{Bmatrix} \bar{i}_r \\ \bar{j}_r \\ \bar{k}_r \end{Bmatrix} = \begin{bmatrix} \cos\Omega t & \sin\Omega t & 0 \\ -\sin\Omega t & \cos\Omega t & 0 \\ 0 & 0 & 1 \end{bmatrix} \begin{Bmatrix} \bar{i}_f \\ \bar{j}_f \\ \bar{k}_f \end{Bmatrix} \tag{1}$$

where t represents time and Ωt represents the instantaneous angle between the two systems. The rotating gyroscope coordinate system also exhibits the same relationship to the shaft rotating coordinate system which will be used in later sections as was noted for the fixed gyroscope system versus the fixed shaft system.

The local gyroscope coordinate system, dG subscripts, has its origin at the center of gravity of the gyroscope (point G) and translates as the gyroscope translates. The z_{dG} axis always coincides with the principal axis of inertia of the gyroscope that is perpendicular to the plane of the gyroscope. The other two mutually orthogonal axes lie in the plane of the gyroscope such that if the plane of the gyroscope is parallel to the rotating coordinate system the x and y axes of the local coordinate system would be in the same direction as the x and y axes of the rotating coordinate system. This coordinate system is presented in general concept with the other two coordinate systems in Figure 4. The orientation of the local gyroscope coordinate system (x_{dG}, y_{dG}, z_{dG}) relative to the rotating coordinate system (x_r, y_r, z_r) is obtained by performing three successive orthogonal rotations; ϕ_{z_r}, ϕ_{y_r}, and ϕ_{x_r}; on the rotating coordinate system as depicted in Figure 5. In terms of the unit vectors of the two coordinate systems and the perturbation rotations relating these coordinate systems, the relation of the local gyroscope system to the rotating gyroscope system assuming small angle approximations is expressed by the coordinate transformation

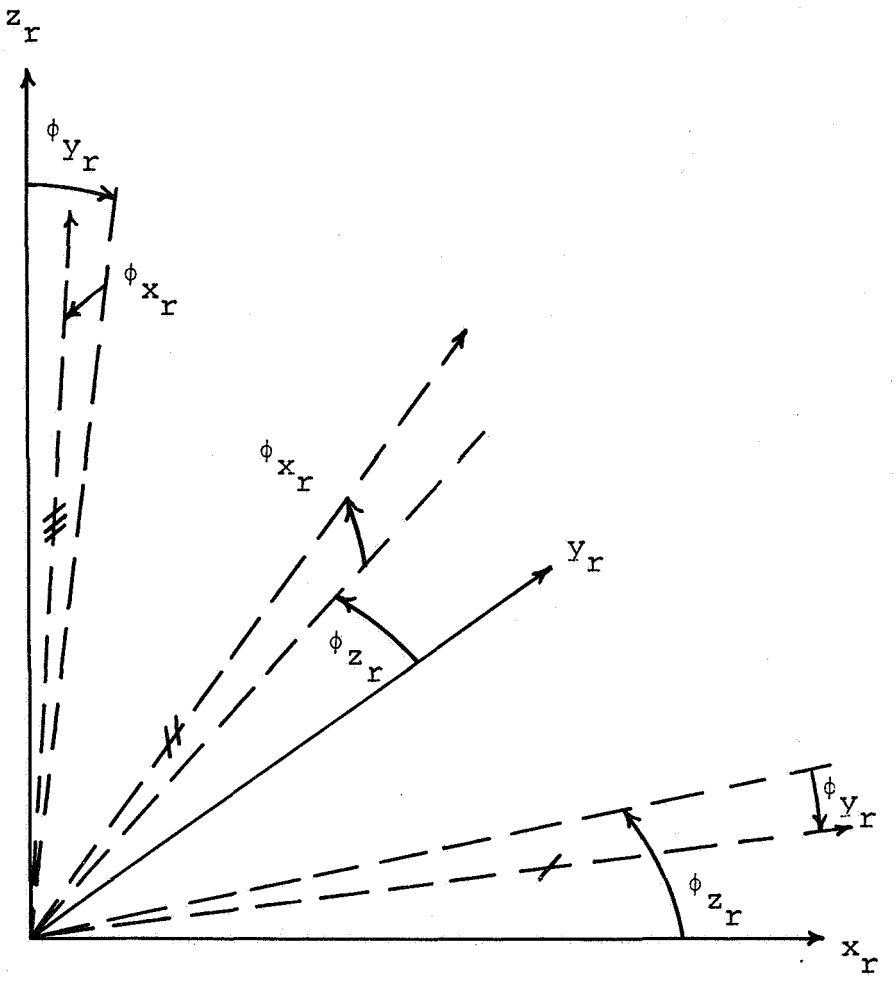

Figure 5. Gyroscope local coordinate system orientation, slash marks refer to x_{dG},y_{dG}, and z_{dG} axes, respectively

$$\begin{Bmatrix} \bar{i}_{dG} \\ \bar{j}_{dG} \\ \bar{k}_{dG} \end{Bmatrix} = \begin{bmatrix} 1 & \phi_{z_r} & -\phi_{y_r} \\ -\phi_{z_r} & 1 & \phi_{x_r} \\ \phi_{y_r} & -\phi_{x_r} & 1 \end{bmatrix} \begin{Bmatrix} \bar{i}_r \\ \bar{j}_r \\ \bar{k}_r \end{Bmatrix} . \tag{2}$$

Neglecting second order terms the inverse transformation is

$$\begin{Bmatrix} \bar{i}_r \\ \bar{j}_r \\ \bar{k}_r \end{Bmatrix} = \begin{bmatrix} 1 & -\phi_{z_r} & \phi_{y_r} \\ \phi_{z_r} & 1 & -\phi_{x_r} \\ -\phi_{y_r} & \phi_{x_r} & 1 \end{bmatrix} \begin{Bmatrix} \bar{i}_{dG} \\ \bar{j}_{dG} \\ \bar{k}_{dG} \end{Bmatrix} . \tag{3}$$

Real-time analytical derivation.- The real-time analysis for representation of the gyroscope control system requires the development of the equations of motion of the gyroscope. These equations of motion are developed considering the perturbation rotation related equations to be independent of the translational equation of motion. In regard to the analysis presented in this section; notation of the form, $\dot{a}$, is used to represent the first time derivative of the variable, a, and notation of the form, $\ddot{a}$, is used to represent the second time derivative of the variable, a. In addition, the time derivative of a vector quantity includes a contribution due to the vector product of the rotational vector and the vector of interest.

The rotational velocity (angular velocity) vector of the rotating coordinate system can be represented by

$$\bar{\Omega} = \Omega \ \bar{k}_f . \tag{4}$$

The angular velocity of the gyroscope is given by

$$\bar{\Omega}_{gyro} = \Omega\bar{k}_f + \dot{\phi}_{x_r} \bar{i}_r + \dot{\phi}_{y_r} \bar{j}_r + \dot{\phi}_{z_r} \bar{k}_r \tag{5}$$

referred to the x_r, y_r, z_r rotating coordinate system or

$$\bar{\Omega}_{gyro} = (\dot{\phi}_{x_r} - \phi_{y_r}\Omega)\bar{i}_{dG} + (\dot{\phi}_{y_r} + \phi_{x_r}\Omega)\bar{j}_{dG} + (\dot{\phi}_{z_r} + \Omega)\bar{k}_{dG} \tag{6}$$

as referred to the body local system of axes with the components being along the instantaneous direction of the axes.

The inertia dyadic of the gyroscope at its center of gravity G, referred to the axes x_{dG}, y_{dG}, z_{dG} is

$$\tilde{I}_G = I_{Gx}\,\bar{i}_{dG}\,\bar{i}_{dG} + I_{Gy}\,\bar{j}_{dG}\,\bar{j}_{dG} + I_{Gz}\,\bar{k}_{dG}\,\bar{k}_{dG} \tag{7}$$

The angular momentum vector of the gyroscope at its center of gravity (principal axes) is, from Equations (6) and (7)

$$\underline{L}_G = I_{Gx}(\dot{\phi}_{x_r} - \phi_{y_r}\Omega)\bar{i}_{dG} + I_{Gy}(\dot{\phi}_{y_r} + \phi_{x_r}\Omega)\bar{j}_{dG} + I_{Gz}(\Omega + \dot{\phi}_{z_r})\bar{k}_{dG}\ . \tag{8}$$

Referring to the x_r, y_r, z_r rotating coordinate system the angular momentum is given by

$$\begin{aligned}\underline{L}_G = {} & [I_{Gx}(\dot{\phi}_{x_r} - \phi_{y_r}\Omega) + \phi_{y_r} I_{Gz}\Omega]\bar{i}_r \\ & + [I_{Gy}(\dot{\phi}_{y_r} + \phi_{x_r}\Omega) - \phi_{x_r} I_{Gz}\Omega]\bar{j}_r \\ & + [I_{Gz}(\Omega + \dot{\phi}_{z_r})]\bar{k}_r\end{aligned} \tag{9}$$

or rearranging

$$\begin{aligned}\underline{L}_G = {} & [I_{Gx}\,\dot{\phi}_{x_r} + (I_{Gz} - I_{Gx})\Omega\phi_{y_r}]\bar{i}_r \\ & + [I_{Gy}\,\dot{\phi}_{y_r} + (I_{Gy} - I_{Gz})\Omega\phi_{x_r}]\bar{j}_r \\ & + [I_{Gz}(\Omega + \dot{\phi}_{z_r})]\bar{k}_r\ .\end{aligned} \tag{10}$$

Then, it follows that

$$\dot{\underline{L}}_G = [I_{Gx}\ddot{\phi}_{x_r} + (I_{Gz} - I_{Gx} - I_{Gy})\Omega\dot{\phi}_{y_r} - (I_{Gy} - I_{Gz})\Omega^2\phi_{x_r}]\bar{i}_r$$

$$+ [I_{Gy}\ddot{\phi}_{y_r} + (I_{Gy} - I_{Gz} + I_{Gx})\Omega\dot{\phi}_{x_r} + (I_{Gz} - I_{Gx})\Omega^2\phi_{y_r}]\bar{j}_r$$

$$+ [I_{Gz}\ddot{\phi}_{z_r}]\bar{k}_r \ . \tag{11}$$

The moment acting on the gyroscope from the support system is

$$\bar{M}_s = -(\phi_{x_r}\ \phi_{y_r})\begin{bmatrix} \bar{K} + K'\cos 2\Omega t & -K'\sin 2\Omega t \\ -K'\sin 2\Omega t & \bar{K} - K'\cos 2\Omega t \end{bmatrix}\begin{Bmatrix} \bar{i}_r \\ \bar{j}_r \end{Bmatrix}$$

$$-(\dot{\phi}_{x_r}\ \dot{\phi}_{y_r})\begin{bmatrix} \bar{C} + C'\cos 2\Omega t & -C'\sin 2\Omega t \\ -C'\sin 2\Omega t & \bar{C} - C'\cos 2\Omega t \end{bmatrix}\begin{Bmatrix} \bar{i}_r \\ \bar{j}_r \end{Bmatrix}$$

$$+\Omega(\phi_{x_r}\ \phi_{y_r})\begin{bmatrix} C'\sin 2\Omega t & -\bar{C} + C'\cos 2\Omega t \\ \bar{C} + C'\cos 2\Omega t & -C'\sin 2\Omega t \end{bmatrix}\begin{Bmatrix} \bar{i}_r \\ \bar{j}_r \end{Bmatrix} \tag{12}$$

where $\bar{K} = \frac{K_{Gx}+K_{Gy}}{2}$, $K' = \frac{K_{Gx}-K_{Gy}}{2}$, $\bar{C} = \frac{C_{Gx}+C_{Gy}}{2}$, $C' = \frac{C_{Gx}-C_{Gy}}{2}$,

with K_{Gx}, K_{Gy} being the lateral and longitudinal stiffnesses of the gyroscope support system and C_{Gx}, C_{Gy} being the lateral and longitudinal damping coefficients of the gyroscope support system.

The moment acting from the blade on the gyroscope is

$$\bar{M}_b = -\sum_{m=1}^{N_b} \bar{r}_m \times P_m(t)\bar{k}_r \tag{13}$$

or replacing $\bar{r}_m$ with its equivalent

$$\bar{M}_b = R_p \sum_{m=1}^{N_b} P_m(t) \left[\cos(\phi_m - \phi_{mp})\bar{j}_r - \sin(\phi_m - \phi_{mp})\bar{i}_r\right] \qquad (14)$$

where N_b is the number of blades,

$P_m(t)$ is the force in the $m^{\underline{th}}$ control rod,

R_p is the radius of the gyroscope,

ϕ_m is the starting azimuthal position of each blade, and

ϕ_{mp} is the perturbation on ϕ_m (blade wrap-up angle).

The governing equation of motion of the gyroscope for rotations is

$$\dot{\underline{L}}_G = \bar{M}_s + \bar{M}_b \ . \qquad (15)$$

The governing equation of motion of the gyroscope for vertical translation is

$$M_G \frac{d^2 z_r}{dt^2} + C_G \frac{dz_r}{dt} + K z_r = - \sum_{m=1}^{N_b} P_m(t) \qquad (16)$$

where M_G is the mass of the gyroscope,

K is the collective stiffness, and

C_G is the collective damping.

The final real-time equation of motion of the gyroscope rotations is obtained in vector form by insertion of Equations (11), (12), and (14) into Equation (15) and replacing the $\sin(2\Omega t)$ and $\cos(2\Omega t)$ by their exponential equivalents. Since Equation (15) must hold on a vector component basis, two expressions are obtained by considering only the terms multiplying the $\bar{i}_r$ and $\bar{j}_r$, independently. The resulting real-time equations of motion for gyroscope rotations are

$$\left[I_{Gx} \frac{d^2}{dt^2} + \Omega^2 (I_{Gz} - I_{Gy}) + K_1^1 + K_{-1}^{-1} + \bar{K} + \bar{C} \frac{d}{dt}\right] \phi_{x_r}$$

$$+ \left[\Omega (I_{Gz} - I_{Gx} - I_{Gy}) \frac{d}{dt} + iK_1^1 - iK_{-1}^{-1} - \Omega \bar{C} \right] \phi_{y_r}$$

$$= - R_p \sum_{m=1}^{N_b} P_m(t) \sin(\phi_m - \phi_{mp}) \qquad (\bar{i}_r \text{ terms}) \tag{17}$$

$$\left[- \Omega (I_{Gz} - I_{Gy} - I_{Gx}) \frac{d}{dt} + iK_1^1 - iK_{-1}^{-1} + \Omega \bar{C} \right] \phi_{x_r}$$

$$+ \left[I_{Gy} \frac{d^2}{dt^2} + \Omega^2 (I_{Gz} - I_{Gx}) - K_1^1 - K_{-1}^{-1} + \bar{K} + \bar{C} \frac{d}{dt} \right] \phi_{y_r}$$

$$= R_p \sum_{m=1}^{N_b} P_m(t) \cos(\phi_m - \phi_{mp}) \qquad (\bar{j}_r \text{ terms}) \tag{18}$$

where for convenience

$$K_b^a = e^{2ai\Omega t} (K' + b\Omega C'i + C' \frac{d}{dt})/2 \quad .$$

The final real-time governing equation of motion for gyroscope translation is obtained by rewriting Equation (16) in the form

$$(M_G \frac{d^2}{dt^2} + C_G \frac{d}{dt} + K) z_r = - \sum_{m=1}^{N_b} P_m(t) \quad . \tag{19}$$

Application of Laplace transforms.- The final real-time gyroscope governing equations are Laplace transformed to eliminate the derivative type of representation and replace it with an algebraic form in addition to providing compatibility with the blade equations which will be developed. In taking the Laplace transforms of the governing equations of motion quiescent boundary conditions are assumed and the following Laplace transformations required:

(a) $L_t [F(t)] = \bar{F}(s)$,

(b) $L_t [\dot{F}(t)] = s \bar{F}(s)$,

(c) $L_t [\ddot{F}(t)] = s^2 \bar{F}(s)$

$$(d)\ L_t\left[e^{iat}\,F(t)\right] = \bar{F}(s-ia)$$

$$(e)\ L_t\left[e^{iat}\,\dot{F}(t)\right] = (s-ia)\,\bar{F}(s-ia)$$

where F(t) is a function of time. With these definitions, the Laplace transformed versions of the necessary equations can be obtained.

The Laplace transformed versions of Equations (17), (19), and (18) are

$$\begin{aligned}
&[I_{Gx}\,s^2 + \Omega^2(I_{Gz} - I_{Gy}) + \bar{K} + \bar{C}\,s]\,\bar{\phi}_{x_r}(s) + K_1\,\bar{\phi}_{x_r}(s + 2i\Omega) \\
&\quad + K_{-1}\,\bar{\phi}_{x_r}(s - 2i\Omega) + [\Omega(I_{Gz} - I_{Gx} - I_{Gy})\,s - \Omega\,\bar{C}]\,\bar{\phi}_{y_r}(s) \\
&\quad - iK_1\,\bar{\phi}_{y_r}(s + 2i\Omega) + iK_{-1}\,\bar{\phi}_{y_r}(s - 2i\Omega) \\
&\quad = -R_p \sum_{m=1}^{N_b} \bar{P}_m(s)\,\sin(\phi_m - \phi_{mp})
\end{aligned} \tag{20}$$

$$M_G\,s^2\,\bar{z}(s) + C_G\,s\,\bar{z}(s) + K\,\bar{z}(s) = -\sum_{m=1}^{N_b} \bar{P}_m(s) \tag{21}$$

$$\begin{aligned}
&[-\Omega(I_{Gz} - I_{Gy} - I_{Gx})\,s + \Omega\bar{C}]\,\bar{\phi}_{x_r}(s) - iK_1\,\bar{\phi}_{x_r}(s + 2i\Omega) \\
&\quad + iK_{-1}\,\bar{\phi}_{x_r}(s - 2i\Omega) + [I_{Gy}\,s^2 + \Omega^2(I_{Gz} - I_{Gx}) + \bar{K} + \bar{C}\,s]\,\bar{\phi}_{y_r}(s) \\
&\quad - K_1\,\bar{\phi}_{y_r}(s + 2i\Omega) - K_{-1}\,\bar{\phi}_{y_r}(s - 2i\Omega) \\
&\quad = R_p \sum_{m=1}^{N_b} \bar{P}_m(s)\,\cos(\phi_m - \phi_{mp})
\end{aligned} \tag{22}$$

where for convenience

$$K_b = (K' + b\Omega C'i + C's)/2$$

The control rod forces $\bar{P}_m(s)$ couple the rotor blade motions to the gyroscope motions. The relations expressed by Equations (20), (21), and (22) are the objective of this section and will be used in a later section of this report.

Derivation of the Governing Equations for an Anisotropically Supported Swashplate

The form of control system utilized in the majority of helicopter rotor systems is of a swashplate type. In this section the analysis for a general form of swashplate control system is developed. This analysis provides the necessary representation for the swashplate control system behavior and for the coupling which occurs between this control system and the blade behavior.

Swashplate control system model.- Even though the basic swashplate model has been previously described there exist additional model capabilities. The general swashplate control system model as shown in Figure 6 consists of:

(1) a flexible ring having uniform mass consisting of two parts which are allowed to translate only along the shaft axis but may rotate about the mutually orthogonal axes perpendicular to the shaft axis and where the upper portion is also rotating about the shaft axis,

(2) a set of supports which have stiffness and damping characteristics which allow anisotropic supporting of the flexible ring and which may be attached to the ring an offset distance from the ring radius,

(3) a single collective support which has stiffness and damping characteristics in series with the previous group,

(4) control rods with stiffness and damping characteristics connecting the blades to the flexible ring and which may be attached to the ring an offset distance from the ring radius,

(5) a collective base plate which is allowed to only translate in the shaft axis direction, and

(6) torsional spring-damper units which counteract the local bending slope and twist of the ring at each azimuthal location of the supports of (2) (shown on Figure 6 at

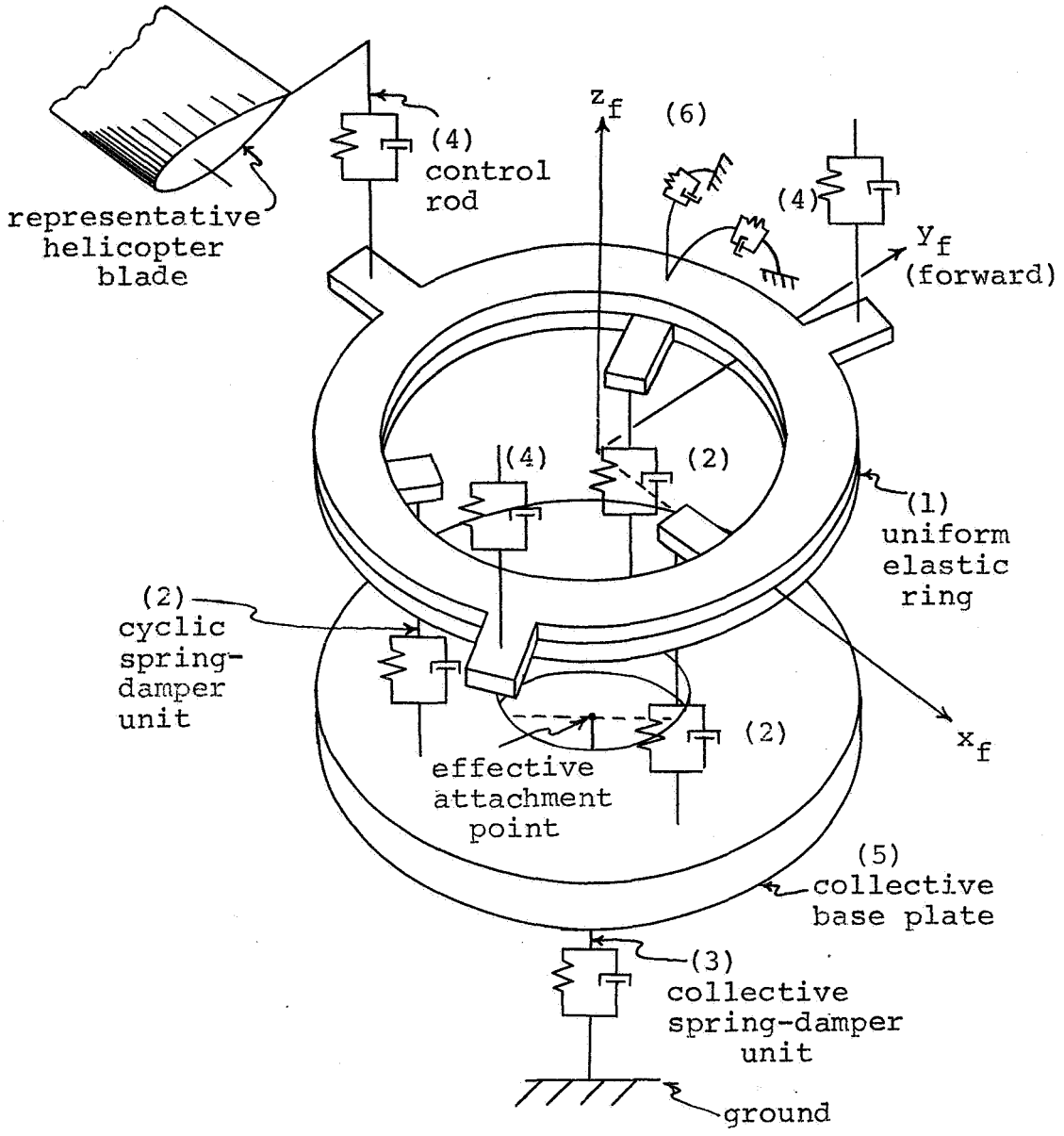

Figure 6. Swashplate system model

only one location).

Due to the generality of the configuration various swashplate systems can be represented by choice of the parameters used in the swashplate control system analysis.

Coordinate systems involved.- Two mutually orthogonal coordinate systems are utilized in the development of the analysis representing the swashplate behavior. The first coordinate system is a fixed (non-rotating) coordinate system whose orientation in space is identical to the shaft (hub) and gyroscope fixed coordinate system. However, the origins of these three fixed coordinate systems may be at different positions on the shaft axis (shaft centerline). In these systems; the y-axis is perpendicular to the shaft axis and in a direction toward the nose of the helicopter, the x-axis is perpendicular to the shaft axis and in a direction toward the helicopter's starboard side (advancing blade position), and the z-axis is coincident with the shaft axis. The swashplate fixed coordinate system has been included in Figure 6.

The second swashplate coordinate system is a rotating coordinate system whose origin and z-axis coincide with the swashplate fixed coordinate system but is rotating at a rotational speed, Ω, such that the same relationship between the rotating and fixed swashplate coordinate systems exists as was depicted for the gyroscope coordinate systems in Figure 4. The swashplate, gyroscope, and shaft rotating coordinate systems all have the same orientation as a function of time.

Real-time analytical derivation.- The governing equations of motion of an elastic ring in terms of variables which are defined relative to the fixed swashplate coordinate system are used to obtain a governing differential equation for deflection behavior of the swashplate relative to the swashplate rotating coordinate system. The final form of the governing equation can not be obtained without the use of Laplace transformations.

Fixed-frame governing equations involving loading functions: The governing differential equations for motion of an elastic ring involving variables which are a function of θ, the azimuthal location of a point of interest on the ring relative to the x_f-axis, and time, t, consist of the equilibrium, stress-strain, and strain-displacement equations:

$$\frac{1}{R_{sp}} \frac{\partial (V_y^{sp})}{\partial \theta} = \mu \frac{\partial^2 v(\theta,t)}{\partial t^2} - Q(\theta,t) \qquad (23)$$

$$\frac{1}{R_{sp}} \frac{\partial (M_z^{sp})}{\partial \theta} = - V_y^{sp} - \frac{T^{sp}}{R_{sp}} - \sigma(\theta,t) \tag{24}$$

$$\frac{1}{R_{sp}} \frac{\partial (T^{sp})}{\partial \theta} = \frac{M_z^{sp}}{R_{sp}} - \beta(\theta,t) \tag{25}$$

$$\frac{1}{R_{sp}} \frac{\partial \Theta(\theta,t)}{\partial \theta} = - \frac{1}{R_{sp}} \Phi(\theta,t) + \frac{M_z^{sp}}{EJ_z} \tag{26}$$

$$\frac{1}{R_{sp}} \frac{\partial v(\theta,t)}{\partial \theta} = \Theta(\theta,t) \tag{27}$$

$$\frac{1}{R_{sp}} \frac{\partial \Phi(\theta,t)}{\partial \theta} = \frac{\Theta(\theta,t)}{R_{sp}} + \frac{T^{sp}}{GJ_t} \tag{28}$$

where V_y^{sp}, M_z^{sp}, and T^{sp} are shear force, bending moment, and torque, respectively;

$v(\theta,t)$ is the local displacement of the swashplate;

μ is the mass per unit arc length of the swashplate ring;

$\Theta(\theta,t)$ and $\Phi(\theta,t)$ are the local bending slope and twist angle of the ring;

R_{sp} is the swashplate radius;

EJ_z is the bending stiffness of the ring;

GJ_t is the torsional stiffness of the ring;

$\sigma(\theta,t)$ is the applied moment per unit length acting on the ring;

$\beta(\theta,t)$ is the applied torque per unit length acting on the ring; and

$Q(\theta,t)$ is the applied force per unit length acting on the ring.

The effects of concentrated moments or torques applied to the swashplate on the swashplate behavior are incorporated in terms appearing in Equations (24) and (25). The orientation of each of the variables used in Equation (23) through (28) are shown in Figure 7.

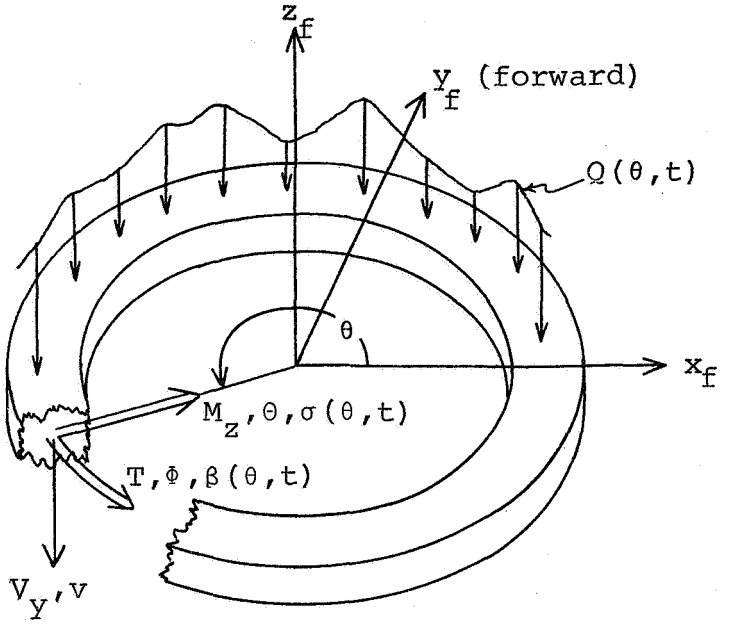

Figure 7. Coordinates of swashplate variables

The dependence of the governing swashplate partial differential equations may be removed by going to a Fourier transform. Since each of the quantities $v(\theta,t)$, $\Phi(\theta,t)$, $\theta(\theta,t)$, T^{sp}, V_y^{sp}, and M_z^{sp} are periodic with respect to θ, each of these variables satisfies relationships of the form exemplified by $v(\theta,t)$ in the two Equations, (29) and (30).

$$v(\theta,t) = \sum_{\ell=-\infty}^{\infty} v_\ell(t) e^{i\ell\theta} \tag{29}$$

$$v_\ell(t) = \frac{1}{2\pi} \int_0^{2\pi} v(\theta,t) e^{-i\ell\theta}\, d\theta \tag{30}$$

Thus, Equations (23) through (28) are multiplied by

$$e^{-i\ell\theta}\, d\theta$$

and the integration is performed over θ from 0 to 2π. After using the conditions of periodicity and the definitions exemplified by Equation (30) above, the following set of ordinary differential equations with time as the single independent variable result.

$$i\ell \frac{(V_y)_\ell}{R_{sp}} = \mu \frac{\partial^2 v_\ell(t)}{\partial t^2} - Q_\ell(t) \tag{31}$$

$$i\ell \frac{(M_z)_\ell}{R_{sp}} = -(V_y)_\ell - \frac{T_\ell}{R_{sp}} - \sigma_\ell(t) \tag{32}$$

$$i\ell \frac{T_\ell}{R_{sp}} = \frac{(M_z)_\ell}{R_{sp}} - \beta_\ell(t) \tag{33}$$

$$i\ell \frac{\Theta_\ell(t)}{R_{sp}} = -\frac{\Phi_\ell(t)}{R_{sp}} + \frac{(M_z)_\ell}{EJ_z} \tag{34}$$

$$i\ell \frac{v_\ell(t)}{R_{sp}} = \Theta_\ell(t) \tag{35}$$

$$i\ell \frac{\Phi_\ell(t)}{R_{sp}} = \frac{\Theta_\ell(t)}{R_{sp}} + \frac{T_\ell}{GJ_t} \tag{36}$$

The same set of equations are also obtainable by direct substitution of variable definitions based on the form of Equation (29) into Equations (23) through (28) and taking the equations corresponding to a specific value of ℓ.

Equations (31) through (36) can be combined to construct the following equation for $v_\ell(t)$ in terms of the applied loading variable harmonics.

$$\mu \frac{\partial^2 v_\ell(t)}{\partial t^2} + \frac{F(\ell)}{R_{sp}^3} v_\ell(t) = Q_\ell(t) - \frac{i\ell}{R_{sp}} \sigma_\ell(t) + S_\ell\, \beta_\ell(t) \tag{37}$$

where for convenience

$$F(a) = \frac{a^2 \ (a^2-1)^2}{\left(\frac{1}{GJ_t} + \frac{a^2}{EJ_z}\right) R_{sp}}$$

and

$$S_a = \frac{a^2 \ (GJ_t + EJ_z)}{(a^2 \ GJ_t + EJ_z) \ R_{sp}}$$

When $\ell = 0$ or ± 1, $F(\ell)$ and S_ℓ are zero and swashplate stiffnesses have no effect on $v_\ell(t)$ since these are rigid body degrees of freedom of the swashplate. During the manipulation of Equations (31) through (36) to obtain Equation (37), additional equations can be obtained to represent the remaining swashplate slopes, moments, and shear variables in terms of the swashplate deflection and applied loading functions. These equations are

$$(V_y)_\ell = \frac{i \ F(\ell)}{\ell \ R_{sp}^2} v_\ell(t) - \frac{i \ S_\ell \ R_{sp}}{\ell} \beta_\ell(t) - \sigma_\ell(t) \qquad (37a)$$

$$(M_z)_\ell = - \frac{\ell^2 \ (\ell^2-1)}{R_{sp}^2 \ P_\ell} v_\ell(t) + \frac{R_{sp}}{GJ_t \ P_\ell} \beta_\ell(t) \qquad (37b)$$

$$T_\ell = \frac{i\ell \ (\ell^2-1)}{R_{sp}^2 \ P_\ell} v_\ell(t) + \frac{i\ell \ R_{sp}}{EJ_t \ P} \beta_\ell(t) \qquad (37c)$$

$$\Phi_\ell(t) = S_\ell \ v_\ell(t) + \frac{R_{sp}^2}{EJ_z \ GJ_t \ P_\ell} \beta_\ell(t) \qquad (37d)$$

$$\Theta_\ell(t) = \frac{i\ell}{R_{sp}} v_\ell(t) \qquad (37e)$$

where for convenience

$$P_\ell = \left(\frac{1}{GJ_t} + \frac{\ell^2}{EJ_z}\right)$$

The variables defined by Equation (37) and Equations (37a) through (37e) and the loading functions involved in these expressions correspond to the amplitude of the $\ell^{\underline{th}}$ harmonic of the related time dependent variable at the azimuthal position on the swashplate corresponding to the x_f axis of the fixed coordinate system ($\theta = 0$). However, in order to couple the swashplate motion with the motion of the rotor blades, it is necessary to have both motions determined relative to either fixed coordinate systems or rotating coordinate systems. It has proven to be more convenient to use the swashplate deflections measured relative to a rotating reference frame corresponding to the blade rotating frame.

Governing deflection equation in rotating frame involving fixed frame loading functions: By defining

$$w(\phi,t) = v(\Omega t + \phi,t) \tag{38}$$

where Ω is the operating speed of the rotor, the quantity $w(\phi,t)$ is equal to the downward vertical displacement of the swashplate at time, t, measured at an azimuth angle, ϕ radians, in advance of the reference blade. This assumes that the reference blade makes an angle Ωt with the x-axis as shown in Figure 6.

By exercising the Fourier representation as shown in Equation (29)

$$w(\phi,t) = \sum_{\ell=-\infty}^{\infty} w_\ell(t)\ e^{i\ell\phi}$$

and

$$v(\Omega t + \phi,t) = \sum_{\ell=-\infty}^{\infty} v_\ell(t)\ e^{i\ell(\Omega t+\phi)} .$$

Substitution of these expressions into Equation (38) and taking advantage of the characteristic that the resulting equation must hold for each harmonic

$$v_\ell(t)\ e^{i\ell(\Omega t+\phi)} = w_\ell(t)\ e^{i\ell\phi}$$

or in an alternate form

$$v_\ell(t) = e^{-i\ell\Omega t}\ w_\ell(t) \tag{39}$$

where

$$w_\ell(t) = \frac{1}{2\pi}\int_0^{2\pi} w(\phi,t)\ e^{-i\ell\phi}\ d\phi . \tag{40}$$

The $w_\ell(t)$ deflections, defined at the reference blade position as it rotates, will be the dependent swashplate unknowns from this point on. Once these quantities are found, the actual swashplate displacements can be found from either of the following two equations:

rotating frame

$$w(\phi,t) = \sum_{\ell=-\infty}^{\infty} e^{i\ell\phi}\, w_\ell(t), \tag{41}$$

non-rotating frame

$$v(\theta,t) = \sum_{\ell=-\infty}^{\infty} e^{i\ell(\theta-\Omega t)}\, w_\ell(t). \tag{42}$$

Substitution of the expression for $v_\ell(t)$ as given by Equation (39) into Equation (37) and multiplying by the factor $e^{i\ell\Omega t}$ yields the governing equation for each $w_\ell(t)$ which is

$$\mu\left[\frac{\partial^2 w_\ell(t)}{\partial t^2} - 2i\ell\Omega\,\frac{\partial w_\ell(t)}{\partial t} - \ell^2\Omega^2\, w_\ell(t)\right] + \frac{F(\ell)}{R_{sp}^3}\, w_\ell(t)$$

$$= e^{i\ell\Omega t}\left[Q_\ell(t) - \frac{i\ell}{R_{sp}}\,\sigma_\ell(t) + S_\ell\,\beta_\ell(t)\right]. \tag{43}$$

Definition of applied loading function.- The harmonics of swashplate loadings required by the right hand side of this equation can be obtained in terms of the swashplate displacement, twist, bending slope and collective base deflection.

Recall that $Q_\ell(t)$ was obtained from the Fourier transform of Equation (23) so that

$$Q_\ell(t) = \frac{1}{2\pi}\int_0^{2\pi} Q(\theta,t)\, e^{-i\ell\theta}\, d\theta \tag{44}$$

and similarily from Equations (24) and (25)

$$\sigma_\ell(t) = \frac{1}{2\pi}\int_0^{2\pi} \sigma(\theta,t)\, e^{-i\ell\theta}\, d\theta \tag{45}$$

and

$$\beta_{\ell}(t) = \frac{1}{2\pi}\int_0^{2\pi} \beta(\theta,t)e^{-i\ell\theta}\, d\theta \tag{46}$$

One contribution to $Q(\theta,t)$ comes from the discrete forces due to the rotating control rods which couple the swashplate with the rotor blades. The other contribution comes from the forces in the spring-damper units shown as item (2) in Figure 6.

A Dirac delta representation of the concentrated forces, moments, and torques leads to the following expressions for $\beta(\theta,t)$, $Q(\theta,t)$ and $\sigma(\theta,t)$;

$$\beta(\theta,t = \sum_{m=1}^{N_b} P_m(t)d_m\delta(\theta - \Omega t - \phi_m + \phi_{mp})$$

$$+ \sum_{j=1}^{N_{e.s.}} \delta(\theta - \chi_j)b_j\left(k_j + c_j \frac{\partial}{\partial t}\right) d(\theta,t)$$

$$- \sum_{j=1}^{N_{e.s.}} \delta(\theta - \chi_j)\left(k_{\phi_j} + c_{\phi_j} \frac{\partial}{\partial t}\right) \Phi(\theta,t) \tag{47}$$

$$Q(\theta,t) = \sum_{m=1}^{N_b} P_m(t)\delta(\theta - \Omega t - \phi_m + \phi_{mp})$$

$$- \sum_{j=1}^{N_{e.s.}} \delta(\theta - \chi_j)\left(k_j + c_j \frac{\partial}{\partial t}\right) \quad d(\theta,t) \tag{48}$$

and

$$\sigma(\theta,t) = - \sum_{j=1}^{N_{e.s.}} \delta(\theta - \chi_j)\left(k_{\theta_j} + c_{\theta_j} \frac{\partial}{\partial t}\right) \Theta(\theta,t) \tag{49}$$

where $d(\theta,t) = v(\theta,t) - b_j\Phi(\theta,t) - u_0(t)$,

N_b is the number of blades,

$P_m(t)$ is the force in the $m^{\underline{th}}$ control rod,

d_m is the rigid offset of the $m^{\underline{th}}$ control rod attachment point from the neutral axis of the ring, positive outward,

$\phi_m = \frac{(m-1)2\pi}{N_b}$ for equal spacing between control rods,

ϕ_{mp} = blade wrap-up angle,

$N_{e.s.}$ is the number of spring-damper units directly supporting the swashplate,

χ_j is the azimuthal angle locating the $j^{\underline{th}}$ support relative to swashplate x_f- axis

b_j is the offset of the $j^{\underline{th}}$ linear spring attachment point from the neutral axis of the ring, positive inward

k_j and c_j are the linear stiffness and damping values for the $j^{\underline{th}}$ spring-damper unit,

k_{θ_j} and c_{θ_j} are the torsional stiffness and damping values the $j^{\underline{th}}$ torsional spring-damper unit counteracting local lateral swashplate rotation,

k_{ϕ_j} and c_{ϕ_j} are the torsional stiffness and damping values for the $j^{\underline{th}}$ torsional spring-damper unit counteracting local longitudinal swashplate rotation,

$u_0(t)$ is the vertical downward displacement of the base which supports the spring-damper units,

and $\delta(\theta-\theta_0)$ is defined such that

$$\int_0^{2\pi} f(\theta)\delta(\theta - \theta_0)R_{sp}\, d\theta = f(\theta_0) \qquad (50)$$

(θ_0 being an arbitrary azimuthal angle).

The variable, ϕ_m, is further defined as the azimuthal location (phase angle) of the $m^{\underline{th}}$ blade relative to the swashplate x_f-axis when t equals zero and ϕ_{mp} is taken as zero in value.

The required expressions for $\beta_\ell(t)$, $Q_\ell(t)$, and $\sigma_\ell(t)$, needed in Equation (43), are obtained by substituting the forms for $\beta(\theta,t)$, $Q(\theta,t)$, and $\sigma(\theta,t)$, as given by Equations (47), (48), and (49), into the integrand of Equations (46), (44), and (45), respectively. Taking proper care with regard to the integral of the Dirac delta functions, the Fourier transforms of $\beta(\theta,t)$, $Q(\theta,t)$, and and $\sigma(\theta,t)$ are

$$\beta_\ell(t) = \frac{1}{2\pi R_{sp}} \sum_{m=1}^{N_b} P_m(t)\, d_m\, e^{-i\ell(\Omega t + \phi_m - \phi_{mp})}$$

$$+ \frac{1}{2\pi R_{sp}} \sum_{j=1}^{N_{e.s.}} \left(k_j + c_j \frac{\partial}{\partial t}\right) b_j\, d(\chi_j,t)\, e^{-i\ell\chi_j}$$

$$- \frac{1}{2\pi R_{sp}} \sum_{j=1}^{N_{e.s.}} \left(k_{\phi_j} + c_{\phi_j} \frac{\partial}{\partial t}\right) \Phi(\chi_j,t)\, e^{-i\ell\chi_j} \qquad (51)$$

$$Q_\ell(t) = \frac{1}{2\pi R_{sp}} \sum_{m=1}^{N_b} P_m(t)\, e^{-i\ell(\Omega t + \phi_m - \phi_{mp})}$$

$$- \frac{1}{2\pi R_{sp}} \sum_{j=1}^{N_{e.s.}} \left(k_j + c_j \frac{\partial}{\partial t}\right) d(\chi_j,t)\, e^{-i\ell\chi_j} \qquad (52)$$

$$\sigma_\ell(t) = - \frac{1}{2\pi R_{sp}} \sum_{j=1}^{N_{e.s.}} \left(k_{\theta_j} + c_{\theta_j} \frac{\partial}{\partial t}\right) \Theta(\chi_j,t)\, e^{i\ell\chi_j} \qquad (53)$$

where $d(\chi_j,t) = v(\chi_j,t) - b_j\, \Phi(\chi_j,t) - u_0(t)$.

The quantities; $v(\chi_j,t)$, $\Theta(\chi_j,t)$, $\Phi(\chi_j,t)$ and $d(\chi_j,t)$; in the previous equations represent the swashplate; local deflection, local bending slope, local twist and local spring-damper unit deflection at the azimuthal location, χ_j, of the $j^{\underline{th}}$ spring-damper unit. These variables can be expressed in terms of the

Fourier harmonic components of the swashplate deflection in the rotating frame.

Replacing θ with the specific value, χ_j, and altering the dummy variable over which the summation is taken, Equation (42) becomes

$$v(\chi_j,t) = \sum_{p=-\infty}^{\infty} w_p(t)\ e^{ip(\chi_j-\Omega t)} \tag{54}$$

Using the same procedure with the form of Equation (29), $\theta(\chi_j,t)$ can be expressed as

$$\theta(\chi_j,t) = \sum_{p=-\infty}^{\infty} \theta_p(t)\ e^{ip\chi_j} \tag{55}$$

Replacing ℓ with p in Equations (39) and (37e), the equations

$$v_p(t) = e^{-ip\Omega t}\ w_p(t) \tag{56}$$

and

$$\theta_p(t) = ip\ v_p(t)\ /\ R_{sp}$$

are obtained. Substitution of Equation (56) into the last equation results in an expression for $\theta_p(t)$ which when inserted into Equation (55) yields the expression

$$\theta(\chi_j,t) = \frac{1}{R_{sp}} \sum_{p=-\infty}^{\infty} ip\ w_p(t)\ e^{ip(\chi_j- t)} \tag{57}$$

The quantity $\Phi(\chi_j,t)$ can be expressed in the same form as $\theta(\chi_j,t)$ in Equation (55), that is

$$\Phi(\chi_j,t) = \sum_{p=-\infty}^{\infty} \Phi_p(t)\ e^{ip\chi_j} \tag{58}$$

Altering the dummy variable, ℓ, to p in Equation (37d) and dropping the $\beta_p(t)$ term since its contribution, based on a comparison of the effects of the terms on $\Phi_p(t)$, is negligible results in

$$\Phi_p(t) = S_p\ v_p(t)$$

Substitution of Equation (56) into this equation yields an expression which when inserted into Equation (58) yields the expression for $\Phi(\chi_j,t)$ in the form

$$\Phi(\chi_j,t) = \sum_{p=-\infty}^{\infty} S_p \, w_p(t) \, e^{ip(\chi_j - \Omega t)} \tag{59}$$

By substituting Equations (54) and (59) into the expression for $d(\chi_j,t)$ following Equation (53), an expression for $d(\chi_j,t)$ as a function of swashplate rotating frame deflections and the collective base plate deflection can be obtained in the form

$$d(\chi_j,t) = \sum_{p=-\infty}^{\infty} \left[(1 - b_j S_p) \, w_p(t) \, e^{ip(\chi_j - \Omega t)} \right] - u_0(t) \tag{60}$$

The collective base deflection, $u_0(t)$, can be related to the deflection of the swashplate by consideration of the force equilibrium of the collective base plate which results in the expression

$$(K + C \frac{\partial}{\partial t}) \, u_0(t) = \sum_{j=1}^{N_{e.s.}} (k_j + c_j \frac{\partial}{\partial t}) \, d(\chi_j,t) \quad . \tag{61}$$

Insertion of Equation (60) into this expression provides a relationship between the base plate and swashplate deflections in the form

$$\left[(K + C \frac{\partial}{\partial t}) + \sum_{j=1}^{N_{e.s.}} (k_j + c_j \frac{\partial}{\partial t}) \right] u_0(t)$$

$$= \sum_{p=-\infty}^{\infty} \sum_{j=1}^{N_{e.s.}} (1 - b_j S_p)(k_j + c_j \frac{\partial}{\partial t}) \, w_p(t) \, e^{ip(\chi_j - \Omega t)} \tag{62}$$

which cannot be solved for $u_0(t)$ without use of Laplace transforms.

Expressions relating the swashplate loading harmonics to the swashplate deflections in the rotating reference frame and the collective base deflection can now be obtained. Insertion of Equations (57), (59), and (60), as required, into Equations (51) through (53) results in the equations

$$\beta_\ell(t) = e^{-i\ell\Omega t} \sum_{m=1}^{N_b} \frac{d_m P_m(t)}{2\pi R_{sp}} e^{-i\ell(\phi_m - \phi_{mp})}$$

$$+ \sum_{p=-\infty}^{\infty} \sum_{j=1}^{N_{e.s.}} \left[b_j (1 - b_j S_p)(k_j + c_j \frac{\partial}{\partial t}) \right.$$

$$\left. - S_p (k_{\phi_j} + c_{\phi_j} \frac{\partial}{\partial t}) \right] \frac{w_p(t)}{2\pi R_{sp}} e^{i(p\chi_j - \ell\chi_j - p\Omega t)}$$

$$- \sum_{j=1}^{N_{e.s.}} b_j (k_j + c_j \frac{\partial}{\partial t}) \frac{u_0(t)}{2\pi R_{sp}} e^{-i\ell\chi_j} \qquad (63)$$

$$Q_\ell(t) = e^{-i\ell\Omega t} \sum_{m=1}^{N_b} \frac{P_m(t)}{2\pi R_{sp}} e^{-i\ell(\phi_m - \phi_{mp})}$$

$$- \sum_{p=-\infty}^{\infty} \sum_{j=1}^{N_{e.s.}} (k_j + c_j \frac{\partial}{\partial t})(1 - b_j S_p) \frac{w_p(t)}{2\pi R_{sp}} e^{i(p\chi_j - \ell\chi_j - p\Omega t)}$$

$$+ \sum_{j=1}^{N_{e.s.}} (k_j + c_j \frac{\partial}{\partial t}) \frac{u_0(t)}{2\pi R_{sp}} e^{-i\ell\chi_j} \qquad (64)$$

$$\sigma_\ell(t) = - \sum_{p=-\infty}^{\infty} \sum_{j=1}^{N_{e.s.}} (k_{\theta_j} + c_{\theta_j} \frac{\partial}{\partial t}) \frac{ip\, w_p(t)}{2\pi R_{sp}^2} e^{i(p\chi_j - \ell\chi_j - p\Omega t)} \qquad (65)$$

Application of Laplace transforms.- The real-time swashplate governing equation is Laplace transformed to replace the derivatives involved with algebraic forms in addition to providing compatibility with the blade equations which will be developed. In addition to the specialized Laplace transformations which were presented previously pertaining to the development of analysis for representation of the gyroscope control system, two more are required for this section. These are

$$(a)\ L_t \left[e^{i\ell\Omega t} w_p(t)\ e^{-ip\Omega t} \right] = \bar{w}_p(s - i\ell\Omega + ip\Omega)$$

$$(b)\ L_t\left[e^{i\ell\Omega t}\frac{\partial}{\partial t}\left(w_p(t)\ e^{-ip\Omega t}\right)\right] = (s-i\ell\Omega)\ \bar{w}_p(s-i\ell\Omega+ip\Omega).$$

The Laplace transformed version of Equation (43) assuming quiescent initial conditions is given by

$$\left[\mu\ (s^2 - 2i\ell\Omega s - \ell^2\Omega^2) + \frac{F(\ell)}{R_{sp}^3}\right]\bar{w}_\ell(s)$$

$$= L_t\left[e^{i\ell\Omega t}\ Q_\ell(t) - e^{i\ell\Omega t}\ \frac{i\ell}{R_{sp}}\ \sigma_\ell(t) + e^{i\ell\Omega t}\ S_\ell\ \beta_\ell(t)\right]. \qquad (66)$$

The Laplace transform of each of the terms appearing on the right hand side of the above equation can be obtained.

Multiplication of Equation (63) by $e^{i\ell\Omega t}$ and application of the Laplace transformation yields the expression

$$L_t\left[e^{i\ell\Omega t}\ Q_\ell(t)\right] = \sum_{m=1}^{N_b}\frac{\bar{P}_m(s)}{2\pi\ R_{sp}}\ e^{-i\ell(\phi_m - \phi_{mp})}$$

$$- \sum_{p=-\infty}^{\infty}\sum_{j=1}^{N_{e.s.}}(1 - b_j S_p)\ \overline{KC}_\ell\ \frac{\bar{w}_p(s-i\ell\Omega+ip\Omega)}{2\pi\ R_{sp}}\ e^{-i\chi_j(\ell-p)}$$

$$+ \sum_{j=1}^{N_{e.s.}}\overline{KC}_\ell\ \frac{\bar{u}_0(s-i\ell\Omega)}{2\pi\ R_{sp}}\ e^{-i\ell\chi_j} \qquad (67)$$

where for convenience

$$\overline{KC}_a = k_j + (s-ia\Omega)\ c_j$$

It is important to realize that the derivatives involved in Equation (63) through (65) do not operate on the multiplying factor, $e^{i\ell\Omega t}$. The quantity, $\bar{w}_p(s-i\ell\Omega+ip\Omega)$, is not to be interpreted as a product but rather as a shifted argument of the function whereas the term, $(s-i\ell\Omega)\ c_j$, does represent a product of two terms.

In a similar manner as was used to obtain Equation (67), Equation (64) and (65) can be used to obtain the expressions

$$L_t\left[e^{i\ell\Omega t}\, S_\ell\, \beta_\ell(t)\right] = S_\ell \sum_{m=1}^{N_b} \frac{d_m\, \bar{P}_m(s)}{2\pi\, R_{sp}}\, e^{-i\ell(\phi_m - \phi_{mp})}$$

$$+ S_\ell \sum_{p=-\infty}^{\infty} \sum_{j=1}^{N_{e.s.}} \left[b_j\, (1 - b_j S_p)\, \overline{KC}_\ell - S_p\, \overline{KC}_{\phi_\ell} \right] \frac{\bar{w}_p(s - i\ell\Omega + ip\Omega)}{2\pi\, R_{sp}}\, e^{-i\chi_j(\ell - p)}$$

$$- S_\ell \sum_{j=1}^{N_{e.s.}} b_j\, \overline{KC}_\ell\, \frac{\bar{u}_0(s - i\ell\Omega)}{2\pi\, R_{sp}}\, e^{-i\ell\chi_j} \tag{68}$$

$$L_t\left[e^{i\ell\Omega t}\, \frac{i\ell}{R_{sp}}\, \sigma_\ell(t)\right]$$

$$= + \sum_{p=-\infty}^{\infty} \sum_{j=1}^{N_{e.s.}} \ell p\, \overline{KC}_{\theta_\ell}\, \frac{\bar{w}_p(s - i\ell\Omega + ip\Omega)}{2\pi\, R_{sp}^3}\, e^{-i\chi_j(\ell - p)} \tag{69}$$

where for convenience

$$\overline{KC}_{\phi_a} = k_{\phi_j} + (s - ia\Omega)\, c_{\phi_j}$$

and

$$\overline{KC}_{\theta_a} = k_{\theta_j} + (s - ia\Omega)\, c_{\theta_j}$$

The Laplace transformed version of Equation (62) makes it convenient to solve for $\bar{u}_0(s)$ as

$$\bar{u}_0(s) = \frac{\sum_{p=-\infty}^{\infty} \sum_{j=1}^{N_{e.s.}} (1 - b_j S_p)\, \overline{KC}_0\, e^{ip\chi_j}\, \bar{w}_p(s + ip\Omega)}{K + C\, s + \sum_{j=1}^{N_{e.s.}} \overline{KC}_0} \tag{70}$$

The expression for $\bar{u}_0(s-i\ell\Omega)$ which is required in Equations (67) and (68) may be obtained by replacing s by $(s-i\ell\Omega)$ (shifting the argument of the function) in Equation (70) which results in

$$\bar{u}_0(s-i\ell\Omega) = \frac{\sum_{p=-\infty}^{\infty} \sum_{j=1}^{N_{e.s.}} (1 - b_j S_p)\ \overline{KC}_\ell\ e^{ip\chi_j}\ \bar{w}_p(s-i\ell\Omega+ip\Omega)}{K + (s-i\ell\Omega)\ C + \sum_{j=1}^{N_{e.s.}} \overline{KC}_\ell}$$

This expression can be substituted into Equations (67) and (68) which with Equation (69) can replace the terms appearing on the right hand side of Equation (66) resulting in the final swashplate control system governing equation of motion. By replacing the index ℓ with q and then the index p with ℓ in the resulting expression, for convenience in later use, and multiplying by $2\pi R_{sp}$, the following system of coupled equations for the Laplace transformed versions of the swashplate unknowns, w_q's, in terms of the control rod forces, $\bar{P}_m(s)$, results.

$$\left[m\ (s^2 - 2iq\Omega s - q^2\Omega^2) + \frac{2\pi\ F(q)}{R_{sp}^2}\right] \bar{w}_q(s)$$

$$+ \sum_{\ell=-\infty}^{\infty} \left[\left(-\sum_{j=1}^{N_{e.s.}} (1 - b_j S_q)\ \overline{KC}_q\ e^{-iq\chi_j} \right) \frac{\left(\sum_{j=1}^{N_{e.s.}} (1 - b_j S_\ell)\ \overline{KC}_q\ e^{i\ell\chi_j} \right)}{\left(K + (s-iq\Omega)\ C + \sum_{j=1}^{N_{e.s.}} \overline{KC}_q \right)} \right.$$

$$+ \sum_{j=1}^{N_{e.s.}} \left((1 - b_j S_\ell)\ (1 - b_j S_q)\ \overline{KC}_q + \frac{q\ell}{R_{sp}^2}\ \overline{KC}_{\theta_q} \right.$$

$$\left. \left. + S_q\ S_\ell\ \overline{KC}_{\phi_q} \right) e^{-i\chi_j(q-\ell)} \right] \bar{w}_\ell(s-iq\Omega+i\ell\Omega)$$

$$= \sum_{m=1}^{N_b} (1 + d_m S_q)\ \bar{P}_m(s)\ e^{iq(\phi_m - \phi_{mp})} \qquad (71)$$

where m is the mass of the swashplate and is equal to $2\pi R_{sp}\mu$.

When the governing matrix equations for the rotor blades are developed in the next section it will be the control rod forces ($P_m(s)$) which couple the swashplate equations or the gyroscope equations to the blade equations. These relations will be used to develop the final complete set of equations for the control system-coupled rotor blade system.

Representation of Rotor Blades by Transfer Matrices

In this section the analysis, using a transfer matrix approach, is developed for representation of the blade behavior due to forces and moments of aerodynamic, mass, and inertia origin acting on the blade. Since the transfer matrix method is complicated by consideration of aerodynamic blade sections, the matrix approach is presented, initially, for sections not involving aerodynamic considerations and then extended to the form required for aerodynamic representation. The resultant analysis provides the necessary representation for blade behavior including coupling with the control system behavior.

General blade model.- A lumped parameter approach has been utilized as the means of representing the allowed blade distributed properties which were listed previously in the section pertaining to helicopter rotor system modeling. Each rotor blade is represented by a specified number of basic sections. Each blade section can have either (1) concentrated mass and inertia, uniform elastic properties, and geometric characteristics such as offsets, precone, presweep, and blade twist, or (2) aerodynamic and certain geometric characteristics. The separation of aerodynamic characteristics, section type (2), from the characteristics of section type (1) is necessary for proper determination of the modified aerodynamic forces acting on the blade section when the free-wake coupled solution method is to be applied. However, if the free-wake coupled iteration solution is not to be applied to the model of interest, the model can consist of sections each having both type (1) and type (2) characteristics. The general construction of a blade section showing the order in which specific characteristics are considered in going outboard to inboard along the section is illustrated in Figure 8.

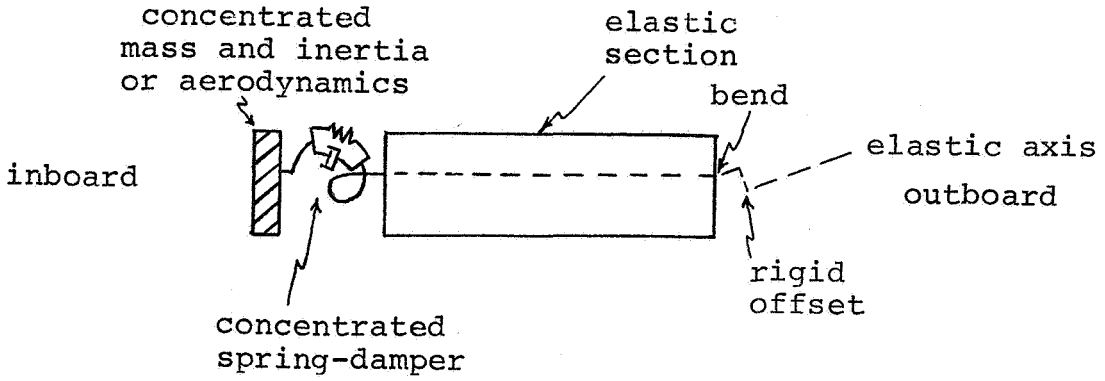

Figure 8. A general blade section

It should be noted that concentrated spring-damper units, bends, and rigid offsets are allowed in three mutually perpendicular directions and that the section center of mass and elastic axis may be offset from the quarter chord (pitch axis) of the blade.

Coordinate system involved.- The coordinate systems defined for representation of blade behavior consist of a fixed (non-rotating) coordinate system, rotating coordinate systems,and local blade coordinate systems. The orientation of the axis of the fixed shaft (hub) coordinate system has been specified previously in the discussion concerning the swashplate coordinate systems. The origin of this system is taken to be on the shaft centerline in the plane of the rotor blades when the blades are not preconed or preswept. The shaft (blade) rotating coordinate systems have their x and y axis in the same plane as the respective axes of the non-rotating shaft coordinate system but are rotating at a speed of Ω relative to the fixed shaft system. For each blade there exists a rotating shaft coordinate system whose x-axis is located along the spanwise axis of the blade when in the unconed and unswept position and which can be related to the shaft fixed coordinate system by the coordinate transformation.

$$\begin{Bmatrix} \bar{i}_{rm} \\ \bar{j}_{rm} \\ \bar{k}_{rm} \end{Bmatrix} = \begin{bmatrix} \cos(\Omega t+\phi_m) & \sin(\Omega t+\phi_m) & 0 \\ -\sin(\Omega t+\phi_m) & \cos(\Omega t+\phi_m) & 0 \\ 0 & 0 & 1 \end{bmatrix} \begin{Bmatrix} \bar{i}_f \\ \bar{j}_f \\ \bar{k}_f \end{Bmatrix} \qquad (72a)$$

where Ωt and ϕ_m have been defined.

The blade local coordinate system (x_{rb}, y_{rb}, z_{rb}) is obtained

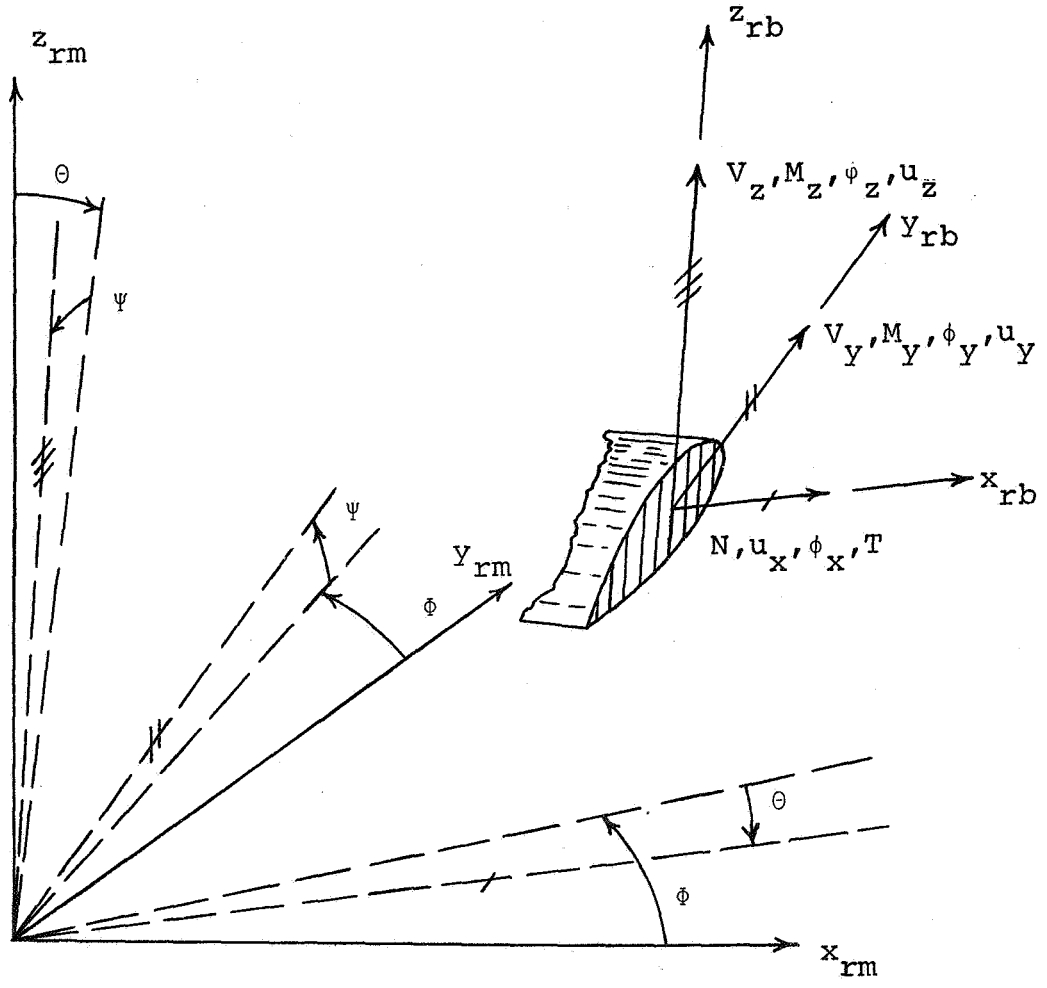

Figure 9. Blade local coordinate system and state variable orientation, slash marks refer to x_{rb}, y_{rb}, and z_{rb} blade coordinates, respectively

from the associated shaft rotating coordinate system (x_{rm}, y_{rm}, z_{rm}) by performing three orthogonal rotations; Φ, θ, and Ψ; in consecutive order where

Φ corresponds to forward presweep

θ corresponds to downward precone, and

Ψ corresponds to nose-up pre-twist and/or collective angle of attack

The relationship between the blade local coordinate system and its associated shaft rotating coordinate system is depicted in Figure 9. The mathematical relationship between the two coordinate systems is represented by the coordinate transformation

$$\begin{Bmatrix} i_{rb} \\ j_{rb} \\ k_{rb} \end{Bmatrix} = \begin{bmatrix} C\Phi\ C\theta & S\Phi\ C\Psi & -S\theta \\ -S\Phi\ C\Psi + C\Phi\ S\theta\ S\Psi & C\Phi\ C\Psi + S\Phi\ S\theta\ S\Psi & C\theta\ S\Psi \\ S\Phi\ S\Psi + C\Phi\ S\theta\ C\Psi & -C\Phi\ S\Psi + S\Phi\ S\theta\ C\Psi & C\theta\ C\Psi \end{bmatrix} \begin{Bmatrix} i_{rm} \\ j_{rm} \\ k_{rm} \end{Bmatrix} \quad (72b)$$

where a short form of denoting the sine and cosine functions has been utilized, (e.g., $S\Phi$ represents $\sin\Phi$ and $C\Phi$ represents $\cos\Phi$). Since the transfer matrix approach which will be developed in the next section relates the blade deflections, slopes, forces, and moments along the blade relative to its local coordinate system, the transformation shown above can be used to obtain blade variables in the disk plane.

Transfer matrix representation of blade model without aerodynamic loading and hinge or bearing discontinuities.- The transfer matrix approach utilized for a blade without aerodynamics included in the blade model is presented initially to provide a mathematical foundation for the presentation of the modified transfer matrix approach required for representation of aerodynamic effects on the blade behavior. The basic transfer matrices to be utilized in this section consist of essentially three basic types. These are (1) section individual transfer matrices which are used to construct (2) section transfer matrices which in turn are used to construct (3) associated transfer matrices. Corresponding to these types of transfer matrices there also will be involved corresponding types of forcing functions. Each type of transfer matrix and forcing function can be represented in a real-time form which upon application of Laplace transforms results in

a related transfer matrix involving complex variable notations. In this initial analytical development for representation of the rotor blade behavior it is convenient to consider the basic real-time relationships only briefly and carry out the development of analysis utilizing Laplace transformed representation.

A section transfer matrix can be developed which relates a state vector at either end of a section such that

$$\left\{S\right\}_m^{(i)-} = \left[G\right]_m^{(i)} \left\{S\right\}_m^{(i)+} + \left\{F\right\}_m^{(i)} \tag{73}$$

The + and - signs in Equation (73) refer, respectively, to the outboard and inboard ends of the ith section of mth blade, the sections being numbered outboard to inboard. The state vector, $\left\{S\right\}$, is a column of twelve quantities expressed as

$$\left\{S\right\} = \left\{u_x \; N \; \phi_x \; T \; u_y \; \phi_z \; M_z \; - V_y \; - u_z \; \phi_y \; M_y \; V_z\right\}$$

where u_x, u_y, u_z are blade displacements in the blade local x, y, and z directions;

N, V_y, V_z are axial force, edgewise shear force, and flapwise shear force, respectively;

ϕ_x, ϕ_y, ϕ_z are local torsional deflection, flapwise bending slope and edgewise bending slope, respectively; and

T, M_y, M_z are local pitching moment, flapwise bending moment, and edgewise bending moment, respectively.

The positive sense of the twelve state variables comprising the state vector has been shown in Figure 9 as they would act on the outboard end of the next inboard section from the section to which the transfer matrix has been applied. The vector, $\{F\}$, in Equation (73) is a section individual forcing function consisting of mass, inertia, and maneuver loading effects on the shear and moment variables in the state vector and may also be considered to be the section forcing function since aerodynamic considerations are being omitted initially. Contributions to the section forcing function due to other individual characteristic portions of a section do not occur.

In general the transfer matrix is a 12 x 12 array whose elements are differential operators when each of the state variables is a real time quantity. By taking the Laplace transform of

Equation (72) the differential operators are converted to complex linear algebraic equations. Assuming quiescent initial conditions the transformed version of Equation (73) is

$$\left\{\bar{S}\right\}_m^{(i)-} = \left[\bar{G}\right]_m^{(i)} \left\{\bar{S}\right\}_m^{(i)+} + \left\{\bar{F}\right\}_m^{(i)} . \tag{74}$$

The section transfer matrix $\left[G\right]_m^{(i)}$ can be expressed in terms of more fundamental transfer matrices which are associated with the mass, elastic, and geometric properties of the section, individually. Thus

$$\left[G\right]_m^{(i)} = \left[A\right]_m^{(i)} \left[SK\right]_m^{(i)} \left[E\right]_m^{(i)} \left[B\right]_m^{(i)} \left[R\right]_m^{(i)} \tag{75}$$

where the individual transfer matrices are constructed such that

- $\left[R\right]$ accounts for a rigid offset in the elastic axis or a translation of the local coordinate system;
- $\left[B\right]$ accounts for a bend in the elastic axis or more generally a rotation of local coordinates;
- $\left[E\right]$ accounts for a uniform elastic section with centrifugal stiffness included;
- $\left[SK\right]$ accounts for a concentrated spring-damper (used normally for lead-lag hinge only); and
- $\left[A\right]$ accounts for a concentrated mass and inertia.

Taking the Laplace transform, it can be shown that

$$\left[\bar{G}\right]_m^{(i)} = \left[\bar{A}\right]_m^{(i)} \left[\overline{SK}\right]_m^{(i)} \left[\bar{E}\right]_m^{(i)} \left[\bar{B}\right]_m^{(i)} \left[\bar{R}\right]_m^{(i)} \tag{76}$$

where each matrix consists of time independent terms and/or Laplace operators. In practice some of the individual transfer matrices may not be necessary in representing a blade section and would be omitted from Equation (76).

In order to develop the associated matrix across a rotor blade, consider the transfer across the (i+1)th blade section which from Equation (74) is given by

$$\left\{\bar{S}\right\}_m^{(i+1)-} = \left[\bar{G}\right]_m^{(i+1)} \left\{\bar{S}\right\}_m^{(i+1)+} + \left\{\bar{F}\right\}_m^{(i+1)} \tag{77}$$

However,

$$\left\{\bar{S}\right\}^{(i+1)+} = \left\{\bar{S}\right\}^{(i)-} \tag{78}$$

Substitution of Equation (74) into Equation (78) and insertion of the resulting expression into Equation (77) yields the equation

$$\left\{\bar{S}\right\}_m^{(i+1)-} = \left[\bar{G}\right]_m^{(i+1)}\left[\bar{G}\right]_m^{(i)}\left\{\bar{S}\right\}_m^{(i)+} + \left[\bar{G}\right]_m^{(i+1)}\left\{\bar{F}\right\}_m^{(i)} + \left\{\bar{F}\right\}_m^{(i+1)} \tag{79}$$

for transferring across the (i+1)th and ith blade section. Extending Equation (79), the expression which relates the state vector at the inboard position of the ith section to the state vector at the blade tip can be written in the form

$$\left\{\bar{S}\right\}_m^{(i)-} = \left[\prod_{j=1}^{i}\left[\bar{G}\right]_m^{(j)}\right]\left\{\bar{S}\right\}_m^{(Tip)} + \sum_{j=1}^{i-1}\left[\left[\prod_{k=j+1}\left[\bar{G}\right]_m^{(k)}\right]\left\{\bar{F}\right\}_m^{(j)}\right] + \left\{\bar{F}\right\}_m^{(i)} \tag{80}$$

The blade tip state vector denoted by $\left\{\bar{S}\right\}_m^{(Tip)}$ has the moments and shears equal to zero due to the free boundary condition. It is convenient to use this fact in the blade transfer process and define

$$\begin{Bmatrix} \bar{u}_x \\ \bar{N} \\ \bar{\phi}_x \\ \bar{T} \\ \bar{u}_y \\ \bar{\phi}_z \\ \bar{M}_z \\ -\bar{V}_y \\ -\bar{u}_z \\ \bar{\phi}_y \\ \bar{M}_y \\ \bar{V}_z \end{Bmatrix}_m^{(Tip)} \triangleq \begin{bmatrix} 1 & 0 & 0 & 0 & 0 & 0 \\ 0 & 0 & 0 & 0 & 0 & 0 \\ 0 & 1 & 0 & 0 & 0 & 0 \\ 0 & 0 & 0 & 0 & 0 & 0 \\ 0 & 0 & 1 & 0 & 0 & 0 \\ 0 & 0 & 0 & 1 & 0 & 0 \\ 0 & 0 & 0 & 0 & 0 & 0 \\ 0 & 0 & 0 & 0 & 0 & 0 \\ 0 & 0 & 0 & 0 & 1 & 0 \\ 0 & 0 & 0 & 0 & 0 & 1 \\ 0 & 0 & 0 & 0 & 0 & 0 \\ 0 & 0 & 0 & 0 & 0 & 0 \end{bmatrix}_m \begin{Bmatrix} \bar{u}_x \\ \bar{\phi}_x \\ \bar{u}_y \\ \bar{\phi}_z \\ -\bar{u}_z \\ \bar{\phi}_y \end{Bmatrix}_m^{(Tip)} \tag{81}$$

This matrix equation can be rewritten as

$$\left\{\bar{S}\right\}_m^{(Tip)} = \left[\bar{\lambda}\right]_m^{Tip}\left\{\bar{S}\right\}_m^{*(Tip)} \tag{82}$$

The reason for writing Equation (81) in the form shown is connected with the modified transfer matrix procedure used to solve the final system of equations for the dynamic forced response.

The fact that the $\left[\bar{\lambda}\right]_m^{Tip}$ matrix is a 12 x 6 instead of a 12 x 12 reduces the number of computations required to obtain the associated transfer matrix for the whole blade.

On insertion of Equation (82) into Equation (80), the equation

$$\left\{\bar{S}\right\}_m^{(i)-} = \left[\bar{B}\right]_m^{(i)}\left\{\bar{S}\right\}_m^{*(Tip)} + \left\{\bar{H}\right\}_m^{(i)} \tag{83}$$

is obtained where the associated matrix is defined as

$$\left[\bar{B}\right]_m^{(i)} \triangleq \left[\prod_{j=1}^{i}\left[\bar{G}\right]_m^{(j)}\right]\left[\bar{\lambda}\right]_m^{Tip} \tag{84}$$

and the associated forcing function column is defined as

$$\left\{\bar{H}\right\}_m^{(i)} \triangleq \sum_{j=1}^{i-1}\left[\left[\prod_{k=j+1}^{i}\left[\bar{G}\right]_m^{(k)}\right]\left\{\bar{F}\right\}_m^{(j)}\right] + \left\{\bar{F}\right\}_m^{(i)} \tag{85}$$

Equation (83) is the blade matrix equation which is valid for any section which is outboard of all possible hinge and bearing discontinuities in the blade model.

Representation of blade hinge and bearing discontinuities without aerodynamics.- The analysis being developed includes the representation necessary for consideration of flap hinge, pitch bearing, and rocker arm attachment point discontinuities in the blade model. At these locations there are discontinuities in flap angle, torsional deflection, and blade torque, respectively.

The state vector relationship across the pitch bearing discontinuity location may be written in the form

$$\left\{\bar{S}\right\}_m^{(fea)-} = \left\{\bar{S}\right\}_m^{(fea)+} - \left\{\bar{\Delta}\right\}_m^{fea} \tag{86}$$

where the column vector

$$\left\{\bar{\Delta}\right\}_m^{fea} = \left\{0\ 0\ \overline{\Delta\phi}_x\ 0\ 0\ 0\ 0\ 0\ 0\ 0\ 0\ 0\right\}_m \quad . \tag{87}$$

The state vector relationship across the flap hinge discontinuity location, provided there exists a flap hinge in the blade model, is given by

$$\left\{\bar{S}\right\}_m^{(flap)-} = \left\{\bar{S}\right\}_m^{(flap)+} - \left\{\bar{\Delta}\right\}_m^{flap} \tag{88}$$

where the column vector

$$\left\{\bar{\Delta}\right\}_m^{flap} = \left\{0\ 0\ 0\ 0\ 0\ 0\ 0\ 0\ 0\ \overline{\Delta\phi}_y\ 0\ 0\right\}_m \quad . \tag{89}$$

In transferring across the rocker arm attachment point it is assumed that only the torque applied to the blade from the control system is significant. Thus the transfer inboard across the control torque point can be written as

$$\left\{\bar{S}\right\}_m^{(c.t.)-} = \left\{\bar{S}\right\}_m^{(c.t.)+} - \left\{\bar{\Delta}\right\}_m^{c.t.} \tag{90}$$

where the column vector

$$\left\{\bar{\Delta}\right\}_m^{c.t.} = \left\{0\ 0\ 0\ \overline{\Delta T}\ 0\ 0\ 0\ 0\ 0\ 0\ 0\ 0\right\}_m \quad . \tag{91}$$

The quantities $\overline{\Delta T}$, $\overline{\Delta\phi}_x$, and $\overline{\Delta\phi}_y$ are additional blade unknowns which are to be solved for in the final system of equations.

Equations (90), (86), and (88) can then be replaced by the matrix equations

$$\left\{\bar{S}\right\}_m^{(c.t.)-} = \left\{\bar{S}\right\}_m^{(c.t.)+} - \left\{\bar{\lambda}\right\}_m^{c.t.}\left\{\bar{\Delta}\right\}_m^{*c.t.} \tag{92}$$

$$\left\{\bar{S}\right\}_m^{(fea)-} = \left\{\bar{S}\right\}_m^{(fea)+} - \left\{\bar{\lambda}\right\}_m^{fea}\left\{\bar{\Delta}\right\}_m^{*fea} \tag{93}$$

$$\left\{\bar{S}\right\}_m^{(flap)-} = \left\{\bar{S}\right\}_m^{(flap)+} - \left\{\bar{\lambda}\right\}_m^{flap}\left\{\bar{\Delta}\right\}_m^{*flap} \tag{94}$$

where the following arrays only have one element:

$$\left\{\bar{\Delta}\right\}_m^{*c.t.} \triangleq \left\{\overline{\Delta T}\right\}_m \; ; \; \left\{\bar{\Delta}\right\}_m^{*fea} \triangleq \left\{\overline{\Delta\phi_x}\right\}_m \; ; \; \left\{\bar{\Delta}\right\}_m^{*flap} \triangleq \left\{\overline{\Delta\phi_y}\right\}_m \tag{95}$$

and

$$\left\{\bar{\lambda}\right\}_m^{c.t.} = \begin{Bmatrix} 0\\0\\0\\1\\0\\0\\0\\0\\0\\0 \end{Bmatrix}_m \; ; \quad \left\{\bar{\lambda}\right\}_m^{fea} = \begin{Bmatrix} 0\\0\\1\\0\\0\\0\\0\\0\\0\\0 \end{Bmatrix}_m \; ; \quad \left\{\bar{\lambda}\right\}_m^{flap} = \begin{Bmatrix} 0\\0\\0\\0\\0\\0\\0\\1\\0\\0 \end{Bmatrix}_m . \tag{96}$$

Expression (83) can now be replaced by the matrix equation which provides the state vector at the inboard end of an arbitrary blade section which is

$$\left\{\bar{S}\right\}_m^{(i)-} = \left[\bar{B}\right]_m^{(i)}\left\{\bar{S}\right\}_m^{*(Tip)} - \left\{\bar{b}\right\}_m^{(i)}\left\{\bar{\Delta}\right\}_m^{*c.t.} - \left\{\bar{c}\right\}_m^{(i)}\left\{\bar{\Delta}\right\}_m^{*fea} - \left\{\bar{d}\right\}_m^{(i)}\left\{\bar{\Delta}\right\}_m^{*flap} + \left\{\bar{H}\right\}_m^{(i)} \tag{97}$$

where by letting $N_{c.t.}$, N_{fea}, and N_{flap} be the blade section numbers immediately inboard of which the control torque, pitch bearings, and flap hinge are respectively located, the new matrices appearing in Equation (97) are defined as

$$\left\{\bar{b}\right\}_m^{(i)} \triangleq \left[\bar{G}\right]_m^{(i)}\left[\bar{G}\right]_m^{(i-1)} \cdots \left[\bar{G}\right]_m^{(N_{c.t.}+1)}\left\{\bar{\lambda}\right\}_m^{c.t.} \qquad i > N_{c.t.}$$

$$\triangleq \left\{\bar{\lambda}\right\}_m^{c.t.} \qquad i = N_{c.t.}$$

$$\triangleq \left\{0\right\} \qquad i < N_{c.t.} \tag{98}$$

$$\left\{\bar{c}\right\}_m^{(i)} \triangleq \left[\bar{G}\right]_m^{(i)} \left[\bar{G}\right]_m^{(i-1)} \cdots \left[\bar{G}\right]_m^{(N_{fea}+1)} \left\{\bar{\lambda}\right\}_m^{fea} \qquad i > N_{fea}$$

$$\triangleq \left\{\bar{\lambda}\right\}_m^{fea} \qquad i = N_{fea}$$

$$\triangleq \left\{0\right\} \qquad i < N_{fea} \qquad (99)$$

$$\left\{\bar{d}\right\}_m^{(i)} \triangleq \left[\bar{G}\right]_m^{(i)} \left[\bar{G}\right]_m^{(i-1)} \cdots \left[\bar{G}\right]_m^{(N_{flap}+1)} \left\{\bar{\lambda}\right\}_m^{flap} \qquad i > N_{flap}$$

$$\triangleq \left\{\bar{\lambda}\right\}_m^{flap} \qquad i = N_{flap}$$

$$\triangleq \left\{0\right\} \qquad i < N_{flap} \qquad (100)$$

With the above definitions the state vector, $\left\{\bar{S}\right\}_m^{(i)-}$, when evaluated at i equal to $N_{c.t.}$, N_{fea}, or N_{flap} will be immediately inboard of the control torque point, the pitch bearings or the flap hinge, respectively.

Application of blade root and discontinuity boundary conditions when no aerodynamic loading.- By use of the boundary conditions which occur at the blade root and the conditions which must occur at the control torque point, pitch bearing, and flap hinge, the governing blade equations in terms of blade tip unknowns and discontinuity unknowns can be obtained when aerodynamic sections are not allowed.

Displacement and slope boundary condition applications: Letting NS be the number of blade sections, the state vector at the blade root is determined from Equation (97) by letting i equal NS. If the boundary conditions at the root of each blade are such that all displacements and slopes vanish, then these conditions are expressed by the matrix equation

$$\left[\alpha\right]\left\{\bar{S}\right\}_m^{NS-} = \left\{0\right\} \qquad (101)$$

Or, from Equation (97)

$$\left[\alpha\right]\left[\overline{B}\right]_m^{(NS)}\left\{\overline{S}\right\}_m^{*(Tip)} - \left[\alpha\right]\left\{\overline{b}\right\}_m^{(NS)}\left\{\overline{\Delta}\right\}_m^{*c.t.} - \left[\alpha\right]\left\{\overline{c}\right\}_m^{(NS)}\left\{\overline{\Delta}\right\}_m^{*fea}$$

$$- \left[\alpha\right]\left\{\overline{d}\right\}_m^{(NS)}\left\{\overline{\Delta}\right\}_m^{*flap} + \left[\alpha\right]\left\{\overline{H}\right\}_m^{(NS)} = \left\{0\right\} \quad (102)$$

where

$$\left[\alpha\right] \triangleq \begin{bmatrix} 1 & 0 & 0 & 0 & 0 & 0 & 0 & 0 & 0 & 0 & 0 & 0 \\ 0 & 0 & 1 & 0 & 0 & 0 & 0 & 0 & 0 & 0 & 0 & 0 \\ 0 & 0 & 0 & 0 & 1 & 0 & 0 & 0 & 0 & 0 & 0 & 0 \\ 0 & 0 & 0 & 0 & 0 & 1 & 0 & 0 & 0 & 0 & 0 & 0 \\ 0 & 0 & 0 & 0 & 0 & 0 & 0 & 0 & 1 & 0 & 0 & 0 \\ 0 & 0 & 0 & 0 & 0 & 0 & 0 & 0 & 0 & 0 & 1 & 0 \end{bmatrix} \quad (103)$$

Equation (102) provides six equations for each blade. However, there are nine possible unknowns due to the control torque, pitch bearing, and flap discontinuities. The other three equations are obtained from the condition of zero bending moment and torque at the flap hinges and pitch bearings respectively, in addition to the relationship between the control torque and the blade torsional deflection at the rocker arm attachment point.

Application of zero torque condition at pitch bearing: Consider the condition of zero torque at the blade pitch bearings. The state vector at the pitch bearings is given by $\left\{\overline{S}\right\}_m^{(N_{fea})}$. In order for the torque (which is the fourth quantity in the state vector) to vanish the equation

$$\left(r_4\right)\left\{\overline{S}\right\}_m^{(N_{fea})-} = 0 \quad (104)$$

must be satisfied. Or equivalently

$$\left(r_4\right)\left[\overline{B}\right]_m^{(N_{fea})}\left\{\overline{S}\right\}_m^{*(Tip)} - \left(r_4\right)\left\{\overline{b}\right\}_m^{(N_{fea})}\left\{\overline{\Delta}\right\}_m^{*c.t.}$$

$$- \left(r_4\right)\left\{\overline{d}\right\}_m^{(N_{fea})}\left\{\overline{\Delta}\right\}_m^{*flap} + \left(r_4\right)\left\{\overline{H}\right\}_m^{(N_{fea})} = 0 \quad (105)$$

where $\{r_4\} = (0\ 0\ 0\ 1\ 0\ 0\ 0\ 0\ 0\ 0\ 0\ 0)$.

Application of control torgue condition for coupling with swashplate or gyroscope control system: The equation for the control torque must reflect the coupling between the blade and the swashplate or gyroscope motion, In real time the balance of forces on the mth control rod which connects the rocker arm to the swashplate is given by

$$(\Delta T)_m = a_m k_m (1 + \tau_m \frac{\partial}{\partial t}) \left[a_m (\phi_x)_m^{(N_{c.t.})} - \sum_{\ell=-\infty}^{\infty} (1 + d_m S_\ell) w_\ell(t) e^{i\ell(\phi_m - \phi_{mp})} \right] \tag{106}$$

where k_m and τ_m are the linear stiffness and damping coefficients of the mth control rod, respectively, and a_m is the distance of control rod rocker arm attachment point aft of quarter chord. Dividing by k_m and taking the Laplace transform yields

$$k_m^{-1} (\overline{\Delta T})_m - a_m^2 (1 + \tau_m s) (\overline{\phi}_x)_m^{(N_{c.t.})} + \sum_{\ell=-\infty}^{\infty} (1 + d_m S_\ell) a_m (1 + \tau_m s) e^{i\ell(\phi_m - \phi_{mp})} \bar{w}_\ell(s) = 0. \tag{107}$$

Referring to Equations (90), (91), and (92)

$$(\overline{\Delta T})_m = \{r_4\} \left\{\bar{\lambda}\right\}_m^{c.t.} \left\{\bar{\Delta}\right\}_m^{*c.t.} \tag{108}$$

and also

$$(\overline{\phi}_x)_m^{(N_{c.t.})} = \{r_3\} \left\{\bar{S}\right\}_m^{(N_{c.t.})} = \{r_3\} \bar{B}_m^{(N_{c.t.})} \left\{\bar{S}\right\}_m^{*(Tip)} - \{r_3\} \left\{\bar{d}\right\}_m^{(N_{c.t.})} \left\{\bar{\Delta}\right\}_m^{*flap} + \{r_3\} \left\{\bar{H}\right\}_m^{(N_{c.t.})} \tag{109}$$

where $\{r_3\} = (0\ 0\ 1\ 0\ 0\ 0\ 0\ 0\ 0\ 0\ 0\ 0)$.

Thus, the control torque equation can be written in terms of the blade tip and internal discontinuity unknowns as

$$- a_m^2(1 + \tau_m s)\left(r_3\right)\left[\bar{B}\right]_m^{(N_{c.t.})}\left\{\bar{S}\right\}_m^{*(Tip)} + k_m^{-1}\left(r_4\right)\left\{\bar{\lambda}\right\}_m^{c.t.}\left\{\bar{\Delta}\right\}_m^{*c.t.}$$

$$- a_m^2(1 + \tau_m s)\left(r_3\right)\left\{\bar{H}\right\}_m^{(N_{c.t.})} + a_m^2(1 + \tau_m s)\left(r_3\right)\left\{\bar{d}\right\}_m^{(N_{c.t.})}\left\{\bar{\Delta}\right\}_m^{*flap}$$

$$+ \sum_{\ell=-\infty}^{\infty}(1 + d_m S_\ell)a_m(1 + \tau_m s)e^{i\ell(\phi_m - \phi_{mp})}\bar{w}_\ell(s) = 0 \quad . \tag{110}$$

If the swashplate is replaced by a gyroscopic control system, the equation for the control torque must reflect the coupling between the rotor blade and the rigid body motion of the gyroscope. In real time the balance of forces on the mth control rod which connects the rocker arm to the gyroscope is given by

$$(\Delta T)_m = a_m k_m\left(1 + \tau_m \frac{\partial}{\partial t}\right)\left[a_m(\phi_x)_m^{(N_{c.t.})} - \sum_{\ell=-1}^{1} w'_\ell(t)\right] \tag{111}$$

where the w_ℓ quantities now stand for the rigid body motions of the gyroscope (i.e., see Equations (17), (18), and (19) for equations of motion of the gyroscope) and are given as

$$\begin{aligned} w'_{-1} &= -\phi_{x_r} R_p \sin(\phi_m - \phi_{mp}) \\ w'_0 &= -z_r \\ w'_1 &= \phi_{y_r} R_p \cos(\phi_m - \phi_{mp}) \end{aligned} \tag{112}$$

Dividing by k_m and taking the Laplace transform yields

$$k_m^{-1}(\Delta\bar{T})_m - a_m^2(1 + \tau_m s)(\bar{\phi}_x)_m^{(N_{c.t.})} + \sum_{\ell=-1}^{1} a_m(1 + \tau_m s)\bar{w}'_\ell(s) = 0 \quad . \tag{113}$$

Therefore, whether the rotor blades are coupled through the swashplate or the gyroscope, the general formulation is essentially the same with the only difference being the functionality involving the $(\phi_m - \phi_{mp})$ term.

Application of flapwise moment condition at flap hinge: If a flap hinge is present the condition that the flapwise moment vanish gives the last equation needed. Since the flapwise

moment is the eleventh quantity in the state vector, this condition is satisfied provided

$$\left[r_{11}\right]\left\{\bar{S}\right\}_m^{(N_{flap})} = 0 \tag{114}$$

where $\left[r_{11}\right] = (0\ 0\ 0\ 0\ 0\ 0\ 0\ 0\ 0\ 0\ 1\ 0)$.

Referring back to Equation (97), the zero flap hinge moment is expressed by

$$\left[r_{11}\right]\left[\bar{B}\right]_m^{(N_{flap})}\left\{\bar{S}\right\}_m^{*(Tip)} - \left[r_{11}\right]\left\{\bar{b}\right\}_m^{(N_{flap})}\left\{\bar{\Delta}\right\}_m^{*c.t.} - \left[r_{11}\right]\left\{\bar{c}\right\}_m^{(N_{flap})}\left\{\bar{\Delta}\right\}_m^{*fea} + \left[r_{11}\right]\left\{\bar{H}\right\}_m^{(N_{flap})} = 0. \tag{115}$$

For a blade without aerodynamic loading, Equation (97) relates the state vector variables at the inboard end of the ith section of the mth blade to the blade tip unknowns and discontinuity unknowns and thus may be utilized to obtain the blade shape if all unknowns have been determined. Values for the unknowns are obtained by use of Equations (102), (105), (115), and either (110) or (113) depending on the type of control system involved.

Shift of transform variable in sectional transfer matrix Equation and its interpretation.- Prior to the inclusion of aerodynamic blade sections into the blade model which compounds the complexity of the transfer matrix approach, consideration of the representation implied by the use of Laplace transform shifted and unshifted variables will be advantageous.

In the previous development of the transfer matrix equation, Equation (74), the Laplace transformed arrays are a function of the Laplace transform variable, s, although this dependency was not explicitly shown. This dependency is directly observable by rewriting Equation (74) in the form

$$\left\{\bar{S}(s)\right\}_m^{(i)-} = \left[\bar{G}(s)\right]_m^{(i)}\left\{\bar{S}(s)\right\}_m^{(i)+} + \left\{\bar{F}(s)\right\}_m^{(i)} . \tag{116}$$

In the dynamic response type of solution the total state vectors and forcing function corresponding to those in the above expression are expressible in real-time notation in a Fourier series form exemplified for the state vector by

$$\left\{S(t)\right\}_m^{(i)-} = \sum_{n=-\infty}^{\infty}\left\{S^n\right\}_m^{(i)-} e^{in\Omega t}$$

where the S^n harmonic coefficients may be complex variables and correspond to the commonly denoted; 0/rev., ±1/rev., and etc.; blade responses and forcing functions for the state vectors and forcing function arrays, respectively. Substitution of $iNp\Omega$ for the Laplace transform variable, s, in Equation (116) provides the transfer matrix equation relating Np/rev. coefficients of the state vectors on both ends of a section and of the forcing function on the section.

This can be shown by first applying the Laplace transform operations as specified in Equation (116) to the real-time state vectors and forcing function such that

$$\sum_{n=-\infty}^{\infty}\left\{\frac{S^n}{(s-in\Omega)}\right\}_m^{(i)-} = \left[\bar{G}(s)\right]_m^{(i)} \sum_{n=-\infty}^{\infty}\left\{\frac{S^n}{(s-in\Omega)}\right\}_m^{(i)+} + \sum_{n=-\infty}^{\infty}\left\{\frac{F^n}{(s-in\Omega)}\right\}_m^{(i)}$$

results. Multiplication of both sides of the above expression by $(s-iNp\Omega)$ yields the equation

$$\left\{S^{Np}\right\}_m^{(i)-} + \sum_{\substack{n=-\infty \\ n\neq Np}}^{\infty}\left\{\frac{(s-iNp\Omega)\ S^n}{(s-in\Omega)}\right\}_m^{(i)-} = \left[G(s)\right]_m^{(i)} \sum_{\substack{n=-\infty \\ n\neq Np}}^{\infty}\left\{\frac{(s-iNp\Omega)\ S^n}{(s-in\Omega)}\right\}_m^{(i)+}$$

$$+ \left[\bar{G}(s)\right]_m^{(i)}\left\{S^{Np}\right\}_m^{(i)+} + \left\{F^{Np}\right\}_m^{(i)} + \sum_{\substack{n=-\infty \\ n\neq Np}}^{\infty}\left\{\frac{(s-iNp\Omega)\ F^n}{(s-in\Omega)}\right\}_m^{(i)}$$

which in the limit as s approaches $iNp\Omega$ reduces to the form

$$\left\{S^{Np}\right\}_m^{(i)-} = \left[\bar{G}(iNp\Omega)\right]_m^{(i)}\left\{S^{Np}\right\}_m^{(i)+} + \left\{F^{Np}\right\}_m^{(i)}$$

relating the Np/rev. harmonic coefficients of the state vectors and forcing function involved. Thus, substitution of $iNp\Omega$ for **s** in Equation (116) corresponds to the relationship shown in the last expression.

Shifted Laplace transform variables of the form $(s-ik\Omega)$ represent harmonics relative to the main harmonic of interest denoted by the value of s. By shifting the argument of Equation (116), that is, replacing s by $(s-ik\Omega)$, the expression

$$\left\{\bar{S}(s-ik\Omega)\right\}_m^{(i)-} = \left[G(s-ik\Omega)\right]_m^{(i)}\left\{\bar{S}(s-ik\Omega)\right\}_m^{(i)+} + \left\{\bar{F}(s-ik\Omega)\right\}_m^{(i)} \quad (117)$$

is obtained. Application of the same procedure that was used on Equation (116) to Equation (117) yields when s is replaced by iNpΩ

$$\left\{S^{Np-k}\right\}_m^{(i)-} = \left[\overline{G}(i(Np-k)\Omega)\right]_m^{(i)} \left\{S^{Np-k}\right\}_m^{(i)+} + \left\{F^{Np-k}\right\}_m^{(i)}$$

which relates the (Np-k)/rev. harmonic coefficients of the state vectors and the forcing function. In this equation and Equation (117) a positive value for k corresponds to a downward shift in the harmonic from that specified by s whereas a negative k denotes an upward shift in harmonic. The quantity, s, taken as iNpΩ in Equation (117) provides the relationship shown in the last expression. This shifted Laplace transform concept is valid for any originally time dependent variable used in this report.

For convenience in the representation of the transfer matrix approach when aerodynamic sections are included in the blade model Equation (117) can be written in the subscripted form

$$\left\{\overline{S}_k\right\}_m^{(i)-} = \left[\overline{G}_k\right]_m^{(i)} \left\{\overline{S}_k\right\}_m^{(i)+} + \left\{\overline{F}_k\right\}_m^{(i)} \tag{118}$$

Transfer matrix representation of transfer across an aerodynamic section.- The transfer across an aerodynamic section in real-time notation can be represented by the matrix relationship

$$\left\{S\right\}^{(i)-} = \left[C\right]^{(i)} \frac{d}{dt}\left\{S\right\}^{(i)+} + \left[D\right]^{(i)}\left\{S\right\}^{(i)+} + \left\{d\right\}^{(i)} \tag{119}$$

where $\left[C\right]^{(i)}$ and $\left[D\right]^{(i)}$ are transfer arrays involving periodic functions and the column vector, $\left\{d\right\}^{(i)}$, is the aerodynamic forcing function also consisting of periodic functions. Each of these arrays can be expanded in a Fourier series form. For example,

$$\left[C\right]^{(i)} = \sum_{n=-\infty}^{\infty} \left[C_n\right]^{(i)} e^{in\Omega t} \quad . \tag{120}$$

Defining $\left[C_n\right]_m^{(i)}$ relative to the initial position of the first blade and replacing Ωt with $(\Omega t+\phi_m-\phi_{mp})$, Equation (120) becomes for the mth blade

$$\left[C\right]_m^{(i)} = \sum_{n=-\infty}^{\infty} \left[C_n\right]_m^{(i)} e^{in(\Omega t+\phi_m-\phi_{mp})} \quad . \tag{121}$$

Applying the same procedure to the other two arrays appearing in Equation (119) and substituting into Equation (119) results in

$$\left\{S\right\}_m^{(i)-} = \sum_{n=-\infty}^{\infty} e^{in(\Omega t+\phi_m-\phi_{mp})}\left[\left[C_n\right]_m^{(i)}\frac{d}{dt} + \left[D_n\right]_m^{(i)}\right]\left\{S\right\}_m^{(i)+}$$

$$+ \sum_{n=-\infty}^{\infty} e^{in(\Omega t+\phi_m-\phi_{mp})}\left\{d_n\right\}_m^{(i)} \quad . \tag{122}$$

The Laplace transform of Equation (122), assuming quiescent initial conditions and also shifting the Laplace transform variable, s, is

$$\left\{\bar{S}_k\right\}_m^{(i)-} = \sum_{n=-\infty}^{\infty}\left[(s-ik\Omega-in\Omega)\left[\bar{C}_n\right]_m^{(i)} + \left[\bar{D}_n\right]_m^{(i)}\right]\left\{\bar{S}_{n+k}\right\}_m^{(i)+} e^{in(\phi_m-\phi_{mp})}$$

$$+ \sum_{n=-\infty}^{\infty} \frac{\left\{d_n\right\}_m^{(i)} e^{in(\phi_m-\phi_{mp})}}{(s-ik\Omega-in\Omega)} \quad . \tag{123}$$

The summation on the first term of the above expression can be taken from $n=-N_f$ to N_f where N_f is the number of harmonics above and coupled to the frequency being solved for. The summation on the second term can be taken from $n=-N_{ff}$ to N_{ff} where N_{ff} is maximum number of aerodynamic forcing function variable harmonics not including the steady, that are obtainable.

However, when these limits are placed on the respective summations involved in Equation (123), it can be observed that the equation representing shifted harmonics of the state vector, k not zero, involves harmonics further removed from the main harmonic of interest. For example, if N_f is taken as 1 corresponding to inclusion of interharmonic coupling 1/rev. above and below the harmonic corresponding to k equal to zero, the version of Equation (123) for k equal 1 would include a term involving (n+k) equal to 2 which corresponds to a harmonic 2/rev. below the main harmonic and similarily, for k equal -1, a term involving (n+k) equal to -2 results. This addition of extra harmonics above and below the range specified by the value for N_f is not desired since these additional harmonics would in turn have to be represented and thereby result in further additional harmonics and so on.

To overcome this problem the summation involved in the first term of Equation (123) can be taken from $n=-N_f-k$ to N_f-k. However, since n includes (-k) the same result is obtained if the

summation is taken over $n=-N_f$ to N_f and n in Equation (123) in the first term is replaced by (n-k). This yields

$$\left\{\bar{S}_k\right\}_m^{(i)-} = \sum_{n=-N_f}^{N_f}\left[(s-in\Omega)\left[\bar{C}_{n-k}\right]_m^{(i)}+\left[\bar{D}_{n-k}\right]_m^{(i)}\right]\left\{\bar{S}_n\right\}_m^{(i)}+e^{i(n-k)(\phi_m-\phi_{mp})}$$

$$+\sum_{n=-N_{ff}}^{N_{ff}}\frac{\left\{d_n\right\}_m^{(i)}e^{in(\phi_m-\phi_{mp})}}{(s-ik\Omega-in\Omega)} \qquad (124)$$

which can be written in the form

$$\left\{\bar{S}_k\right\}_m^{(i)-} = \sum_{n=-N_f}^{N_f}\left[\bar{C}_{n-k,n}\right]_m^{(i)}\left\{\bar{S}_n\right\}_m^{(i)}+e^{i(n-k)(\phi_m-\phi_{mp})}$$

$$+\sum_{n=-N_{ff}}^{N_{ff}}\frac{\left\{d_n\right\}_m^{(i)}e^{in(\phi_m-\phi_{mp})}}{(s-ik\Omega-in\Omega)} \qquad (125)$$

where $\left[\bar{C}_{n-k,n}\right]_m^{(i)}$ represents the aerodynamic section transfer matrix for a given section with (n-k) denoting which harmonic of the C and D matrices is involved and n representing the shift on s inherent in the matrix.

Transfer matrix representation of blade model with aerodynamics but without hinge or bearing discontinuities.- Equation (118) representing the transfer across a non-aerodynamic section and Equation (125) representing the transfer across an aerodynamic section provide the fundamental relationships necessary to construct the associated transfer matrix representation relating the state vector at the inboard end of a blade section to the blade tip unknowns.

In order to include the aerodynamic interharmonic coupling effects, Equation (83) is modified to the form

$$\left\{\bar{S}_k\right\}_m^{(i)-} = \sum_{n=-N_f}^{N_f}\left[\bar{E}_{k,n}\right]_m^{(i)}\left\{\bar{S}_n\right\}_m^{*(Tip)}+\left\{\bar{H}_k\right\}_m^{(i)} \qquad (126)$$

where the k and n subscripts denote the degree of harmonic shift relative to the harmonic specified by the Laplace transform variable, s, as previously noted. The modified associated transfer matrices of the form, $\left[\bar{B}_{k,n}\right]_m^{(i)}$, represent the effects of n-shifted harmonic coefficients of the blade tip slopes and deflections on the k-shifted harmonic coefficients of the state vector variables at the inboard end of the ith section and for the mth blade. The modified associated forcing function vectors of the form, $\left\{\bar{H}_k\right\}_m^{(i)}$, represents the effects of the k-shifted forcing function harmonic coefficients on the k-shifted harmonic coefficients of the state vector variables at the inboard end of the ith section due to aerodynamic, mass, and inertia loadings on and outboard of this blade section.

Since inclusion of aerodynamics into the blade model results in interharmonic coupling which is apparent in Equation (125), the subscripted associated transfer matrix arrays and associated forcing function vectors cannot be expressed in the simple forms exemplified by Equations (84) and (85) when aerodynamics are included. Instead, the relationships between the associated transfer arrays and forcing functions at the inboard end of a section and the associated transfer arrays and forcing functions at the outboard end of a section for the two types of blade sections can be determined.

For a non-aerodynamic section, Equation (126) with the (i) superscripts replaced by (i-1) superscripts can be inserted into Equation (118) for the (i)+ superscripted state vector (making use of the form of Equation (78)) such that the equation

$$\left\{\bar{S}_k\right\}_m^{(i)-} = \left[\bar{G}_k\right]_m^{(i)} \sum_{n=-N_f}^{N_f} \left[\bar{B}_{k,n}\right]_m^{(i-1)} \left\{S_n\right\}_m^{*(Tip)} + \left[\bar{G}_k\right]_m^{(i)} \left\{\bar{H}_k\right\}_m^{(i-1)} + \left\{\bar{F}_k\right\}_m^{(i)}$$

results. From a comparison of this expression and Equation (126), the relationships of the associated transfer matrices and associated forcing function vectors of a section to those of the previous section can be expressed as

$$\left[\bar{B}_{k,n}\right]_m^{(i)} = \left[\bar{G}_k\right]_m^{(i)} \left[\bar{B}_{k,n}\right]_m^{(i-1)}, \text{ and} \tag{127}$$

$$\left\{\bar{H}_k\right\}_m^{(i)} = \left[\bar{G}_k\right]_m^{(i)} \left\{\bar{H}_k\right\}_m^{(i-1)} + \left\{\bar{F}_k\right\}_m^{(i)} \tag{128}$$

For an aerodynamic section the same form of comparison can be used. In this case, the superscript in Equation (126) is altered in the previous manner but the k subscript is replaced by p such that when the resulting expression is inserted into a form of Equation (125) where the dummy index n has been replaced by p in the first term the following equation results

$$\left\{\bar{S}_k\right\}_m^{(i)-} = \sum_{p=-N_f}^{N_f}\left[\left[\bar{C}_{p-k,p}\right]_m^{(i)} e^{i(p-k)(\phi_m-\phi_{mp})}\left[\left\{\bar{H}_p\right\}_m^{(i-1)} + \sum_{n=-N_f}^{N_f}\left[\bar{B}_{p,n}\right]_m^{(i-1)}\left\{\bar{S}_n\right\}^{*(Tip)}\right]\right] + \sum_{n=-N_{ff}}^{N_{ff}} \frac{\left\{d_n\right\}_m^{(i)} e^{in(\phi_m-\phi_{mp})}}{(s-ik\Omega-in\Omega)} \tag{129}$$

Referring back to Equation (126)

$$\left[\bar{B}_{k,n}\right]_m^{(i)} = \sum_{p=-N_f}^{N_f}\left[\bar{C}_{p-k,p}\right]_m^{(i)}\left[\bar{B}_{p,n}\right]_m^{(i-1)} e^{i(p-k)(\phi_m-\phi_{mp})} \tag{130}$$

and

$$\left\{\bar{H}_k\right\}_m^{(i)} = \sum_{n=-N_f}^{N_f}\left[\bar{C}_{n-k,n}\right]_m^{(i)}\left\{\bar{H}_n\right\}_m^{(i-1)} e^{i(n-k)(\phi_m-\phi_{mp})} + \sum_{n=-N_{ff}}^{N_{ff}} \frac{\left\{d_n\right\}_m^{(i)} e^{in(\phi_m-\phi_{mp})}}{(s-ik\Omega-in\Omega)} \tag{131}$$

It should be noted that the associated transfer matrices for k not equal to n consist of all zero elements until an aerodynamic section is encountered since non-aerodynamic stations do not provide interharmonic coupling. This can be observed by noting that the definition of tip state vectors in terms of the tip unknowns by application of tip boundary conditions is represented by a subscript form of Equation (82) which is

$$\left\{\bar{S}_k\right\}_m^{(Tip)} = \left[\bar{\lambda}_k\right]_m^{Tip} \left\{\bar{S}_k\right\}_m^{*(Tip)}$$

where the matrix $\left[\bar{\lambda}_k\right]_m^{Tip}$ is defined for each value of k as previously defined by Equation (81). The above expression can be extended to the form

$$\left\{\bar{S}_k\right\}_m^{(Tip)} = \sum_{n=-N_f}^{N_f} \left[\bar{\lambda}_{k,n}\right]_m^{(Tip)} \left\{\bar{S}_n\right\}_m^{*(Tip)} \tag{132}$$

where the $\left|\bar{\lambda}_{k,n}\right|_m^{(Tip)}$ array is defined for k equal to n as in Equation (81) and consists of all zero elements if k is not equal to n. Thus, if the first section is a non-aerodynamic section, Equation (127) would be replaced by

$$\left[\bar{B}_{k,n}\right]_m^{(1)} = \left[\bar{G}_k\right]_m^{(1)} \left[\bar{\lambda}_{k,n}\right]_m^{Tip}$$

based on a subscript form of Equation (84) when i is equal to 1. Thus, from this expression and Equation (127), the associated transfer matrices for k not equal to n can be seen to consist of all zeroes until an aerodynamic section is crossed at which point the associated transfer matrices for k not equal to n receive a contribution due to interharmonic coupling as shown by Equation (130).

With the inclusion of aerodynamic sections, Equation (126) has become the general matrix transfer equation for sections outboard of hinge or bearing discontinuities where the associated transfer matrices are related by either Equation (127) or (130) and the associated forcing function vectors are related by Equations (128) or (131)

Hinge and bearing discontinuities representation modifications due to inclusion of aerodynamics.- The state vector at the inboard end of any arbitrary blade section on extending Equation (97) to a subscripted form is defined by

$$\left\{\bar{S}_k\right\}_m^{(i)-} = \sum_{n=-N_f}^{N_f}\left[\left[\bar{B}_{k,n}\right]_m^{(i)}\left\{\bar{S}_n\right\}_m^{*(Tip)} - \left\{\bar{b}_{k,n}\right\}_m^{(i)}\left\{\bar{\Delta}_n\right\}_m^{*c.t.}\right]$$

$$- \sum_{n=-N_f}^{N_f}\left[\left\{\bar{c}_{k,n}\right\}_m^{(i)}\left\{\bar{\Delta}_n\right\}_m^{*fea} + \left\{\bar{d}_{k,n}\right\}_m^{(i)}\left\{\bar{\Delta}_n\right\}_m^{*flap}\right] + \left\{\bar{H}_k\right\}_m^{(i)} \tag{133}$$

Since, normally, an aerodynamic section would not occur inboard of the flap hinge, pitch bearings, or rocker arm attachment point Equations (98), (99), and (100) can be extended to

$$\left\{\bar{b}_{k,n}\right\}_m^{(i)} = \left[\bar{G}_k\right]_m^{(i)} \cdots \left[\bar{G}_k\right]_m^{(N_{c.t.}+1)}\left\{\bar{\lambda}_{k,n}\right\}_m^{c.t.}$$

$$\left\{\bar{c}_{k,n}\right\}_m^{(i)} = \left[\bar{G}_k\right]_m^{(i)} \cdots \left[\bar{G}_k\right]_m^{(N_{fea}+1)}\left\{\bar{\lambda}_{k,n}\right\}_m^{fea}$$

$$\left\{\bar{d}_{k,n}\right\}_m^{(i)} = \left[\bar{G}_k\right]_m^{(i)} \cdots \left[\bar{G}_k\right]_m^{(N_{flap}+1)}\left\{\bar{\lambda}_{k,n}\right\}_m^{flap} \tag{134}$$

where $\left\{\bar{\lambda}_{k,n}\right\}_m^{c.t.}$, $\left\{\bar{\lambda}_{k,n}\right\}_m^{fea}$, and $\left\{\bar{\lambda}_{k,n}\right\}_m^{flap}$ are defined in Equation (96) when k is equal to n and consist of all zeroes if k is not equal to n. If an aerodynamic section does occur inboard of the flap hinge, pitch bearings or rocker arm attachment point, then, as the result of a transfer across this section, the arrays defined in Equation (134) are altered such that, for example,

$$\left\{\bar{b}_{k,n}\right\}_m^{(i)} = \sum_{p=-N_f}^{N_f}\left[\bar{C}_{p-k,p}\right]_{(m)}^{(i)}\left\{\bar{b}_{p,n}\right\}_m^{(i-1)} e^{i(p-k)(\phi_m-\phi_{mp})} \tag{135}$$

and similar equations occur for $\left\{\bar{c}_{k,n}\right\}_m^{(i)}$ and $\left\{\bar{d}_{k,n}\right\}_m^{(i)}$

Application of blade root and discontinuity boundary conditions with aerodynamics.- From the general form for the state vector inboard of any arbitrary section as represented by Equa-

tion (133) the boundary conditions at the blade root and the discontinuity conditions can be applied as in Equations (101) through (115) to yield the representative equations when aerodynamic sections are included.

Displacement and slope boundary condition applications: With the slopes and displacements being zero in value at the blade root irrespective of the value of k, the insertion of Equation (133) for i equal to NS into Equation (101) with k subscript added to the blade root state vector yields

$$\left[\alpha\right]\sum_{n=-N_f}^{N_f}\left[\left[\bar{B}_{k,n}\right]_m^{(NS)}\left\{\bar{S}_n\right\}_m^{*(Tip)} - \left\{\bar{b}_{k,n}\right\}_m^{(NS)}\left\{\bar{\Delta}_n\right\}_m^{*c.t.}\right] + \left[\alpha\right]\left\{\bar{H}_k\right\}_m^{(NS)}$$

$$- \left[\alpha\right]\sum_{n=-N_f}^{N_f}\left[\left\{\bar{c}_{k,n}\right\}_m^{(NS)}\left\{\bar{\Delta}_n\right\}_m^{*fea} + \left\{\bar{d}_{k,n}\right\}_m^{(NS)}\left\{\bar{\Delta}_n\right\}_m^{*flap}\right] = 0 \quad . \tag{136}$$

Application of zero torque condition at pitch bearing: The condition of zero torque at the blade pitch bearing is achieved if the Laplace shifted (subscripted) form of Equation (104) which is

$$\left(r_4\right)\left\{\bar{S}_k\right\}_m^{(N_{fea})-} = 0$$

is satisfied. Insertion of Equation (133) with i replaced by N_{fea} into the above expression and noting that the fourth element in each $\left\{\bar{c}_{k,n}\right\}_m^{(N_{fea})}$ is zero in value the pitch bearing discontinuity equation

$$\left(r_4\right)\sum_{n=-N_f}^{N_f}\left[\left[\bar{B}_{k,n}\right]_m^{(N_{fea})}\left\{\bar{S}_n\right\}_m^{*(Tip)} - \left\{\bar{b}_{k,n}\right\}_m^{(N_{fea})}\left\{\bar{\Delta}_n\right\}_m^{*c.t.}\right]$$

$$-\left(r_4\right)\sum_{n=-N_f}^{N_f}\left\{\bar{d}_{k,n}\right\}_m^{(N_{fea})}\left\{\bar{\Delta}_n\right\}_m^{*flap} + \left(r_4\right)\left\{\bar{H}_k\right\}_m^{(N_{fea})} = 0 \quad . \tag{137}$$

Application of control torque condition for coupling with swashplate or gyroscope control systems: The equation representing the coupling between the blade and the swashplate motion when aerodynamics are allowed can be obtained by first considering

the modifications necessary to Equations (107), (108), and (109). Shifting of the Laplace transform variable of Equation (107) yields

$$k_m^{-1}(\overline{\Delta T}_k)_m - a_m \bar{Y}_m^k (\bar{\phi}_{xk})_m^{(N_{c.t.})} + \sum_{\ell=-\infty}^{\infty} (1 + d_m S_\ell)\bar{Y}_m^k e^{i\ell(\phi_m - \phi_{mp})} \bar{w}_\ell(s-ik\Omega) = 0 \qquad (138)$$

where

$$\bar{Y}_m^k \triangleq a_m\left[1 + \tau_m(s-ik\Omega)\right]$$

Equations (108) and (109) can be extended to the subscripted forms

$$(\overline{\Delta T}_k)_m = \left(r_4\right) \sum_{n=-N_f}^{N_f} \left\{\bar{\lambda}_{k,n}\right\}_m^{c.t.} \left\{\bar{\Delta}_n\right\}_m^{*c.t.}$$

and

$$(\bar{\phi}_{xk})_m^{(N_{c.t.})} = \left(r_3\right)\left\{\bar{S}_k\right\}_m^{(N_{c.t.})} = \left(r_3\right) \sum_{n=-N_f}^{N_f} \left[\bar{B}_{k,n}\right]_m^{(N_{c.t.})} \left\{\bar{S}_n\right\}_m^{*(Tip)}$$

$$- \left(r_3\right) \sum_{n=-N_f}^{N_f} \left\{\bar{d}_{k,n}\right\}_m^{(N_{c.t.})} \left\{\bar{\Delta}_n\right\}_m^{*flap} + \left(r_3\right)\left\{\bar{H}_k\right\}_m^{(N_{c.t.})}$$

in which the $\left\{\bar{b}_{k,n}\right\}_m^{(N_{c.t.})}$ terms have been dropped since the third element in each array is zero in value and the $\left\{\bar{c}_{k,n}\right\}_m^{(N_{c.t.})}$ terms have been neglected since the pitch bearing should occur at or inboard of the control torque application point. The substitution of these last two equations into Equation (138) yields the control torque discontinuity equation in the form

$$- a_m \bar{Y}_m^k(r_3)\left[\sum_{n=-N_f}^{N_f}\left[\bar{B}_{k,n}\right]_m^{(N_{c.t.})}\left\{\bar{S}_n\right\}_m^{*(Tip)} + \left\{\bar{H}_k\right\}_m^{(N_{c.t.})}\right]$$

$$- \sum_{N=-N_f}^{N_f}\left[a_m \bar{Y}_m^k(r_3)\left\{\bar{d}_{k,n}\right\}_m^{(N_{c.t.})}\left\{\bar{\Delta}_n\right\}_m^{*flap} + k_m^{-1}(r_4)\left\{\bar{\lambda}_{k,n}\right\}_m^{c.t.}\left\{\bar{\Delta}_n\right\}_m^{*c.t.}\right]$$

$$+ \sum_{\ell=-\infty}^{\infty}(1 + d_m S_\ell)\bar{Y}_m^k e^{i\ell(\phi_m - \phi_{mp})}\bar{w}_\ell(s-ik\Omega) = 0 \qquad (139)$$

For a gyroscope control system the last term in Equation (139) is replaced with a summation from ℓ=-1 to +1 of the term $\bar{Y}_m^k \bar{w}_\ell'(s-ik\Omega)$.

Application of flapwise moment condition at flap hinge: The condition of zero flapwise moment at the flap hinge is achieved if the Laplace shifted (subscripted) form of Equation (114) which is

$$(r_{11})\left\{\bar{S}_k\right\}_m^{(N_{flap})} = 0$$

is satisfied. Insertion of Equation (133) with i replaced by N_{flap} into the above expression and noting that the eleventh element in each $\left\{\bar{d}_{k,n}\right\}_m^{(N_{flap})}$ is zero in value results in the flapwise discontinuity equation

$$(r_{11})\sum_{n=-N_f}^{N_f}\left[\left[\bar{B}_{k,n}\right]_m^{(N_{flap})}\left\{\bar{S}_n\right\}_m^{*(Tip)} - \left\{\bar{b}_{k,n}\right\}_m^{(N_{flap})}\left\{\bar{\Delta}_n\right\}_m^{*c.t.}\right]$$

$$- (r_{11})\sum_{n=-N_f}^{N_f}\left\{\bar{c}_{k,n}\right\}_m^{(N_{flap})}\left\{\bar{\Delta}_n\right\}_m^{*fea} + (r_{11})\left\{\bar{H}_k\right\}_m^{(N_{flap})} = 0 . \qquad (140)$$

In conjunction with the swashplate equations of motion, Equations (136), (137), (139), and (140) provide the necessary relations to obtain the solution when aerodynamic coupling is included. The state vector at any section can be obtained by use of Equation (133) after the values for tip unknowns have been obtained.

Development of the Final Matrix Equations Governing Dynamic Forced Response Behavior of Rotor Blades Coupled Through a Swashplate

The basic governing equations have been developed which are necessary to represent the dynamic forced response behavior of a rotor blade system coupled with a swashplate or gyroscope control system. These equations, however, have not been combined to construct the final form of the matrix Equations which must be solved in order to obtain blade tip and control system unknowns. To accomplish this, the swashplate governing equations will be reduced to a coefficient form suitable for inclusion with an array coefficient form of the blade representation into a final matrix form. In addition, a similar coefficient form of the gyroscope equations will be constructed to replace the swashplate representation if this type of control is desired.

General coefficient representation of swashplate governing equations of motion.- The swashplate governing equation of motion, Equation (71), can be written in the form

$$\sum_{n=-\infty}^{\infty} \sum_{\ell=-\infty}^{\infty} \left\{ \left[m(s^2 - 2i\ell\Omega s - \ell^2\Omega^2) + \frac{2\pi F(\ell)}{R_{sp}^2} \right. \right.$$

$$- \left(\sum_{j=1}^{N_{e.s.}} (1 - b_j S_\ell) \overline{KC}_\ell e^{-i\ell\chi_j} \right) \frac{\left(\sum_{j=1}^{N_{e.s.}} (1 - b_j S_\ell) \overline{KC}_\ell e^{i\ell\chi_j} \right)}{\left(K + (s - i\ell\Omega) C + \sum_{j=1}^{N_{e.s.}} \overline{KC}_\ell \right)}$$

$$\left. + \sum_{j=1}^{N_{e.s.}} \left((1 - b_j S_\ell)^2 \overline{KC}_\ell + \frac{\ell^2}{R_{sp}^2} \overline{KC}_{\theta_\ell} + S_\ell^2 \overline{KC}_{\phi_\ell} \right) \right] \delta_q^\ell \delta_0^n$$

$$\left. + \left[\sum_{j=1}^{N_{e.s.}} \left(S_q S_\ell \overline{KC}_{\phi_q} + \frac{q\ell}{R_{sp}^2} \overline{KC}_{\theta_q} \right) e^{-i\chi_j(q-\ell)} \right] \right.$$

$$- \left(\sum_{j=1}^{N_{e.s.}} (1 - b_j S_q) \, \overline{KC}_q \, e^{-iq\chi_j} \right) \frac{\left(\sum_{j=1}^{N_{e.s.}} (1 - b_j S_\ell) \, \overline{KC}_q \, e^{i\ell\chi_j} \right)}{K + (s - iq\Omega) \, C + \sum_{j=1}^{N_{e.s.}} \overline{KC}_q}$$

$$+ \left[\sum_{j=1}^{N_{e.s.}} (1 - b_j S_\ell) \, (1 - b_j S_q) \, \overline{KC}_q \, e^{-i\chi_j (q-\ell)} \right]_{q \neq \ell} \delta^n_{q-\ell} \Bigg\} \bar{w}_\ell (s - in\Omega)$$

$$= \sum_{m=1}^{N_b} (1 + d_m S_q) \, \frac{(\overline{\Delta T})_m}{a_m} \, e^{-iq(\phi_m - \phi_{mp})} \qquad (141)$$

where δ^i_j is the Kronecker delta function defined such that

$$\delta^i_j = 1 \quad \text{for } i = j$$

and

$$\delta^i_j = 0 \quad \text{for } i \neq j \ .$$

Also, in obtaining Equation (141), the force in the control rods, $P_m(s)$, has been replaced by the control torques, $(\overline{\Delta T})_m$, divided by the respective control rod attachment point offset.

On observation of Equation (141), it appears that there would be more unknowns than equations because of the shifting of the Laplace transform variable. There is, however, an implicit relationship between $\bar{w}_\ell(s)$ and $\bar{w}_\ell(s - in\Omega)$. In this analysis, more equations are constructed from the basic ones by additional shifting of the Laplace transform variable such that s is replaced by $(s - ik\Omega)$ throughout Equation (141). The end result in general form is

$$\sum_{n=-\infty}^{\infty} \left[\sum_{\ell=-\infty}^{\infty} \bar{Z}^\ell_n \, \delta^\ell_q \, \delta^n_k + \sum_{\substack{\ell=-\infty \\ \ell \neq q}}^{\infty} \bar{X}^{k,n}_{q,\ell} \, \delta^{n+\ell}_{k+q} \right] \bar{w}_\ell (s - in\Omega)$$

$$= \sum_{m=1}^{N_b} (1 + d_m S_q) \frac{(\overline{\Delta T}_k)_m}{a_m} e^{-iq(\phi_m - \phi_{mp})} \qquad (142)$$

where

$$\overline{Z}_n^{\ell} = m\left[(s-in\Omega)^2 - 2i\ell\Omega(s-in\Omega) - \ell^2\Omega^2\right] + \frac{2\pi F(\ell)}{R_{sp}^2}$$

$$- \frac{\left[\sum_{j=1}^{N_{e.s.}} (1 - b_j S_\ell)\, \overline{KC}_{\ell+n}\, e^{-i\ell\chi_j}\right]\left[\sum_{j=1}^{N_{e.s.}} (1 - b_j S_\ell)\, \overline{KC}_{\ell+n}\, e^{i\ell\chi_j}\right]}{\left[K + (s-in\Omega-i\ell\Omega)\, C + \sum_{j=1}^{N_{e.s.}} \overline{KC}_{\ell+n}\right]}$$

$$+ \sum_{j=1}^{N_{e.s.}} \left[(1 - b_j S_\ell)^2\, \overline{KC}_{\ell+n} + \frac{\ell^2}{R_{sp}^2}\, \overline{KC}_{\theta\,\ell+n} + S_\ell^2\, \overline{KC}_{\phi\,\ell+n}\right] , \qquad (143)$$

$$\overline{X}_{q,\ell}^{k,n} = \sum_{j=1}^{N_{e.s.}} \left[S_q\, S_\ell\, \overline{KC}_{\phi\,\ell+n} + \frac{q\ell}{R_{sp}^2}\, \overline{KC}_{\theta\,\ell+n}\right] e^{-i\chi_j(q-\ell)}$$

$$- \frac{\left[\sum_{j=1}^{N_{e.s.}} (1 - b_j S_q)\, \overline{KC}_{\ell+n}\, e^{-iq\chi_j}\right]\left[\sum_{j=1}^{N_{e.s.}} (1 - b_j S_\ell)\, \overline{KC}_{\ell+n}\, e^{i\ell\chi_j}\right]}{\left[K + (s-in\Omega-i\ell\Omega)\, C + \sum_{j=1}^{N_{e.s.}} \overline{KC}_{\ell+n}\right]}$$

$$+ \sum_{j=1}^{N_{e.s.}} (1 - b_j S_\ell)\, (1 - b_j S_q)\, \overline{KC}_{\ell+n}\, e^{-i\chi_j(q-\ell)} \qquad (144)$$

Note that $(\overline{\Delta T}_k)_m$ which appears in Equation (142) is the same term which appears in Equation (138) and defined following that equation.

Final matrix form of equation for determination of unknown quantities.- The complete set of equations representing the coupled rotor-swashplate system can be written for the k denoted harmonic relative to that specified by the value used for the Laplace transform variable in the matrix form

$$\sum_{n=-N_f}^{N_f} \left[\bar{T}_{k,n}\right]\left\{\bar{q}_n\right\}^* + \left\{\bar{F}_k\right\}^* = \left\{0\right\} \qquad k = 0, \pm 1, \ldots \pm N_f \tag{145}$$

where $\left[\bar{T}_{k,n}\right]$ is representative of the terms multiplying the unknown quantities $\left\{\bar{q}_n\right\}^*$ and $\left\{\bar{F}_k\right\}^*$ consists of the forcing function terms for all blades and swashplate. All the terms involved may be obtained from Equations (136), (137), (139), (140) and (142).

The $\left[\bar{T}_{k,n}\right]$ array for a three-bladed rotor can be represented, utilizing integers for blade subscripts, as

$$\left[\bar{T}_{k,n}\right] = \begin{array}{|c|c|c|c|} \hline \left[\bar{S}_{k,n}\right] & \left[\bar{D}_{k,n}\right]_1 & \left[\bar{D}_{k,n}\right]_2 & \left[\bar{D}_{k,n}\right]_3 \\ \hline \left[\bar{C}_k\right]_1 \delta_n^k & \left[\bar{B}_{k,n}\right]_1 & 0 & 0 \\ \hline \left[\bar{C}_k\right]_2 \delta_n^k & 0 & \left[\bar{B}_{k,n}\right]_2 & 0 \\ \hline \left[\bar{C}_k\right]_3 \delta_n^k & 0 & 0 & \left[\bar{B}_{k,n}\right]_3 \\ \hline \end{array} \tag{146}$$

where, if the number of spacial harmonics retained in the swashplate is limited by letting the summation over ℓ range from $-N_{max}$ to N_{max}, for N_{max} equal 1 the swashplate impedances from Equation (142) are represented by

$$\left[\bar{S}_{k,n}\right] = \begin{array}{|c|c|c|} \hline \bar{Z}_n^{-1} \delta_k^n & \bar{X}_{-1,0}^{k,n} \delta_{k-1}^n & \bar{X}_{-1,1}^{k,n} \delta_{k-1}^{n+1} \\ \hline \bar{X}_{0,-1}^{k,n} \delta_k^{n-1} & \bar{Z}_n^0 \delta_k^n & \bar{X}_{0,1}^{k,n} \delta_k^{n+1} \\ \hline \bar{X}_{1,-1}^{k,n} \delta_{k+1}^{n-1} & \bar{X}_{1,0}^{k,n} \delta_{k+1}^n & \bar{Z}_n^1 \delta_k^n \\ \hline \end{array} \tag{147}$$

and swashplate coupling to the blade, m, is given by

$$\left[\bar{\mathcal{D}}_{k,n}\right]_m = \begin{bmatrix} & -(1 + d_m S_{-1}) \dfrac{\left[r_4\right]}{a_m}\left\{\bar{\lambda}_{k,n}\right\}_m^{c.t.} e^{i(\phi_m - \phi_{mp})} & 0 \\ \leftarrow 7 \text{ cols.} \rightarrow \text{ of zeros} & -(1 + d_m S_0) \dfrac{\left[r_4\right]}{a_m}\left\{\bar{\lambda}_{k,n}\right\}_m^{c.t.} & 0 \\ & -(1 + d_m S_1) \dfrac{\left[r_4\right]}{a_m}\left\{\bar{\lambda}_{k,n}\right\}_m^{c.t.} e^{-i(\phi_m - \phi_{mp})} & 0 \end{bmatrix} \tag{148}$$

The blade root condition and discontinuity equations provide the generalized impedances of the blade, m, as

$$\left[\bar{\mathcal{B}}_{k,n}\right]_m =$$

$$\begin{bmatrix} \left[\alpha\right]\left[\bar{\mathcal{B}}_{k,n}\right]_m^{(NS)} & -\left[\alpha\right]\left\{\bar{c}_{k,n}\right\}_m^{(NS)} & -\left[\alpha\right]\left\{\bar{b}_{k,n}\right\}_m^{(NS)} & -\left[\alpha\right]\left\{\bar{d}_{k,n}\right\}_m^{(NS)} \\ \left(r_4\right)\left[\bar{\mathcal{B}}_{k,n}\right]_m^{(N_{fea})} & 0 & -\left(r_4\right)\left\{\bar{b}_{k,n}\right\}_m^{(N_{fea})} & -\left(r_4\right)\left\{\bar{d}_{k,n}\right\}_m^{(N_{fea})} \\ -a_m \bar{Y}_m^k \left(r_3\right)\left[\bar{\mathcal{B}}_{k,n}\right]_m^{(N_{c.t.})} & 0 & k_m^{-1}\left(r_4\right)\left\{\bar{\lambda}_{k,n}\right\}_m^{(c.t.)} & a_m \bar{Y}_m^k \left(r_3\right)\left\{\bar{d}_{k,n}\right\}_m^{(N_{c.t.})} \\ \left(r_{11}\right)\left[\bar{\mathcal{B}}_{k,n}\right]_m^{(N_{flap})} & -\left(r_{11}\right)\left\{\bar{c}_{k,n}\right\}_m^{(N_{flap})} & -\left(r_{11}\right)\left\{\bar{b}_{k,n}\right\}_m^{(N_{flap})} & 0 \end{bmatrix} \tag{149}$$

and the blade coupling to the swashplate as

$$\left[\bar{C}_k\right]_m = \begin{bmatrix} & \uparrow \\ & 7 \text{ rows of zeros} \\ & \downarrow & \\ \bar{Y}_m^k (1 + d_m S_\ell) e^{-i(\phi_m - \phi_{mp})} & \bar{Y}_m^k (1 + d_m S_\ell) & \bar{Y}_m^k (1 + d_m S_\ell) e^{i(\phi_m - \phi_{mp})} \\ 0 & 0 & 0 \end{bmatrix} \tag{150}$$

It should be noted that $\left\{\bar{\lambda}_{k,n}\right\}_m^{c.t.}$, appearing in Equations (148) and (149) has a non-zero element only when k is equal to n.

The column of unknowns, $\left\{\bar{q}_n\right\}^*$, represents the blade and swashplate unknowns in the form of

$$\left\{\bar{q}_n\right\}^* = \left\{\begin{array}{c} \left\{\bar{r}_n\right\} \\ \hline \left\{\bar{p}_n\right\}_1 \\ \hline \left\{\bar{p}_n\right\}_2 \\ \hline \left\{\bar{p}_n\right\}_3 \end{array}\right\} \tag{151}$$

where in general,

$$\left\{\bar{r}_n\right\} = \left\{\begin{array}{l} \bar{w}_{-N_{max}}(s\text{-in}\Omega) \\ \vdots \\ \bar{w}_{-1}(s\text{-in}\Omega) \\ \bar{w}_0(s\text{-in}\Omega) \\ \bar{w}_1(s\text{-in}\Omega) \\ \vdots \\ \bar{w}_{N_{max}}(s\text{-in}\Omega) \end{array}\right\} \quad \text{and} \quad \left\{\bar{p}_n\right\}_m = \left\{\begin{array}{c} \left\{\bar{S}_n\right\}_m^{*(Tip)} \\ \hline \left\{\bar{\Delta}_n\right\}_m^{*fea} \\ \hline \left\{\bar{\Delta}_n\right\}_m^{*c.t.} \\ \hline \left\{\bar{\Delta}_n\right\}_m^{*flap} \end{array}\right\}. \tag{152}$$

The forcing function in Equation (145) can be expressed in the form

$$\left\{\bar{F}_k\right\}^* = \begin{Bmatrix} \left\{\bar{F}r_k\right\}^* \\ \hline \left\{\bar{F}p_k\right\}^*_1 \\ \hline \left\{\bar{F}p_k\right\}^*_2 \\ \hline \left\{\bar{F}p_k\right\}^*_3 \end{Bmatrix} \tag{153}$$

where $\left\{\bar{F}r_k\right\}^*$ consists of $(2N_{max}+1)$ zero elements and

$$\left\{\bar{F}p_k\right\}^*_m = \begin{Bmatrix} \left[\alpha\right]\left\{\bar{H}_k\right\}^{(NS)}_m \\ \hline \left(r_4\right)\left\{\bar{H}_k\right\}^{(N_{fea})}_m \\ \hline -a_m \bar{Y}^k_m \left(r_3\right)\left\{\bar{H}_k\right\}^{(N_{c.t.})}_m \\ \hline \left(r_{1,1}\right)\left\{\bar{H}_k\right\}^{(N_{flap})}_m \end{Bmatrix} \tag{154}$$

Modifications of final matrix representation for gyroscope control system.- If a gyro system is used, the Laplace transform variable s can be shifted by $ik\Omega$ in Equations (20), (21) and (22) and manipulated similar to the swashplate governing equation, Equation (71), such that the gyro governing equations can be written in the form similar to Equation (142) as

$$\sum_{n=-N_f}^{N_f} \sum_{\ell=-1}^{1} \left\{ \left[\overline{ZG}^{\ell}_n \delta^{\ell}_q + \overline{VG}^{\ell}_n \delta^{-\ell}_q \right] \delta^n_k + \overline{XG}^{k,n}_{q,\ell} \left[\left(\delta^{\ell}_q + \delta^{-\ell}_q \right) \left(\delta^n_{k-2} + \delta^n_{k+2} \right) \right] \right\} \bar{w}_{\ell}(s-in\Omega)$$

$$= - \sum_{m=1}^{N_b} \frac{(\overline{\Delta T}_k)_m}{a_m} \left(\delta^0_q + R_p \sin(\phi_m - \phi_{mp}) \delta^{-1}_q - R_p \cos(\phi_m - \phi_{mp}) \delta^1_q \right) \tag{155}$$

where

$$\bar{w}_{-1}(s-in\Omega) \triangleq \bar{\phi}_{x_r}(s-in\Omega)$$

$$\bar{w}_0\ (s-in\Omega) \triangleq \bar{z}(s-in\Omega) \tag{156}$$

$$\bar{w}_1\ (s-in\Omega) \triangleq \bar{\phi}_{y_r}(s-in\Omega)$$

and

$$\overline{ZG}_n^{-1} \triangleq I_{Gx}(s-in\Omega)^2 + \Omega^2(I_{Gz} - I_{Gy}) + \bar{K} + \bar{C}(s-in\Omega)$$

$$\overline{ZG}_n^{0} \triangleq M_G(s-in\Omega)^2 + C_G(s-in\Omega) + K$$

$$\overline{ZG}_n^{1} \triangleq I_{Gy}(s-in\Omega)^2 + \Omega^2(I_{Gz} - I_{Gx}) + \bar{K} + \bar{C}(s-in\Omega) \tag{157}$$

$$\overline{VG}_n^{\ell} \triangleq \ell[\Omega(I_{Gz} - I_{Gx} - I_{Gy})(s-in\Omega) - \Omega\bar{C}]$$

$$\overline{XG}_{q,\ell}^{k,n} \triangleq K_{\frac{k-n}{2},k}\left[\ell\frac{(k-n)}{2}\ \frac{(q-\ell)}{2}\ i - \frac{(q+\ell)}{2}\right]$$

where

$$K_{b,k} \triangleq [K' + b\Omega C'i + C'(s-ik\Omega)].$$

From Equation (155), for a gyro instead of a swashplate, Equation (147) would be replaced with

$$\left[\bar{S}_{k,n}\right] = \left[\begin{array}{c|c|c} \overline{ZG}_n^{-1}\delta_k^n + \overline{XG}_{-1,-1}^{k,n}\left(\delta_{k-2}^n + \delta_{k+2}^n\right) & 0 & \overline{VG}_n^{1}\delta_k^n + \overline{XG}_{-1,1}^{k,n}\left(\delta_{k-2}^n + \delta_{k+2}^n\right) \\ \hline 0 & \overline{ZG}_n^{0}\delta_k^n & 0 \\ \hline \overline{VG}_n^{-1}\delta_k^n + \overline{XG}_{1,-1}^{k,n}\left(\delta_{k-2}^n + \delta_{k+2}^n\right) & 0 & \overline{ZG}_n^{1}\delta_k^n + \overline{XG}_{1,1}^{k,n}\left(\delta_{k-2}^n + \delta_{k+2}^n\right) \end{array}\right] \tag{158}$$

where use has been made of the fact that $\overline{XG}^{k,n}_{0,0}$ and $\overline{VG}^{0}$ are zero. In addition, Equation (148) would be replaced with

$$\left[\bar{\mathcal{D}}_{k,n}\right]_m = \begin{bmatrix} & + R_p \frac{\left(r_4\right)}{a_m} \left\{\bar{\lambda}_{k,n}\right\}^{c.t.}_m \sin(\phi_m - \phi_{mp}) & 0 \\ \leftarrow 7 \text{ cols.} \rightarrow \text{ of zeros} & + \frac{\left(r_4\right)}{a_m} \left\{\bar{\lambda}_{k,n}\right\}^{c.t.}_m & 0 \\ & - R_p \frac{\left(r_4\right)}{a_m} \left\{\bar{\lambda}_{k,n}\right\}^{c.t.}_m \cos(\phi_m - \phi_{mp}) & 0 \end{bmatrix} \quad . \quad (159)$$

The control torque discontinuity equation for the gyro representation, Equation (113), would result in the replacement of Equation (150) with

$$\left[\bar{C}_k\right]_m = \begin{bmatrix} & \uparrow \\ & 7 \text{ rows of zeros} \\ & \downarrow & \\ - R_p \bar{Y}^k_m \sin(\phi_m - \phi_{mp}) & -\bar{Y}^k_m & R_p \bar{Y}^k_m \cos(\phi_m - \phi_{mp}) \\ 0 & 0 & 0 \end{bmatrix} \quad (160)$$

Having reduced the analysis to the matrix form of Equation (145), the method of solution and wake iteration scheme can now be presented.

Solution Scheme For Obtaining Forced Response Unknowns and Wake Iteration Procedure

In the previous analytical section, the necessary expressions have been obtained to enable solution for the dynamic response variables for a helicopter rotor system coupled with a swashplate or gyroscope control system. This section is concerned with the basic solution to obtain values for the swashplate and blade tip unknowns, harmonically, and subsequent determination of the state vector variables and with the extension of this basic solution scheme to incorporate the effects of a deformed free wake on the dynamic response variable involved.

Solution scheme to obtain swashplate and blade tip unknowns.- In the development of analysis, use has been made of Laplace transform variables such as $(s-in\Omega)$ where the integer, n, represents the harmonic shift relative to the particular harmonic of interest which has previously been denoted as Np. To solve for the Np/rev. swashplate and blade tip unknowns, the value of s in the analytical expressions necessary to obtain the terms involved in Equation (145) is taken as $iNp\Omega$. Thus, these terms will be dependent on the value of Np in addition to the values of k and/or n. Consideration of Equation (145) for $-N_f \leq k \leq N_f$ results in a matrix equation of the form exemplified by taking $N_f=1$ which is

$$\begin{bmatrix} [\bar{T}_{-1,-1}] & [\bar{T}_{-1,0}] & [\bar{T}_{-1,1}] \\ [\bar{T}_{0,-1}] & [\bar{T}_{0,0}] & [\bar{T}_{0,1}] \\ [\bar{T}_{1,-1}] & [\bar{T}_{1,0}] & [\bar{T}_{1,1}] \end{bmatrix} \begin{Bmatrix} \{\bar{q}_{-1}\}^* \\ \{\bar{q}_0\}^* \\ \{\bar{q}_1\}^* \end{Bmatrix} = - \begin{Bmatrix} \{\bar{F}_{-1}\}^* \\ \{\bar{F}_0\}^* \\ \{\bar{F}_1\}^* \end{Bmatrix} \tag{161}$$

and when multiplied by the inverse of the square matrix yields the solution for the unknowns as

$$\begin{Bmatrix} \{\bar{q}_{-1}\}^* \\ \{\bar{q}_0\}^* \\ \{\bar{q}_1\}^* \end{Bmatrix} = - \begin{bmatrix} [\bar{T}_{-1,1}] & [\bar{T}_{-1,0}] & [\bar{T}_{-1,1}] \\ [\bar{T}_{0,-1}] & [\bar{T}_{0,0}] & [\bar{T}_{0,1}] \\ [\bar{T}_{1,-1}] & [\bar{T}_{1,0}] & [\bar{T}_{1,1}] \end{bmatrix}^{-1} \begin{Bmatrix} \{\bar{F}_{-1}\}^* \\ \{\bar{F}_0\}^* \\ \{\bar{F}_1\}^* \end{Bmatrix} \tag{162}$$

where the $[\bar{T}_{k,n}]$ arrays consist of Laplace transform operators and time dependent constants and the column arrays represent harmonics above, below, and at the harmonic of interest depending on the value of the subscript as referred to in the section pertaining to interpretation of the use of shifted Laplace transform variables. Thus, for a given value of Np, N_f, and N_{max}, Equation (161) can be constructed and solved by Equation (162) for the (Np+1)/rev.,

Np/rev., and (Np-1)/rev. blade tip and swashplate unknowns.

Determination of the total state vector variable distributions.- Once the unknowns are obtained by Equation (162) for s equal to iNpΩ, Equation (133) is used with k equal to zero to determine the Np/rev. state vector variable harmonic coefficients at the inboard end of each blade section. For a particular state vector variable, for example $\bar{V}_z^{(i)},Np$, which is the Np/rev. harmonic coefficient of the shear force in the local z direction inboard of the ith section, is obtained in the form

$$\bar{V}_z^{(i)},Np = A_{Np}^{(i)} + B_{Np}^{(i)}\, i \quad . \tag{163}$$

As previously noted the state vector variables can be expressed in a Fourier series form such that for example

$$V_z^{(i)-}(t) = \sum_{Np=0}^{\infty} \bar{V}_z^{(i)},Np\; e^{iNp\Omega t}$$

Taking advantage of the fact that -n/rev. harmonic coefficients are complex conjugates of the +n/rev. harmonic coefficients, substitution of Equation (163) into the last expression yields

$$V_z^{(i)-}(t) = \sum_{Np=0}^{\infty} \left[\left(A_{Np}^{(i)} + B_{Np}^{(i)} i \right) e^{iNp\Omega t} + \left(A_{Np}^{(i)} - B_{Np}^{(i)} i \right) e^{-iNp\Omega t} \right]_{Np\neq 0} \tag{164}$$

where $B_0 = 0$.

This can also be written in the form

$$V_z^{(i)-}(t) = A_0^{(i)} + 2 \sum_{Np=1}^{\infty} R_{Np}^{(i)} \cos\left(Np\Omega t + \beta_{Np}^{(i)} \right) \tag{165}$$

where

$$R_{Np}^{(i)} = \sqrt{A_{Np}^{(i)\,2} + B_{Np}^{(i)\,2}} \tag{166}$$

and

$$\beta_{Np}^{(i)} = \arctan\left(\frac{B_{Np}^{(i)}}{A_{Np}^{(i)}}\right) \tag{167}$$

If ψ_k represents the azimuthal position of the blade relative to its position at t = 0, Equation (165) can be written as

$$V_z(\psi_k)^{(i)} = A_0^{(i)} + 2\sum_{Np=1}^{\infty} R_{Np}^{(i)} \cos\left(Np\psi_k + \beta_{Np}^{(i)}\right) \tag{168}$$

which represents the real value of the shear force acting perpendicular to the chord at ψ_k for section (i).

Other time dependent state vector variables can be obtained utilizing the same representation as in Equation (168) where the harmonic coefficients used would correspond to the variable of interest. To obtain the total state vector variables as a function of blade radius and azimuthal position the harmonic coefficients for each state vector variable must be determined for successively increasing values of N_p (beginning with zero) until the magnitude of the harmonic coefficients can be considered to be negligible compared to the lower harmonic coefficients. The harmonic coefficients for each state vector variable can then be utilized in the form of Equation (168) with the upper limit on the summation being determined by the highest non-negligible harmonic to obtain the radial and azimuthal distribution of the state variable of interest.

Solution scheme for inclusion of deformed free-wake effects on dynamic response.- The inclusion of the effects of a free wake utilizes the previously discussed solution scheme used when free-wake effects are not included as an integral part of an iterative procedure which allows the blade response and free-wake to interact.

The free-wake effect is initially taken into account by using the wake-induced velocity influence coefficient matrix (σ-matrix) and the bound circulation matrix (Γ-matrix) generated by the free-wake program to compute the wake induced velocities at the blade aerodynamic section azimuthal locations. With the initial induced velocity distribution known, these values are introduced into the analysis for proper determination of angles of attack and aerodynamic loads and moments at azimuthal positions for each aero-

dynamic section. This information allows the construction of the aerodynamic transfer matrices necessary for the determination of the blade dynamic response in terms of a summation of the steady and harmonic response.

From the dynamic response, in particular shear force quantities, a radial and azimuthal lift distribution acting on the blades can be obtained. This distribution includes the effects due to blade response which in turn is a function of the initial velocity field. To facilitate the determination of lift values, the blade sections with aerodynamics representation are taken to consist of only aerodynamic characteristics such that a difference in the shear forces acting on the inboard end of the aerodynamic blade section and inboard end of the previous outboard non-aerodynamic blade section can be utilized to obtain the actual lift forces acting on the aerodynamic blade section. For consistency in shear force vector orientation to insure proper shear difference determination both the aerodynamic and the previous outboard non-aerodynamic blade section must have the same local coordinate system (i.e., the values for Φ, Θ, Ψ must be identical for both sections).

The actual shear forces applied to an aerodynamic blade section, i, at the azimuthal position, ψ_k, due to aerodynamic and blade response effects on this section can be expressed as

$$\Delta\left[V_z(\psi_k)^{(i)}\right] = V_z(\psi_k)^{(i)} - V_z(\psi_k)^{(i-1)}$$

$$\Delta\left[-V_y(\psi_k)^{(i)}\right] = -V_y(\psi_k)^{(i)} - \left[-V_y(\psi_k)^{(i-1)}\right] \tag{169}$$

where the (i-1) superscript denotes the previous outboard non-aerodynamic blade section. The shear force, $V_z(\psi_k)^{(i)}$, which has been defined by Equation (168) is the force acting on the outboard end of the (i+1)th section in the local blade coordinate system z direction (perpendicular to the blade section chordline not perturbed by cyclic pitch). The shear force, $-V_y(\psi_k)^{(i)}$, which is defined by a similar form of Equation (168) is the force acting on the outboard end of the (i+1)th section in the local blade coordinate system -y direction (parallel to the blade section chordline not perturbed by cyclic pitch). It should be noted that the direction of the local blade coordinate system z axis does not coincide with the direction of lift acting on the blade.

The lift distribution acting on the ith aerodynamic blade section at the kth azimuthal position with variable induced velocity and blade response effects included can be defined as

$$L_k^{(i)} = \Delta\left[V_z(\psi_k)^{(i)}\right]\cos\alpha_k^{(i)} - \Delta\left[-V_y(\psi_k)^{(i)}\right]\sin\alpha_k^{(i)} \quad . \qquad (170)$$

where the angle, $\alpha_k^{(i)}$, is the angle between the section chord line (zero cyclic pitch) and the resultant velocity vector acting on the ith aerodynamic blade station at the kth azimuthal position. This angle is defined approximately by the expression

$$\alpha_k^{(i)} \simeq \alpha_{i,k} - \alpha_{c_k}$$

where α_{c_k} is the cyclic pitch, defined positive for airfoil leading edge rotated upward, and $\alpha_{i,k}$ is the angle of attack of airfoil including cyclic pitch at section, i, and azimuthal position denoted by ψ_k determined during the previous blade dynamic response calculations. Thus, in order to determine the lift distribution as in Equation (170) it is necessary to consider several harmonic coefficients of the shear forces for use in the form of Equation (168) and subsequently in Equations (169).

A new nondimensional circulation distribution, $\Gamma_k^{(i)}$, previously termed Γ-matrix, is obtained by use of the expression

$$\Gamma_k^{(i)} \simeq L_k^{(i)} / \left[\rho\, V_k^{(i)}\, L^{(i)}\, \Omega R^2\right] \qquad (171)$$

where $L^{(i)}$ is the effective length of the ith aerodynamic section and $V_k^{(i)}$ is amplitude of the resultant velocity vector determined during the previous blade dynamic response calculations acting on the ith aerodynamic section at the kth azimuthal location. In the aerodynamic representation the aerodynamic loading is applied at a point but the loading values represent that due to an effective spanwise aerodynamic length, $L^{(i)}$, over which length the aerodynamic characteristics such as angle of attack and velocities are identical. This method of determining the new nondimensional circulation distribution is an approximation since both the angle of attack and velocity distributions used are those obtained during the previous dynamic response calculations (iteration) since the exact values are unobtainable.

The new $\Gamma_k^{(i)}$ is combined with the old [σ]-matrix from the free-wake program tc obtain a new nondimensional induced velocity distribution which when multiplied by ΩR results in a new induced velocity distribution reflecting the coupling of the wake to the blade motions. This distribution can then be reinserted into the aerodynamic analysis and a new lift, circulation, and induced velocity distribution obtained. This process can be repeated until the desired degree of accuracy (or repeatability) is established at which time additional higher harmonics, not required during the wake iteration procedure, may be calculated. This section concludes the discussion of the analytical representation required to investigate the effects of a nonuniform swashplate on the dynamic response, and control loads of a helicopter.

APPLICATION OF COMPUTER PROGRAM

The computer program developed on the basis of the analytical study was utilized to obtain the blade dynamic response of a four bladed H-34 rotor system model with various collective and cyclic control system stiffnesses. The results obtained showed only minor effects on blade dynamic response due to changes in the support system stiffness characteristics since the H-34 system is stiff and restricts interblade coupling which would alter the natural frequencies and result in additional frequencies as was seen in the investigation of the much softer OH-6A support system investigated in reference 2. The use of artificial elastic axis and mass offsets originally used to enhance coupling, instead of the zero values the H-34 blade normally has, resulted in steady and harmonic pitch horn loads altered significantly from those obtained from experimental results. This section will be concerned with the flight condition and swashplate control system configurations for which the computer program was executed and some of the results obtained. It should be noted that the SI system of units will be used for purposes of discussion although the British system of units were employed in the actual program execution.

The fundamental H-34 rotor system information was obtained from reference 3. The model of the blade (lumped parameter model) was based on the blade model employed for reference 1 with some modification to reduce the number of stations representing the mass, elastic, and geometric blade characteristics. This data included elastic axis and mass offsets which were originally thought to have little, if any, significant effect on the results. The final blade data employed is presented in Appendix A in tabular form. The aerodynamic effects on the blade were included by using eight aerodynamic stations with effective aerodynamic lengths to represent the NACA 0012 airfoil which begins at 1.397 meters from the axis of rotation and ends at the blade tip. The effective aerodynamic length of the outboard aerodynamic section

was modified to take into account tip losses. The blades had a uniform blade twist of -.139626 radians (outboard sections rotated leading edge down compared to inboard sections) over the blade airfoil length. On the basis of measurements reported in reference 3 the blade steady coning angle used was -.07854 radians (blade coned upward) and the lag angle used was -.10472 radians (blade lagged aft). The pitch bearing (feathering), lead-lag hinge (sweep), and flap hinge were located .3048 meters from the rotor hub centerline and oriented going inboard to outboard in the order; flap, lead-lag, and pitch.

The control rods were attached to the blade shaft by the pitch horn ahead of the blade pitch axis a distance of .20318 meters. Attempts to acquire information concerning the breakdown of the H-34 swashplate support system stiffnesses were not successful. Reference 3 provided a value of approximately 78,638 Newton-meters per radian for the control system stiffness. Using this value as a basis, a collective system stiffness of 32,091 Newton-meters per radian and lateral and longitudinal cyclic control system stiffnesses of 63,307 Newton-meters per radian were chosen as the reference uniform stiffness characteristics of the control system. Torsional response calculations were carried out for five flight conditions consisting of one cruise speed flight, μ=.172; one high speed flight, μ=.291; one right turn, μ=.235 and 1.34g loading; one left turn, μ=.244 and 1.35g loading; and for one pullup, μ=.223 and a 1.4g loading. The values for the advance ratio, μ, given above are based only on the ratio of forward speed to rotational tip speed and do not include induced effects. Of these five flight conditions the first (cruise flight) was not based directly on a flight case in reference 3 since the desired advance ratio was not available whereas the remaining four are based in the order given on the experimental flights referred to as Flight 16, Flight 39, Flight 40, and Flight 89 (Data Table 123), respectively, in reference 3. From these experimental conditions and ones similar to the cruise flight condition, values for the forward speed, rotational speed, air density, shaft tilt angles, collective pitch angle, and cyclic pitch angles were obtained.

The program was initially executed for the five flight conditions with the reference uniform control system stiffness and with uniform downwash velocities based on Gessow and Myers (see reference 4) to ascertain if the necessary thrust was being obtained and also to obtain the steady and one per rev flap motions necessary for the wake geometry program developed in reference 1. The resultant steady thrust values per blade obtained from these runs were much less than the weight of the aircraft. To increase the thrust for each case, the values of lateral and longitudinal cyclic pitch angles were fixed slightly decreased from the original values while maintaining the same azimuthal position of maximum negative cyclic (defined as β radians ahead of the position ψ=0 degrees in our convention or ψ=90 degrees in the standard

convention) and the collective pitch increased. For each flight the effects of an increase in collective pitch angle increased the thrust in essentially a linear fashion (straight line curve) such that the necessary collective pitch values for the desired thrust could be obtained by interpolation. The criterion for the proper thrust per blade in forward flight was that the value for thrust should be between 12,788.6 Newton's (average weight of helicopter divided by the number of blades, four for the H-34 helicopter) and 12,010.2 Newton's (the first value minus the blade weight) since the program internally considers the blade weight effects. For the maneuver type conditions the g factor was applied to the upper and lower limits to obtain the desired thrust range. The resulting collective and cyclic pitch input values obtained for each flight condition to yield the required thrust and, in addition, the uniform downwash velocities and the resultant thrust per blade are presented in Table I. The method utilized to obtain cyclic and collective pitch values represents only a trimming of control variables in regards to thrust values and does not include criteria related to roll and pitch moment values.

The sets of control system stiffness values utilized by the program with various flight conditions were chosen to allow a rough determination of the general effect of changes in collective stiffness, cyclic stiffness, or the control rod stiffness on the blade dynamic response behavior in addition to verification of correct program operation. The parameters which were previously presented, necessary to define the lateral cyclic, longitudinal cyclic and collective control system stiffness, are the linear spring stiffnesses; k_j, K and k_m; the linear offsets; b_j, d_m, and a_m; the location angles; ϕ_m and χ_j; and the integer controls; N_b and $N_{e.s.}$. With the assumption of four blades equally spaced and the offsets b_j and d_m equal to zero, the collective stiffness, lateral cyclic stiffness, and longitudinal cyclic stiffness can be expressed in the form*:

$$K_{coll.} = a_m^2 \Big/ \left(1/k_m + N_b \Big/ \sum_{j=1}^{N_{e.s.}} k_j + N_b / K \right)$$

$$K_{lat.} = \left(a_m^2 \sum_{j=1}^{N_{e.s.}} k_j \cos^2\chi_j \right) \Big/ \left[2 + \left(\sum_{j=1}^{N_{e.s.}} k_j \cos^2\chi_j \right) / k_m \right]$$

$$K_{long.} = \left(a_m^2 \sum_{j=1}^{N_{e.s.}} k_j \sin^2\chi_j \right) \Big/ \left[2 + \left(\sum_{j=1}^{N_{e.s.}} k_j \sin^2\chi_j \right) / k_m \right]$$

*The derivation of these equations is available in reference 5 which is the documentation pertaining to this computer program.

TABLE I

FLIGHT CASE PITCH AND RESULTANT THRUST VALUES

Case	Condition	Collective Pitch (rad)	Cyclic Pitch Amplitude (rad)	β (rad)	Uniform Downwash (m/sec)	Thrust Range (N)	Thrust Obtained (N)
1	forward flight μ=0.291	0.305	0.1412	0.4030	1.8288	12,010.2-12,788.6	12,699.7
2	forward flight μ=0.172	0.263	0.1089	0.4089	2.7432	12,010.2-12,788.6	12,481.7
3	right turn μ=0.235, 1.34g	0.305	0.1223	0.4245	2.7432	16,093.7-17,136.8	16,792.0
4	left turn μ=0.244, 1.35g	0.305	0.1197	0.4785	2.7432	16,217.8-17,264.7	16,769.8
5	pull-up μ=0.223, 1.4g	0.264	0.1293	0.3920	2.7432	16,814.3-17,904.1	17,543.8

These expressions, assuming three equally spaced elastic supports (i.e. $N_{e.s.} = 3$, $\chi_1 = 0$, $\chi_2 = \frac{2\pi}{3}$, and $\chi_3 = \frac{4\pi}{3}$), were used to obtain the control system collective, lateral cyclic, and longitudinal cyclic stiffnesses corresponding to given sets of input values for the variables associated with the linear spring-damper units involved in the representation of the swashplate control system. The input spring-damper stiffness values which were used and the resulting collective, lateral cyclic, and longitudinal cyclic control system stiffnesses are presented in Table II.

Wake iteration program runs were executed for various combinations of flight conditions and control system stiffness configurations using the steady, one per rev., and two per rev. dynamic responses to determine the induced velocity distribution for each subsequent iteration. All of these runs are listed by flight conditions in Table III with information as to the rotor rotational speed, Ω (radians/second); forward flight speed, V (meters/second); air density, ρ (kilograms/cubic meter); and shaft tilt angle, α_s (radians above the position of the shaft parallel to the direction of forward flight). The run code consists of a numeric character signifying the flight condition involved and an alphabetic character denoting the control system stiffness configuration used. The resulting steady blade root; pitch angle (positive leading edge rotated upward), coning angle (positive blade tip rotated downward), lead-lag angle (positive blade tip rotated forward), and thrust per blade are also included.

The blade root angles are obtained by adding the resulting blade root perturbation angles; ϕ_x, ϕ_y, and ϕ_z; in respective order to the collective pitch, coning, and lead-lag input values corresponding to the flight condition involved. The steady blade root pitch, coning, and lead-lag values in Table III are their respective values just outboard of the feathering bearing, flap hinge, and lead-lag hinge, respectively. The changes in the steady blade root coning and lead-lag angles from their respective input values are more pronounced than the changes in the steady blade root pitch angles from their input values. This is due to the fact that the input coning and lead-lag angles are only approximate and define the orientation of the blade spanwise axis in the local coordinate system (reference system for determination of response variables) as if the blade was rigidly rotated about the flap and lead-lag hinge axes. When the blade is allowed to respond to the applied forces and moments, as in a dynamic response calculation, the blade may deflect significantly from the reference positions at each radial section including blade root position. The change in steady root pitch is directly related to the control system collective stiffness which in the runs executed was sufficiently high such that only a very small steady pitch angle perturbation

TABLE II

INPUTTED STIFFNESSES AND RESULTANT SYSTEM STIFFNESS

Case	k_1 (N/m)	k_2, k_3 (N/m)	K (N/m)	k_m (N/m)	$K_{coll.}$ (N-m/rad)	$K_{lat.}$ (N-m/rad)	$K_{long.}$ (N-m/rad)
A	4,159,256.	1,459,388.	5,837,552.	14,593,880.	31,307.4	86,452.6	42,041.0
B	1,489,495.	2,742,934.	6,204,938.	14,593,880.	32,092.3	53,792.5	74,448.1
C	2,284,259.	2,284,259.	6,304,556.	14,593,880.	32,090.9	63,306.8	63,306.8
D	3,160,757.	1,907,318.	6,204,209.	14,593,880.	32,090.9	74,448.4	53,792.7
E	3,160,757.	1,907,318.	6,204,209.	3,648,470.	27,669.7	54,316.4	42,429.6
F	3,160,757.	1,907,318.	6,204,209.	7,296,940.	30,467.9	66,262.0	35,825.9
G	6,958,143.	1,094,541.	5,122,452.	3,648,470.	27,669.9	76,384.2	27,669.9
H	6,958,143.	1,094,541.	5,122,452.	7,296,940.	30,468.0	102,326.0	30,467.9
I	4,568,519.	4,568,519.	12,609,112.	14,593,880.	60,935.7	114,576.4	114,576.4
J	5,064,076.	1,503,170.	7,296,940.	11,675,104.	36,557.5	96,124.5	42,450.8

TABLE III

PROGRAM RUNS EXECUTED

Run	Flight Variable	Steady Root Values			
		Pitch (rad)	Coning (rad)	Lead-lag (rad)	Thrust (N)
1-C	Ω=22.4100 V=55.5993 ρ=1.09775 α_s=1.4661	0.29943	-0.08112	-0.13617	12,082.7
1-D		0.29919	-0.08126	-0.13615	12,108.1
1-I		0.30203	-0.08369	-0.13840	12,428.3
1-J		0.29910	-0.08151	-0.13572	12,147.6
2-C	Ω=22.4000 V=32.9581 ρ=1.08229 α_s=1.5208	0.25773	-0.08147	-0.10053	12,112.5
2-D		0.25754	-0.08145	-0.10003	12,110.7
2-E		0.25672	-0.08070	-0.09983	12,012.4
2-F		0.25726	-0.08119	-0.09997	12,077.8
2-G		0.25495	-0.07952	-0.09814	11,862.5
2-H		0.25548	-0.08001	-0.09828	11,927.0
2-I		0.26019	-0.08367	-0.10123	12,401.6
2-J		0.25748	-0.08159	-0.09943	12,132.5
3-A	Ω=22.8290 V=45.8179 ρ=1.08229 α_s=1.5202	0.29767	-0.10374	-0.11018	15,795.2
3-B		0.29868	-0.10381	-0.11170	15,790.3
4-A	Ω=22.5150 V=46.8479 ρ=1.08229 α_s=1.5179	0.29767	-0.10463	-0.10809	15,782.7
4-B		0.29868	-0.10467	-0.11031	15,773.8
5-A	Ω=23.0380 V=43.7602 ρ=1.08229 α_s=1.6545	0.25697	-0.09688	-0.15158	15,138.2

was necessary to counteract the blade torque at the control torque application point in order to have zero torque at the pitch bearing.

Comparison of blade root thrust values presented in Table I (thrust trim runs) and Table III (wake iteration runs) provides information as to the effect of inclusion of free-wake effects in the induced velocity distribution determination on the blade root thrust value. In the high speed forward flight condition, the thrust value dropped from 12,699.7 Newtons with a uniform induced velocity field to 12,082.7 Newtons with the free-wake generated induced velocity field (∿5% drop) where the same control system stiffness, stiffness case C, was employed. In the cruise speed forward flight condition, the thrust value dropped from 12,481.7 Newtons to 12,112.5 Newtons (∿3% drop). In a similar manner, using thrust values from Table III corresponding to the control system stiffness case B which has essentially the same collective control system stiffness as that in control system stiffness case C, the effect of including the free-wake effects in the maneuver flight conditions resulted in; a drop in the thrust from 16,792.0 Newtons to 15,790.3 Newtons (∿6% drop) for the right turn maneuver, a drop in the thrust from 16,769.8 Newtons to 15,773.8 Newtons (∿6% drop) for the left turn maneuver, and a drop in the thrust from 17,543.8 Newtons to 15,138.2 Newtons (∿14% drop) for the pullup maneuver. Thus, the inclusion of free-wake effects in the blade response calculations significantly reduced the thrust per blade compared to that obtained with blade response calculations utilizing a uniform downwash distribution. However, the above percentages are dependent upon the input uniform induced velocity value used in each flight condition to determine the base thrust value.

The independent effects of the control system; collective stiffness, lateral cyclic stiffness, and longitudinal cyclic stiffness; on the behavior of the four steady root variables presented in Table III cannot be ascertained in detail since the number of control system stiffness configurations for any one flight case is not sufficient to separate the cause and effect relationships involved. However, some general behavior characteristics of the steady root variables can be noted. Except for a few exceptions, the absolute values of the four steady root variables behave in the same manner as a result of a change in control system stiffness configuration. That is, for a given change in control system stiffness parameters all of the variables either increased or decreased in absolute value. Control system collective stiffness changes appear to be the dominant contributing factor to changes in the values for the steady root variables as would be expected. This conclusion is borne out to some extent by noting that of the runs pertaining to the cruise forward flight condition the highest absolute values for the steady root variables were obtained with the stiffest stiffness configuration, stiffness

case I, where the control system collective stiffness was 60,935.7 Newtons-meters/radian and the lowest absolute values for the steady root variables were obtained for stiffness case G in which the control system collective stiffness was 27,669.9 Newton-meters/radian.

The results of the program runs were scanned to verify that the analysis operational in the computer program was performing correctly. The dynamic response variables; blade slopes, blade displacements, blade shears, blade moments, pitch horn loads (control loads), and swashplate control system deflections; resulting from each run in harmonic form were observed to satisfy all boundary conditions and discontinuity conditions employed by the program. Due to the magnitude of the values used in the control system stiffness configurations only minor changes resulted in the dynamic response variables as a result of changes in control system stiffness characteristics. Some of the harmonic results were employed to generate azimuthal distributions for comparison with experimental results obtained in reference 3. With the exception of pitch horn load distributions and torsional moment (blade torque) distributions the results compared favorably with the experimental results considering that the values for collective and cyclic pitch were different than those measured in reference 3 and that only the steady, one per rev. and two per rev. shear responses were utilized to obtain the free-wake generated variable induced velocity fields.

The large discrepancy between the theoretically predicted and experimentally obtained pitch horn loading azimuthal distributions was investigated to ascertain its probable cause. This discrepancy in predicted and experimental pitch horn loadings for the high speed forward flight condition is depicted in Figure 10, which represents the pitch horn loading azimuthal distribution obtained from program run 1-C and that obtained from reference 3. The sign convention for the pitch horn loading was based on assuming the pitch horn load to be positive when its effect is counteracting a positive blade torque (positive for moment tending to rotate the blade leading edge upward). Thus, for the H-34 helicopter rotor system in which the control rod is attached to the pitch horn ahead of the pitch axis, a positive pitch horn load represents a downward force applied to the pitch horn with the control rod being in tension. The azimuthal variable utilized in Figure 10 corresponds to the standard definition of azimuthal location (i.e. $\psi_{standard}$ is zero when blade is directly aft) and not the azimuthal reference variable utilized in the analysis. This required the theoretical pitch horn loading to be determined relative to the reference variable, ψ, used in the analysis and then plotted at $\psi_{standard}$ equal to $\psi + \pi/2$. The values for the pitch horn loading harmonics were obtained by dividing the (ΔT) variable outputted in the solution vector for each harmonic by the distance, a_m,

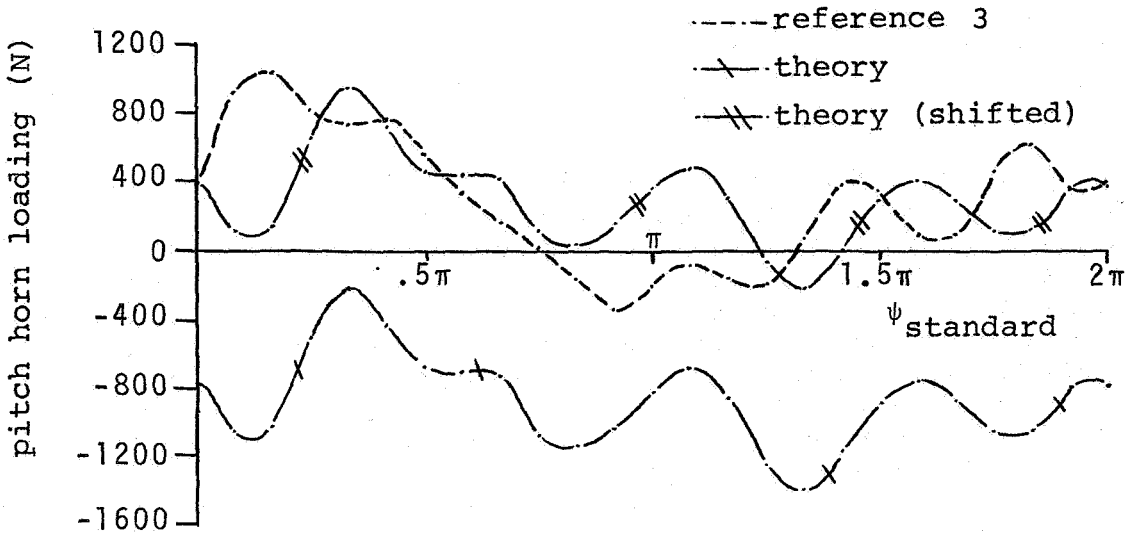

Figure 10. Azimuthal pitch horn loading for the high speed flight

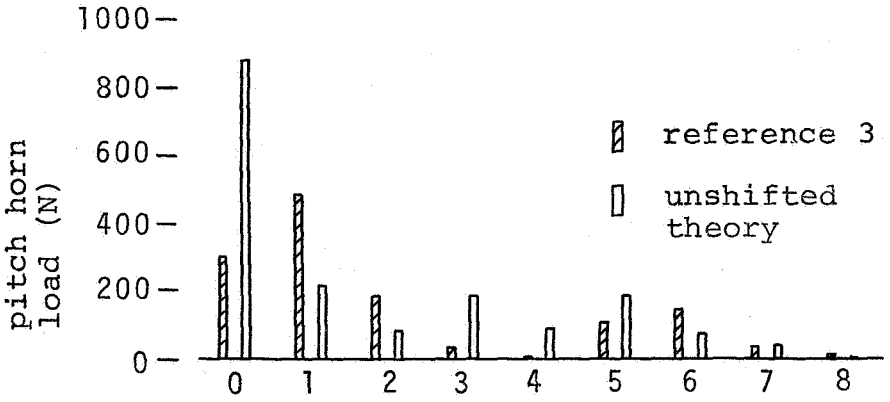

Figure 11. Harmonic content of pitch horn loading for high speed flight

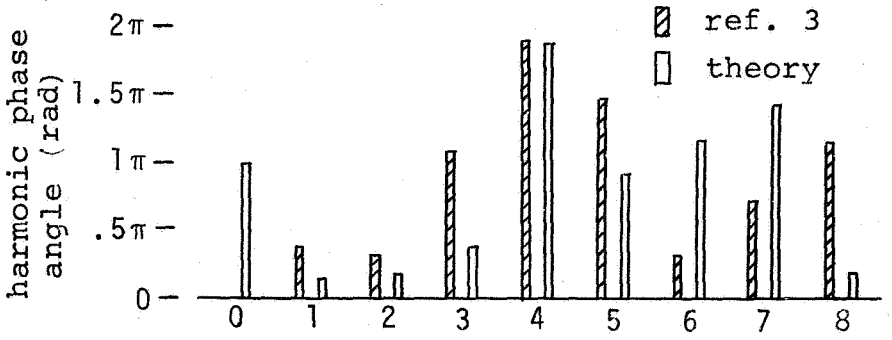

Figure 12. Phasing associated with the harmonic content of pitch horn loading for high speed flight

where, depending on the blade model, the (ΔT) harmonic is equal or approximately equal to the blade torque harmonic of the section outboard of the section inboard of which the control torque is applied.

On comparison of the theoretically and experimentally determined pitch horn loading distributions it is obvious that a significant difference in the steady component occurs. The experimental results obtained from reference 3 were harmonically analyzed to obtain the harmonic amplitudes and associated phase angles for comparison with the corresponding theoretical values. The pitch horn loading harmonic content, amplitude and phasing, of the theoretical and experimental distributions shown in Figure 10 is compared in Figures 11 and 12. The harmonic content shown in these figures has been determined relative to the azimuthal position defined by the reference variable, ψ, equal to zero. By taking the theoretical steady pitch horn to be that of the experimental data and using the theoretical harmonics, a third distribution (shifted) was obtained and added to Figure 10. The shifted theoretical curve is in better agreement with the experimental results. It can be concluded that a primary difference in the experimental and theoretical results is the magnitude and sign of the steady pitch loads.

In an investigation to determine the cause of the large steady negative pitch horn loads, it was found that the mass and elastic offsets reported for the H-34 blade in reference 1 and used in the present analysis were the significant contributors to large steady feathering torques which are directly related to steady pitch horn loadings. In the high speed flight condition the center of mass offsets of 0.00417 meters ahead of the neutral axis combined with perturbation quantities and centrifugal force components for all mass stations occurring outboard of the airfoil cutout was found to contribute approximately 85 percent of the negative feathering torque acting at the control torque discontinuity application point. Roughly, an additional 10 percent of the negative feathering torque was due to the aerodynamic forces acting at quarter chord which was 0.002083 meters aft of the elastic axis. In addition, these artificial offsets may result in differences in the harmonic content of feathering torque and thereby pitch horn loadings both due to their involvement in the analytical rotor system representation for all dynamic response harmonics and due to interharmonic coupling in which the harmonics above and below the harmonic of interest can effect the results obtained for the harmonic of interest. Since these small offsets were not present in the physical system, it was concluded that these offsets were a major cause of the difference between the experimental and predicted results. This effect of the small offsets suggest that the dynamic response of a helicopter rotor system may be much more sensitive to the spanwise distribution of the center of mass and elastic axis locations than previously suspected.

Representative azimuthal plots of the predicted flapwise bending moment, chordwise bending moment, and torsional moment for the same high speed flight condition are compared with the measured results from reference 3 in Figures 13 thru 15. Since the H-34 blade system is highly uncoupled it is not expected that the neutral axis and mass offsets would provide a very significant effect of the high negative torsional loading on the bending moments. This is borne out in that the behavior of the predicted results seems to follow the azimuthal trend of the experimental data. The comparison of experimental and theoretical results would be further improved if additional harmonics were included in the interharmonic coupling representation (one/rev. above and below the harmonic of interest was used in program runs) and in the free-wake induced velocity determination and if the artificial offsets were removed.

CONCLUDING REMARKS AND RECOMMENDATIONS

The program which has been developed for this investigation is a highly sophisticated theoretical representation of helicopter rotor systems. The coded analysis includes the effect of an anisotropically mounted flexible swashplate or a gyroscope control system and the effects of a deformed free-wake. The analysis has the capability of predicting the response characteristics of helicopter rotor systems in both forward flight and steady-state maneuver conditions. The quasi-steady blade aerodynamics representation can utilize an induced velocity field which is either uniform, variably defined, or one which is generated on successive iterations based on information from a free-wake analysis. The programmed analysis includes aerodynamic interharmonic coupling and also structural interharmonic coupling thru the swashplate or gyroscope without the necessity of information concerning the rotor system natural frequencies or related mode shapes. The analytical method employed allows for the straightforward extension of the program to include unsteady phenomena such as transient maneuvers and gust loading effects. Also the program is in a form such that it could be modified to investigate the stability and vibration characteristics of helicopter rotor systems in forward flight or maneuvers.

The blade dynamic response calculations which were carried out indicate that even with the high control system stiffnesses involved that the program provides an effective method of investigating the dynamic response behavior of present or future helicopter rotor systems. Considering the extensive information that can be obtained by use of this program, the program is a very efficient tool for use in investigating the effects of various parameters on the dynamic characteristics of a helicopter rotor system. A significant result of the execution of the program for the H-34 rotor system was the observation that

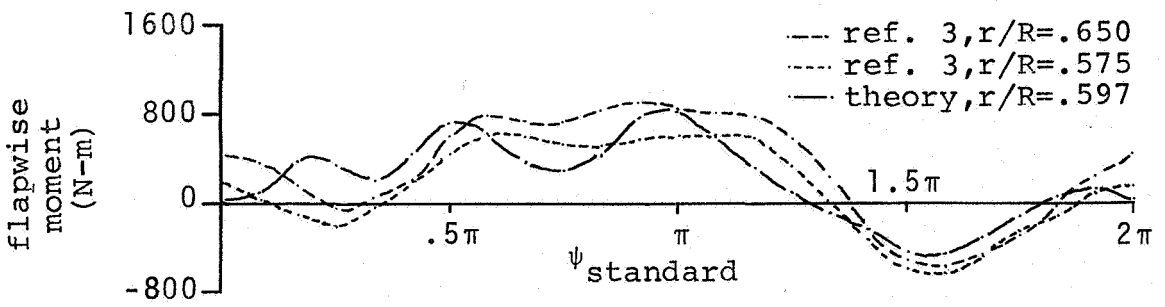

Figure 13. Flapwise bending moments for the high speed flight

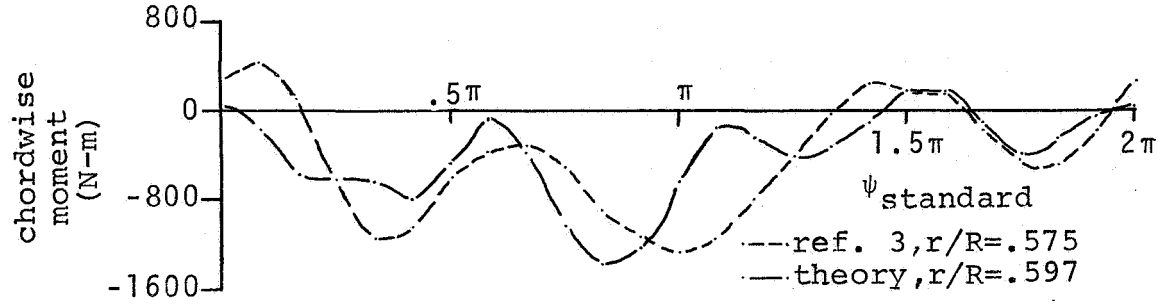

Figure 14. Chordwise bending moments for the high speed flight

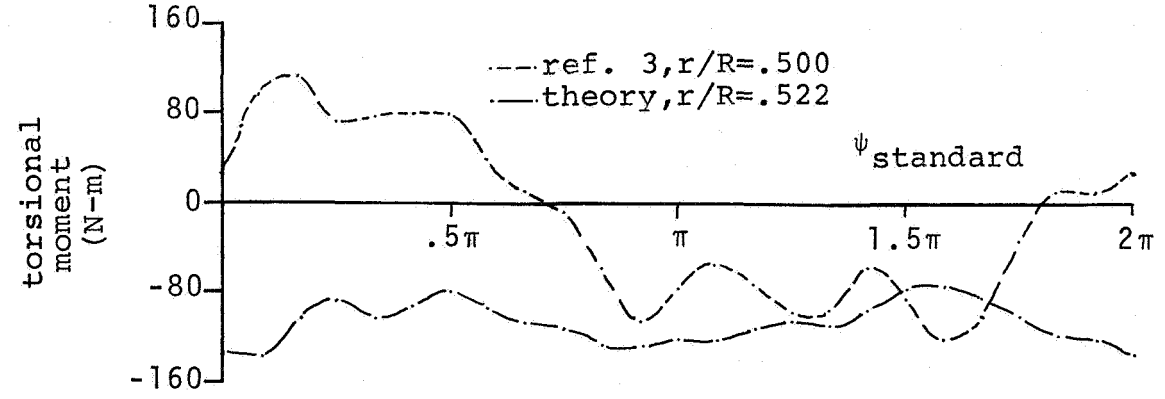

Figure 15. Torsional moments for the high speed flight

there is a significant effect of small offsets of the center of mass from the blade neutral axis and of the blade neutral axis from the blade aerodynamic center on the pitch horn loads and torsional moments. This result suggests that the blade pitch horn control loads may be more sensitive to the spanwise distribution of center of mass, neutral axis, and aerodynamic center locations than previously thought.

It is recommended that the program be extended to represent the unsteady phenomena a helicopter system might encounter as well as altering the program to provide the option of calculating the vibrational or stability characteristics of helicopter rotor systems. In addition, it is recommended that in order to more fully investigate the capabilities of the program and to show the effects of a nonuniform swashplate that the program be used to investigate the dynamic characteristics of a rotor system having a soft control system such as the OH-6A.

APPENDIX A

BLADE SECTION DATA

Section Number	Section Code*	m (kg)	ϵ_{ry} (m)	h_{rx} (m)	h_{ry} (m)	I_x, I_z (kg-m^2)	Φ (rad)	Θ (rad)
1	1000000	1.354093	0.00417	8.534417	0.002083	0.004583	-0.10472	-0.07854
2	1101000	3.745213	0.00417	8.191052	0.002083	0.034869	-0.10472	-0.07854
3	1010001	0.0	0.0	8.191052	0.0	0.0	-0.10472	-0.07854
4	1101000	3.153781	0.00417	7.829687	0.002083	0.025091	-0.10472	-0.07854
5	1010001	0.0	0.0	7.829687	0.0	0.0	-0.10472	-0.07854
6	1101000	3.973169	0.00417	7.434953	0.002083	0.026188	-0.10472	-0.07854
7	1010001	0.0	0.0	7.434953	0.0	0.0	-0.10472	-0.07854
8	1101000	4.078873	0.00417	6.992504	0.002083	0.033712	-0.10472	-0.07854
9	1010001	0.0	0.0	6.992504	0.0	0.0	-0.10472	-0.07854
10	1101000	4.575896	0.00417	6.484271	0.002083	0.056004	-0.10472	-0.07854
11	1010001	0.0	0.0	6.484271	0.0	0.0	-0.10472	-0.07854
12	1101000	5.298761	0.00417	5.877286	0.002083	0.037846	-0.10472	-0.07854
13	1010001	0.0	0.0	5.877286	0.0	0.0	-0.10472	-0.07854
14	1101000	5.394423	0.00417	5.096737	0.002083	0.052946	-0.10472	-0.07854
15	1010001	0.0	0.0	5.096737	0.0	0.0	-0.10472	-0.07854
16	1101000	5.373350	0.00417	4.452764	0.002083	0.060677	-0.10472	-0.07854
17	1101000	5.509700	0.00417	3.808791	0.002083	0.044611	-0.10472	-0.07854
18	1010001	0.0	0.0	3.808791	0.0	0.0	-0.10472	-0.07854
19	1101000	6.300893	0.00417	3.073406	0.002083	0.062014	-0.10472	-0.07854
20	1101000	4.319788	0.00417	2.286005	0.002083	0.043725	-0.10472	-0.07854
21	1101000	3.137684	0.00417	2.006604	0.002083	0.035997	-0.10472	-0.07854
22	1101000	3.130387	0.00417	1.397003	0.002083	0.030709	-0.10472	-0.07854
23	1101000	8.457153	0.0	0.889002	0.0	0.044607	-0.10472	-0.07854
24	1101000	23.452365	0.0	0.635001	0.0	0.073621	-0.10472	-0.07854
25	1101000	16.199207	0.0	0.304801	0.0	0.043929	-0.10472	-0.07854
26	0100000	0.0	0.0	0.0	0.0	0.0	0.0	0.0
27	0100000	0.0	0.0	0.0	0.0	0.0	0.0	0.0
28	0100000	0.0	0.0	0.0	0.0	0.0	0.0	0.0

* The section code consists of integers which if equal to 1 allow inclusion of certain section characteristics. The condition and effects included are; 1st integer =1 - mass effects, 2nd integer =1 - bend effects, 3rd and 7th integers =1 - aerodynamic effects, 4th integer =1 - elastic effects, 5th integer =1 - rigid effects, and 6th integer =1 - torsional spring effects. Section I_y was always taken as zero in value.

BLADE SECTION DATA (Cont.)

Section Number	Ψ (rad)	L (m)	δ_r (m)	C (m)	v * (m/sec)	xxxx (m)	ℓ (m)	(GJ) ($N-m^2$)
1	-0.139626	0.0	0.0	0.41666	0.0	0.0	0.0	0.0
2	-0.132909	0.0	0.0	0.41666	0.0	0.0	0.343365	50,210.5
3	-0.132909	0.352365	0.106249	0.41666	1.5240	8.191052	0.0	0.0
4	-0.125840	0.0	0.0	0.41666	0.0	0.0	0.361364	50,210.5
5	-0.125840	0.378049	0.106249	0.41666	1.5240	7.829687	0.0	0.0
6	-0.118118	0.0	0.0	0.41666	0.0	0.0	0.394734	50,210.5
7	-0.118118	0.418592	0.106249	0.41666	1.5240	7.434953	0.0	0.0
8	-0.109463	0.0	0.0	0.41666	0.0	0.0	0.442450	50,210.5
9	-0.109463	0.475341	0.106249	0.41666	1.5240	6.992504	0.0	0.0
10	-0.099520	0.0	0.0	0.41666	0.0	0.0	0.508233	50,210.5
11	-0.099520	0.557609	0.106249	0.41666	1.5240	6.484271	0.0	0.0
12	-0.087646	0.0	0.0	0.41666	0.0	0.0	0.606985	50,210.5
13	-0.087646	0.693767	0.106249	0.41666	1.5240	5.877286	0.0	0.0
14	-0.072376	0.0	0.0	0.41666	0.0	0.0	0.780549	50,210.5
15	-0.072376	1.034248	0.106249	0.41666	1.5240	5.096737	0.0	0.0
16	-0.059779	0.0	0.0	0.41666	0.0	0.0	0.643973	50,210.5
17	-0.047181	0.0	0.0	0.41666	0.0	0.0	0.643973	50,210.5
18	-0.047181	1.849867	0.106249	0.41666	1.5240	3.808791	0.0	0.0
19	-0.032795	0.0	0.0	0.41666	0.0	0.0	0.735385	50,210.5
20	-0.017391	0.0	0.0	0.41666	0.0	0.0	0.787401	50,210.5
21	-0.011925	0.0	0.0	0.41666	0.0	0.0	0.279401	50,210.5
22	0.0	0.0	0.0	0.41666	0.0	0.0	0.609601	50,210.5
23	0.0	0.0	0.0	0.41666	0.0	0.0	0.508001	60,252.6
24	0.0	0.0	0.0	0.41666	0.0	0.0	0.254000	129,762.1
25	0.0	0.0	0.0	0.41666	0.0	0.0	0.330201	341,513.9
26	0.0	0.0	0.0	0.0	0.0	0.0	0.0	0.0
27	0.0	0.0	0.0	0.0	0.0	0.0	0.0	0.0
28	0.0	0.0	0.0	0.0	0.0	0.0	0.0	0.0

* Values given in this column are only representative. The actual values used for runs employing uniform downwash are given in Table I.

BLADE SECTION DATA (Cont.)

Section Number	$(EI)_y$ ($N-m^2$)	$(EI)_z$ ($N-m^2$)	$\frac{1}{k_x}$ *	$\frac{1}{k_y}$ *	$\frac{1}{k_z}$ *	τ_x (sec)	τ_y (sec)	τ_z (sec)	K_s *
1	0.0	0.0	0.0	0.0	0.0	0.0	0.0	0.0	0.0
2	457,473.3	42,193.3	0.0	0.0	0.0	0.0	0.0	0.0	0.0
3	0.0	0.0	0.0	0.0	0.0	0.0	0.0	0.0	0.0
4	457,473.3	42,193.3	0.0	0.0	0.0	0.0	0.0	0.0	0.0
5	0.0	0.0	0.0	0.0	0.0	0.0	0.0	0.0	0.0
6	475,473.3	42,193.3	0.0	0.0	0.0	0.0	0.0	0.0	0.0
7	0.0	0.0	0.0	0.0	0.0	0.0	0.0	0.0	0.0
8	457,473.3	42,193.3	0.0	0.0	0.0	0.0	0.0	0.0	0.0
9	0.0	0.0	0.0	0.0	0.0	0.0	0.0	0.0	0.0
10	457,473.3	42,193.3	0.0	0.0	0.0	0.0	0.0	0.0	0.0
11	0.0	0.0	0.0	0.0	0.0	0.0	0.0	0.0	0.0
12	457,473.3	42,143.3	0.0	0.0	0.0	0.0	0.0	0.0	0.0
13	0.0	0.0	0.0	0.0	0.0	0.0	0.0	0.0	0.0
14	457,473.3	42,193.3	0.0	0.0	0.0	0.0	0.0	0.0	0.0
15	0.0	0.0	0.0	0.0	0.0	0.0	0.0	0.0	0.0
16	457,473.3	42,193.3	0.0	0.0	0.0	0.0	0.0	0.0	0.0
17	457,473.3	42,193.3	0.0	0.0	0.0	0.0	0.0	0.0	0.0
18	0.0	0.0	0.0	0.0	0.0	0.0	0.0	0.0	0.0
19	457,473.3	42,193.3	0.0	0.0	0.0	0.0	0.0	0.0	0.0
20	457,473.3	42,193.3	0.0	0.0	0.0	0.0	0.0	0.0	0.0
21	457,473.3	42,193.3	0.0	0.0	0.0	0.0	0.0	0.0	0.0
22	457,473.3	42,193.3	0.0	0.0	0.0	0.0	0.0	0.0	0.0
23	493,013.2	49,053.4	0.0	0.0	0.0	0.0	0.0	0.0	0.0
24	680,217.7	202,908.2	0.0	0.0	0.0	0.0	0.0	0.0	0.0
25	1,319,936.5	1,434,821.4	0.0	0.0	0.0	0.0	0.0	0.0	0.0
26	0.0	0.0	0.0	0.0	0.0	0.0	0.0	0.0	0.0
27	0.0	0.0	0.0	0.0	10.54712	0.0	0.0	50,000.0	0.0
28	0.0	0.0	0.0	0.0	0.0	0.0	0.0	0.0	0.0

*rad/(N-m)

APPENDIX B

CONVERSION OF UNITS

The following conversion relationships are those which were utilized to convert variable values originally in the British system of units to the corresponding values in the SI system of units for purposes of discussion in this report.

1 foot = .3048006 meters

1 pound = 4.448222 Newtons

1 slug = 14.59388 kilograms

1 foot/second = .3048006 meters/second

1 foot-pound = 1.355821 Newton-meters

1 pound/foot = 14.59388 Newtons/meter

1 pound-foot^2 = .4132550 Newton-meters^2

1 slug-foot^2 = 1.355821 kilogram-meters^2

1 slug/foot^3 = 515.3750 kilograms/meter^3

1 foot-pound/radian = 1.355821 Newton-meters/radian

1 radian/(foot-pound) = .7375607 radians/(Newton-meter)

REFERENCES

1. Sadler, S. Gene: Main Rotor Free Wake Geometry Effects on Blade Air Loads and Response for Helicopters in Steady Maneuvers, NASA CR-2110, 1972.

2. Piarulli, Vincent J.: The Effects of Nonuniform Swash-plate Stiffness on Coupled Blade-Control System Dynamics and Stability, NASA CR-1817, 1971.

3. Scheiman, James: A Tabulation of Helicopter Rotor-Blade Differential Pressures, Stresses and Motions as Measured in Flight, NASA TM X-952, 1964.

4. Gessow, Albert and Myers, Garry C.: Aerodynamics of the Helicopter, Frederick Unger Publishing Co., 1967.

5. Sutton, Lawrence R. and Rinehart, Stephen A.: Development of an Analysis for the Determination of Coupled Helicopter Rotor System Dynamic Response, Computer Program Documentation, RASA Report 73-09.

NATIONAL AERONAUTICS AND SPACE ADMINISTRATION
WASHINGTON, D.C. 20546

OFFICIAL BUSINESS
PENALTY FOR PRIVATE USE $300

SPECIAL FOURTH-CLASS RATE BOOK

POSTAGE AND FEES PAID
NATIONAL AERONAUTICS AND SPACE ADMINISTRATION
451

U.S. MAIL

POSTMASTER: If Undeliverable (Section 158 Postal Manual) Do Not Return

"The aeronautical and space activities of the United States shall be conducted so as to contribute . . . to the expansion of human knowledge of phenomena in the atmosphere and space. The Administration shall provide for the widest practicable and appropriate dissemination of information concerning its activities and the results thereof."

—NATIONAL AERONAUTICS AND SPACE ACT OF 1958

NASA SCIENTIFIC AND TECHNICAL PUBLICATIONS

TECHNICAL REPORTS: Scientific and technical information considered important, complete, and a lasting contribution to existing knowledge.

TECHNICAL NOTES: Information less broad in scope but nevertheless of importance as a contribution to existing knowledge.

TECHNICAL MEMORANDUMS: Information receiving limited distribution because of preliminary data, security classification, or other reasons. Also includes conference proceedings with either limited or unlimited distribution.

CONTRACTOR REPORTS: Scientific and technical information generated under a NASA contract or grant and considered an important contribution to existing knowledge.

TECHNICAL TRANSLATIONS: Information published in a foreign language considered to merit NASA distribution in English.

SPECIAL PUBLICATIONS: Information derived from or of value to NASA activities. Publications include final reports of major projects, monographs, data compilations, handbooks, sourcebooks, and special bibliographies.

TECHNOLOGY UTILIZATION PUBLICATIONS: Information on technology used by NASA that may be of particular interest in commercial and other non-aerospace applications. Publications include Tech Briefs, Technology Utilization Reports and Technology Surveys.

Details on the availability of these publications may be obtained from:

SCIENTIFIC AND TECHNICAL INFORMATION OFFICE

NATIONAL AERONAUTICS AND SPACE ADMINISTRATION

Washington, D.C. 20546